AFCRL-67-0277 ASE-1602

THE FLUORESCENCE OF AIR AND NITROGEN EXCITED BY ENERGETIC ELECTRONS

ROBERT O'NEIL
GILBERT DAVIDSON

AS&E
AMERICAN SCIENCE AND ENGINEERING, INC.
11 Carleton Street, Cambridge, Massachusetts 02142

CONTRACT AF 19(628)-4080
PROJECT NO. 5710
TASK NO. 571000
WORK UNIT NO. 57100001

CONTRACT MONITOR: GARY CULP
OPTICAL PHYSICS LABORATORY

FINAL REPORT

12 MARCH 1964 - 11 FEBRUARY 1967

1 JANUARY 1968

This research was sponsored by the Defense Atomic Support Agency, Washington, D.C. under Subtask No. 12.505

PREPARED FOR
AIR FORCE CAMBRIDGE RESEARCH LABORATORIES
OFFICE OF AEROSPACE RESEARCH
UNITED STATES AIR FORCE
BEDFORD, MASSACHUSETTS 01730

ASE-1602

AFCRL-67-0277

THE FLUORESCENCE OF AIR AND NITROGEN EXCITED BY ENERGETIC ELECTRONS

Robert O'Neil
Gilbert Davidson

American Science and Engineering, Inc.
11 Carleton Street
Cambridge, Massachusetts 02142

Contract No. AF 19 (628)-4080

Project No. 5710
Task No. 571000
Work Unit No. 57100001

FINAL REPORT

Period Covered: 12 March 1964 through 11 February 1967

1 January 1968

Contract Monitor: Gary Culp, Capt. USAF
Optical Physics Laboratory

Prepared for

Air Force Cambridge Research Laboratories
Office of Aerospace Research
United States Air Force
Bedford, Massachusetts 01730

This research was supported by the
Defense Atomic Support Agency

ABSTRACT

The optical radiation from air and nitrogen bombarded by energetic (kev) electrons has been measured over a wide range of gas pressures. Absolute fluorescent efficiencies of spectra from 3,200 to 11,000 Å are presented for air and nitrogen at both 22 Torr excited by 10 kev electrons and 600 Torr excited by 50 kev electrons. At lower pressures, absolute intensity measurements have been made in the form of electron excitation cross sections for the first negative and Meinel bands of N_2^+. The radiative lifetimes of the Meinel bands are also given.

The pressure dependence of the first and second positive systems of N_2 and the first negative and Meinel systems of N_2^+ has been analyzed. With the exception of the Meinel bands, the Stern-Volmer collisional quenching mechanism accurately describes the pressure dependence of these systems in nitrogen and air. The Meinel bands of N_2^+ are produced by several mechanisms. One excitation process is pressure dependent and effective only at lower pressures. The Stern-Volmer expression describes the intensity-pressure dependence of the Meinel bands at higher pressures where the direct excitation process dominates.

Based on the Stern-Volmer analysis, the absolute intensity of the electron induced fluorescence is determined for various transitions of these four band systems for any pressure of air or nitrogen.

FOREWARD

This report describes research performed under Contract AF 19 (628)-4080 during the period 12 March 1964 to 11 February 1967.

The support and encouragement of Mr. Hervey P. Gauvin, Dr. A. T. Stair, Jr., and Captain G. Culp of Air Force Cambridge Research Laboratories is gratefully acknowledged. The authors also wish to thank Dr. J. W. Carpenter of American Science and Engineering, Incorporated (AS&E) for his continuous technical assistance, and Miss Evelyn Nangle of AS&E for the preparation of this report.

TABLE OF CONTENTS

TABLE OF CONTENTS
(continued)

LIST OF ILLUSTRATIONS

LIST OF ILLUSTRATIONS
(continued)

LIST OF ILLUSTRATIONS
(continued)

LIST OF ILLUSTRATIONS
(continued)

LIST OF TABLES

1. INTRODUCTION

The optical emissions from gases excited by energetic electrons are characteristic of certain paremeters of the gas and the exciting electrons. Defining the nature of the optical emissions for atmospheric constituents excited by energetic electrons in a controlled laboratory experiment is necessary to understand and interpret ionospheric radiative phenomena. These include natural aurora and airglow emissions as well as the optical emissions associated with the detonation of a nuclear device.

As is well-known, thermal X-rays constitute a large fraction of the total yield of an unshielded high altitude nuclear weapon. On encountering the atmosphere much of the thermal X-ray energy is dissipated in the form of electrons produced by the ionization of atmospheric constituents. The electrons, in turn, excite certain molecular and atomic states of the atmospheric gases which may decay with the emission of the optical radiation. This research study was designed to measure the absolute intensities of the optical emissions from atmospheric gases excited by energetic electrons. Very limited experimental measurements have been reported for absolute fluorescent efficiencies (the percentage of an electron's total kinetic energy converted into optical radiation). In addition, other parameters such as radiative lifetimes, quenching cross sections of the atmospheric gases and electron excitation cross sections are necessary to extrapolate from a given experimental condition to other conditions of pressure (altitude) and incident electron energy.

Presented in this report are various forms of absolute intensity measurements made with an experimental system designed to provide high beam currents of electrons with kilovolt energy incident on target gases over a wide range of pressures. The apparatus facilitates the measurement of absolute intensities in the two obvious cases (fluorescent efficiency and excitation cross section) where absolute values of the radiance by a specific molecular or atomic transition may be described in terms of

meaningful parameters. The target gases were restricted to either nitrogen or air.

In the thick target case, the incident energetic electron is stopped within the observation region of the target chamber and measurements of absolute intensity yield fluorescent efficiencies. Fluorescent efficiencies are presented for the spectra observed in nitrogen and air at 22 Torr excited by 10 kev electrons and 600 Torr excited by 50 kev electrons. The spectra were observed from 2,000 to 11,000 Angstroms with 18 Angstrom resolution. Fluorescent efficiencies are presented for resolved spectral features from 3,200 to 11,000 Å. The band systems observed in the nitrogen thick target case were the second positive ($C^3\Pi_u \rightarrow B^3\Pi_g$), first positive ($B^3\Pi_g \rightarrow A^3\Sigma_u^+$), Gaydon-Green and Herman infrared systems of N_2 and the first negative system ($B^2\Sigma_u^+ \rightarrow X^2\Sigma_g^+$) of N_2^+. In addition the NO γ system ($A^2\Sigma^+ \rightarrow X^2\Pi$) and CN violet ($B^2\Sigma^+ \rightarrow X^2\Sigma^+$) and red systems ($A^2\Pi_i \rightarrow X^2\Sigma^+$) were observed as impurities in the target chamber. The spectra observed in the air thick target case consisted of the first and second positive systems of N_2, the first negative system of N_2^+, the NO γ bands and some atomic spectra of nitrogen, oxygen and argon. In addition, the fluorescent efficiency of the (0-0) band of the first negative system of N_2^+ at 3914 Å has been measured for a variety of combinations of incident electron energy from 10 to 60 kev and target gas pressure from 22 to 800 Torr.

When the mean time between collisions approaches the lifetime of a transition, collisional quenching may compete with spontaneous decay as a depopulating mechanism of the excited species. Values of the quenching cross sections of the N_2 and air are given for the 3914 Å band and intense transitions of the N_2 first and second positive systems. Calculation of the collisional deactivation cross section from thick target measurements infers knowledge of the fluorescent efficiency at low pressures where quenching is an ineffective depopulating process. In the case of the N_2 first and second positive bands, this quantity is extrapolated from the thick target

measurements. For the N_2^+ first negative system, the low pressure fluorescent efficiency is based on several established parameters as well as the electron excitation cross section of this experiment.

In the thin target case the energetic primary electron loses a small fraction of its energy in traversing the observation region of the target chamber. In this condition the absolute intensity measurements may yield values for excitation cross sections providing primary electron excitation can be distinguished from emission produced by secondary electrons. The emission from nitrogen in the thin target case (5×10^{-2} Torr) excited by 50 kev electrons has been measured from 2,000 to 11,000 Å. The spectra observed includes the first positive, second positive and Gaydon-Herman singlet systems of N_2, the first negative and Meinel ($A^2\Pi_g \rightarrow X^2\Sigma_g^+$) system of N_2^+ and several atomic transitions of nitrogen. Excitation cross sections have been measured for the (0-0) band of the first negative system and the (2-0), (1-0) and (0-0) bands of the Meinel system. Additional measurements of the (2-0), (1-0) and (0-0) Meinel bands have determined N_2 quenching cross sections and radiative lifetimes for these transitions.

The first negative and Meinel systems of N_2^+ and the first and second positive systems of N_2 are among the most intense atmospheric emissions. Fluorescent efficiencies for electron excitation, radiative lifetimes and the quenching cross sections of the atmospheric constituents are parameters essential for the interpretation of excitation conditions.

2. EXPERIMENTAL APPARATUS

The experimental facility used to record the data presented in this report was developed under a previous contract.[1] An abbreviated description of the basic experimental system is repeated here with subsequent modifications. Previous publications contain a more detailed description of the experimental apparatus[1] and also initial values for absolute fluorescent efficiencies[2] which have been essentially confirmed by subsequent measurements.

The system has been designed to measure the absolute emission from various gases and gas mixtures excited by electrons. Differentially pumped nozzles are used to provide monoenergetic electrons incident on the target gas. The maximum system operating conditions are 10 ma beam current, 60 kev beam energy and 1 atmosphere of air or nitrogen target chamber pressure. Figure 1, a doubly exposed photograph of the differential pumping system, shows a fluorescing volume extending slightly outside the observable region of the target chamber. The beam energy is variable down to approximately 3 kev with a significant decrease in target chamber beam current due to electron gun defocussing effects. The minimum target pressure used in the present measurements was 10^{-4} Torr attained by removing two of the three differentially pumped nozzles used in the high target pressure studies.

2.1 Electronic System

The electron gun was similar to the type used in Van de Graaf accelerators. A series of seven electrodes supplied by a voltage divider network accelerate and focus the electron beam. At the output of the gun assembly a magnetic lens reduced the natural focal length of the electron beam as determined by the focussing electrodes.

The electron gun cathode, a hairpin tungsten filament, was operated at a maximum of 60 kv negative potential. A 30 amp dc filament supply, extraction voltage supply and pulser network rested on an insulated shielded table and were supplied by a 3 kva isolation transformer as shown in Figure 2

DOUBLY EXPOSED PHOTOGRAPH OF EXPERIMENTAL APPARATUS

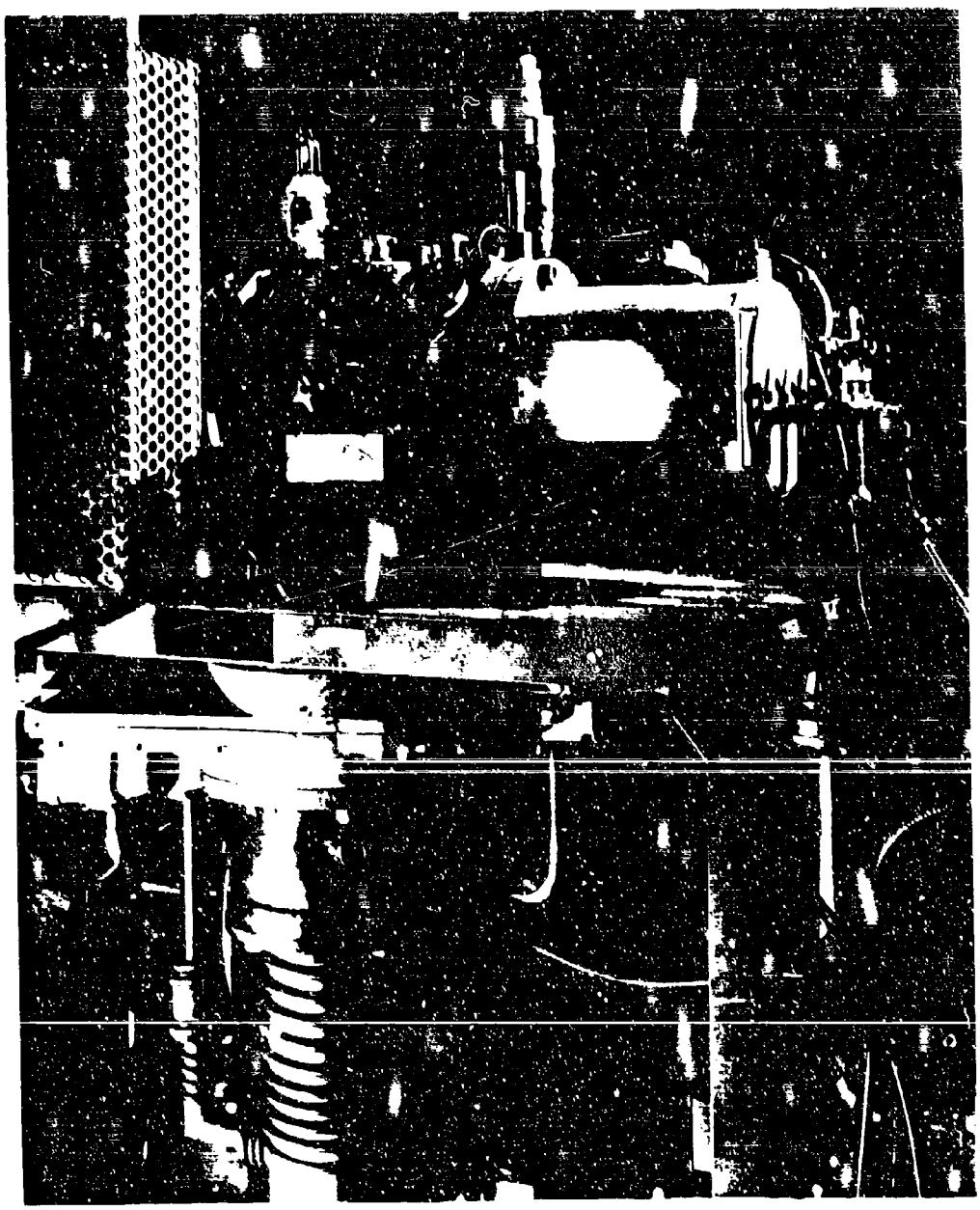

Figure 1

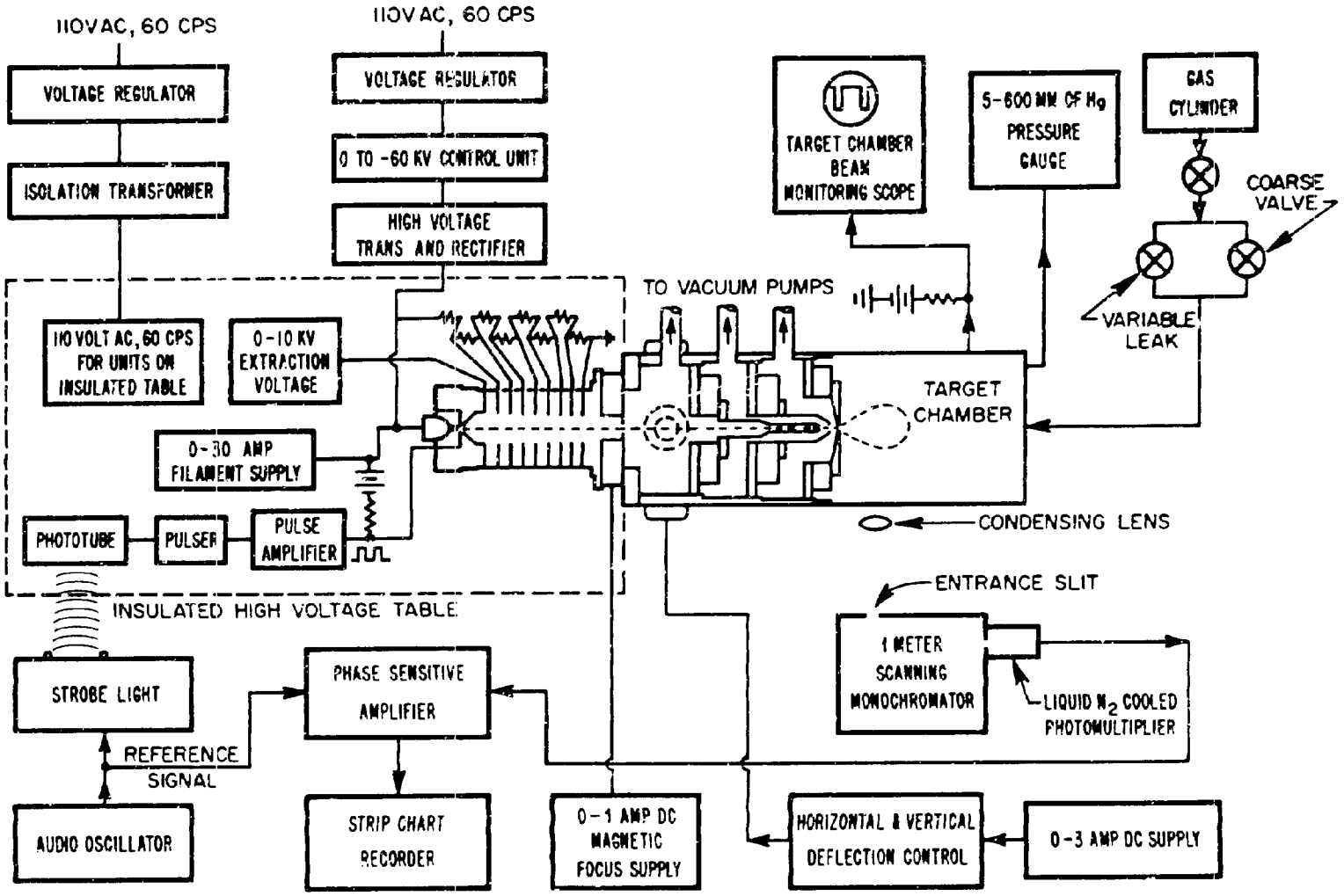

Figure 2

BLOCK DIAGRAM OF EXPERIMENTAL SYSTEM

The electron beam was modulated by a control grid. In one operating mode, the pulse to the control element was supplied by a strobe which was outside the insulated shielded table and detected by a phototube on the table. The phototube output triggered a pulse generator that controlled the duty cycle and amplitude of the modulated electron beam. The primary frequency generator was a precision variable oscillator which triggered the strobe and provided the reference signal for a synchronous detection system. This operating mode was limited to frequencies of less than 450 Hz, the maximum strobe pulse rate.

Another operating mode was used at frequencies greater than 450 Hz and was an alternative to the strobe technique at lower frequencies. In this mode the pulse generator was internally triggered. The beam pulse collected in the target chamber or on one of the differentially pumped nozzles was used as a reference signal for the synchronous detection system.

Two pairs of Helmholtz coils were located beyond the electron gun system in the region of the low pressure chamber. These provided horizontal and vertical beam deflection to aid in the alignment of the electron beam.

2.2 Pumping System

The electron beam system described here used the technique of differentially pumped chambers tc allow passage of the electron beam from the gun to a high pressure target chamber without traversing window material. The system described here was similar to that of Grun[3]. The design parameters have been discussed by Schumacher[4].

This system was composed of three differentially pumped chambers between the electron gun and the target chamber. Chamber 1 (Figure 3) was pumped by an NRC Equipment Corporation HS4-750 Type 161 diffusion pump with a maximum pumping speed of 750 liters/sec unbaffled. Chamber 2 was pumped by an NRC Equipment Corporation B-4 booster pump Type 126B with a maximum pumping speed of 240 liters/sec unbaffled, and Chamber 3 by an F. J. Stokes Corporation 212N microvac pump with a pumping speed of 140 cfm unbaffled. An individually thermostated, optically opaque, cold trap

ELECTRON GUN AND THE DIFFERENTIALLY-PUMPED CHAMBERS

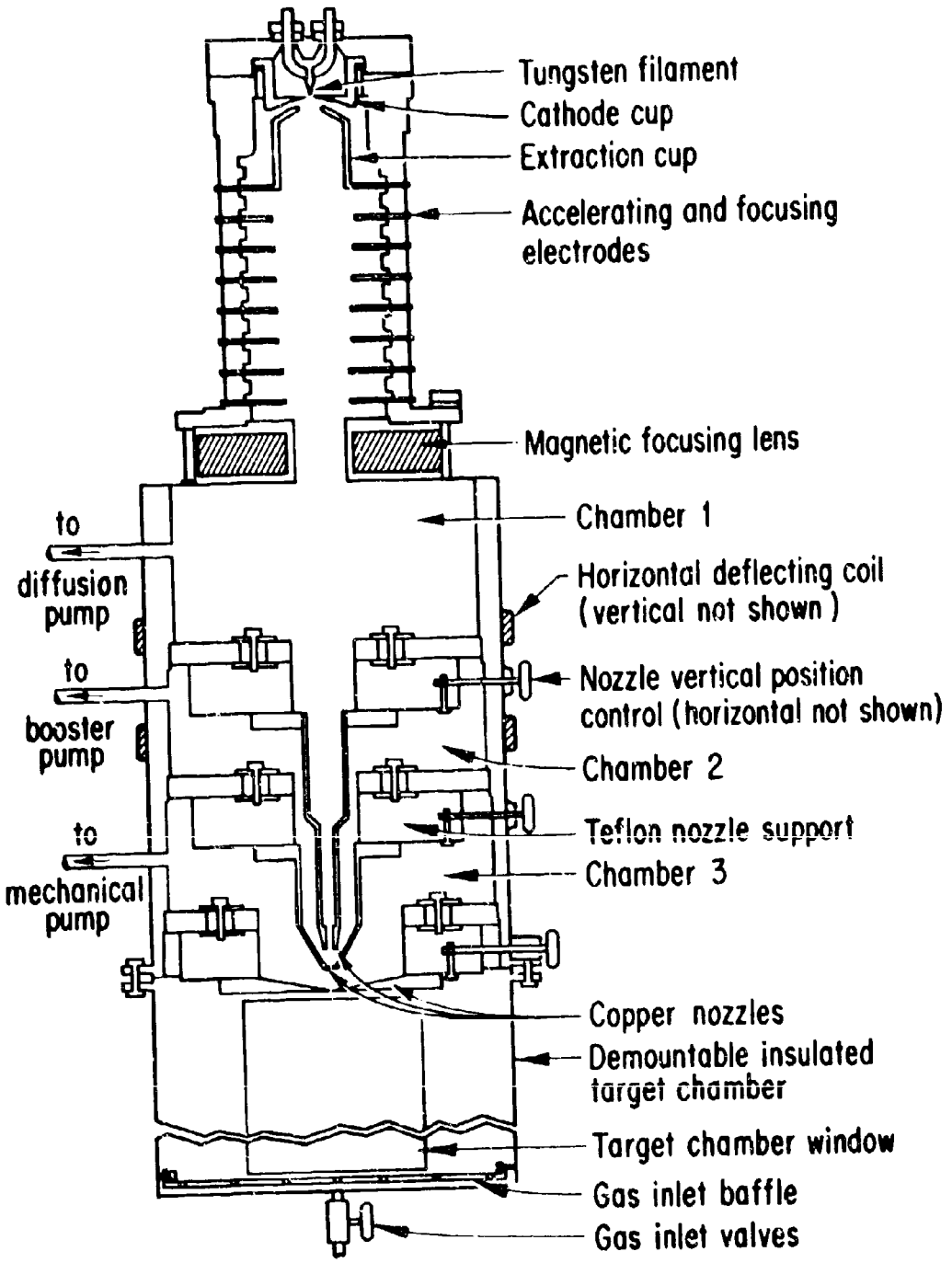

AT041

Figure 3

was maintained at -20°F by a freon refrigeration system between each pump and the vacuum system.

The differentially pumped nozzles were attached to movable teflon supports as shown in Figure 3. These were driven horizontally and vertically by vernier drive screws, controlled outside the chamber. This allowed for alignment of the nozzle system to maximize the beam current entering the target chamber.

The nozzle design, Figure 4, maintained a pressure of 1×10^{-4} Torr in the gun chamber with 800 Torr of air or N_2 in the target chamber. The maximum operating pressure in the gun chamber was limited by high voltage breakdown and reasonable cathode life. For low pressure thin target studies, a single nozzle was used to increase the beam current entering the target chamber and to increase target chamber pumping speed. The higher pumping speed reduced contaminants from residual gases and facilitated target pressure control. A Granville-Phillips Company variable leak was used to regulate target gas pressure.

2.3 Target Chamber

The stainless steel target chamber was 11 inches in length by 8 inches in diameter. The 4 x 10 inch window was either lead glass, pyrex, quartz or arsenic trisulfide depending upon the wavelength region of interest. The chamber was electrically isolated and used as a Faraday cup to measure beam current. A pump port on the target chamber allowed rapid rough-out of the system by the mechanical pump. Internal target chamber design differed in the thick and thin target cases. Details are described in subsequent sections.

2.4 Monitoring and Detection System

The target chamber pressure was measured by a Wallace and Tiernan Gauge (5 to 800 Torr) or an NRC Equipment Corporation "Alphatron" Gauge (10^{-4} to 10^{+4} Torr). The gauges were consistent within five percent in the overlap pressure range.

CONFIGURATION OF THE NOZZLES SEPARATING THE CHAMBERS

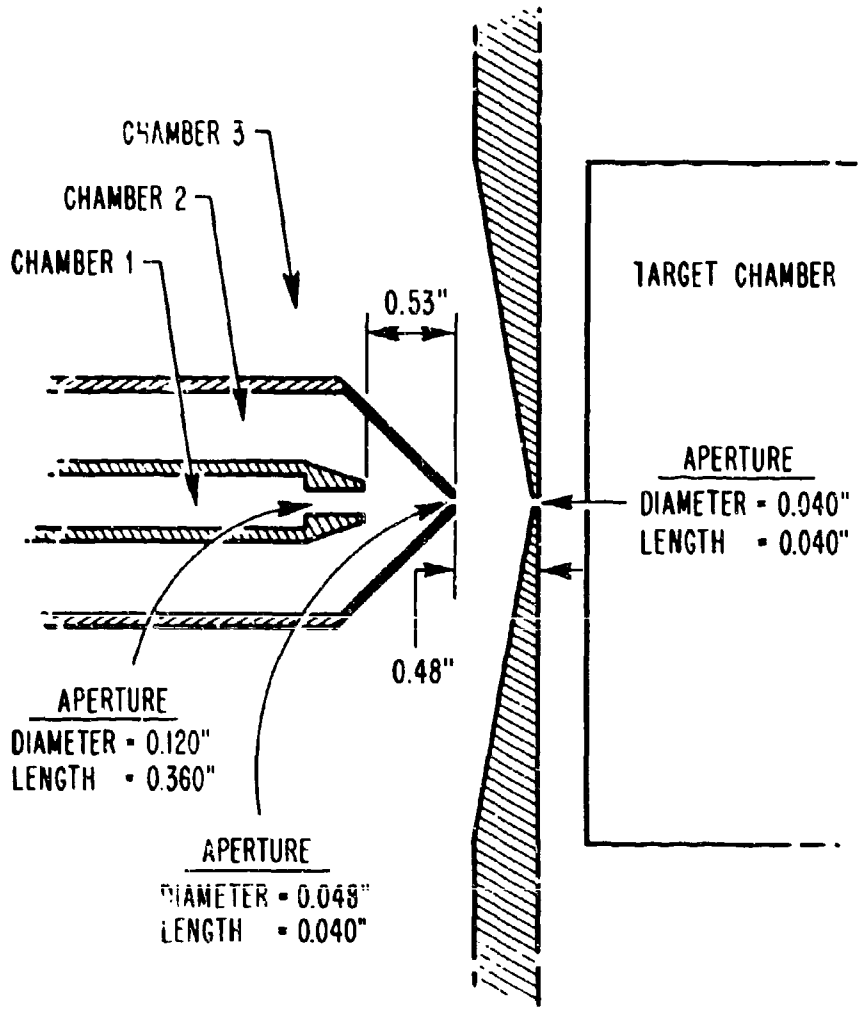

Figure 4

The pulsed beam current striking each nozzle was monitored through a leakage resistor by an oscilloscope. This aided in the initial alignment of the nozzles for maximum beam current in the target chamber. Thermistors monitored the temperature of the copper nozzles and under the usual operating conditions the duration of system operation was unlimited.

The radiation emitted by the target gas was spectrally analyzed by a one meter MacPherson f/10.0 scanning grating monochromator of the Czerny Turner design. For the data presented here, 1200 line/mm Bausch and Lomb gratings blazed at either 7500 Å or 3000 Å were used in the monochromator. Diffraction orders were separated by Corning filters. The detectors used at the exit slit of the monochromator were an EMI 6256 photomultiplier with S-13 response, an RCA 6199 photomultiplier with S-11 response and a liquid nitrogen cooled RCA 7102 photomultiplier with S-1 response.

The modulated electron beam fluorescence was measured by a phase sensitive amplifier (Princeton Applied Research Model JB-4) and recorded by a dual channel strip chart. The second channel was used to record either the electron beam current or a fluorescence monitor signal as provided by a second phase sensitive amplifier. The fluorescence monitor consisted of an optical interference filter mounted on a photomultiplier.

A 10-20% duty cycle was normally used with the electron beam pulse to maximize the ratio of power in the fundamental frequency to total power in the beam. This minimized the general heating effect in the system for a given signal as recorded through the narrow band phase sensitive system.

3. THICK TARGET CONDITIONS

The thick target studies measured the optical emissions excited by energetic electrons stopped within the field of view of the target chamber. With the present chamber, this requirement limits the range of the incident electron to 10 cm or less. Figure 5, a photograph of thick target fluorescence, illustrates that the fluorescing volume approximates a sphere. The two thick target cases considered are 10 kev electrons incident on air and nitrogen at 22 Torr and 50 kev electrons incident on air and nitrogen at 600 Torr. Absolute fluorescent efficiencies have been previously presented for 50 kev electrons incident on air and nitrogen at 600 Torr.[2] Remeasurements have essentially confirmed the absolute fluorescent efficiencies initially reported[2] with revised values, on the order of 10 to 20 percent, for some transitions.

3.1 Target Chamber

The target chamber used in the thick target case is shown in Figure 6. Since the electron beam is stopped within a 10 cm sphere, the electrons are not collected by the walls of the chamber. A thin copper disc with an opening slightly larger than the electron beam entrance opening was mounted on the copper plate containing the entrance hole. The disc was isolated from the plate by a thin film of Teflon. This surface was one of two electron collecting surfaces. The second surface, an innovation since the earlier reports, consisted of a movable copper disc controlled outside the chamber by means of rotary seal. When spectra was being observed, the movable plate was withdrawn outside the range of the incident electrons. In order to measure the absolute beam current incident on the target gas, the movable plate was positioned within 1 cm of the non-movable disc. In this position the incident electron beam strikes the movable copper plate. The two collecting surfaces which are separated by a small fraction of the incident electron range collect all of the electrons incident on the target gas. The difference in beam current measured with the movable plate in its two extreme positions is a function of the relative hole diameters of the differentially pumped plate and the teflon isolated collecting plate, a function of

THICK TARGET FLUORESCENCE

N_2 AT 600 TORR, 50 keV ELECTRONS

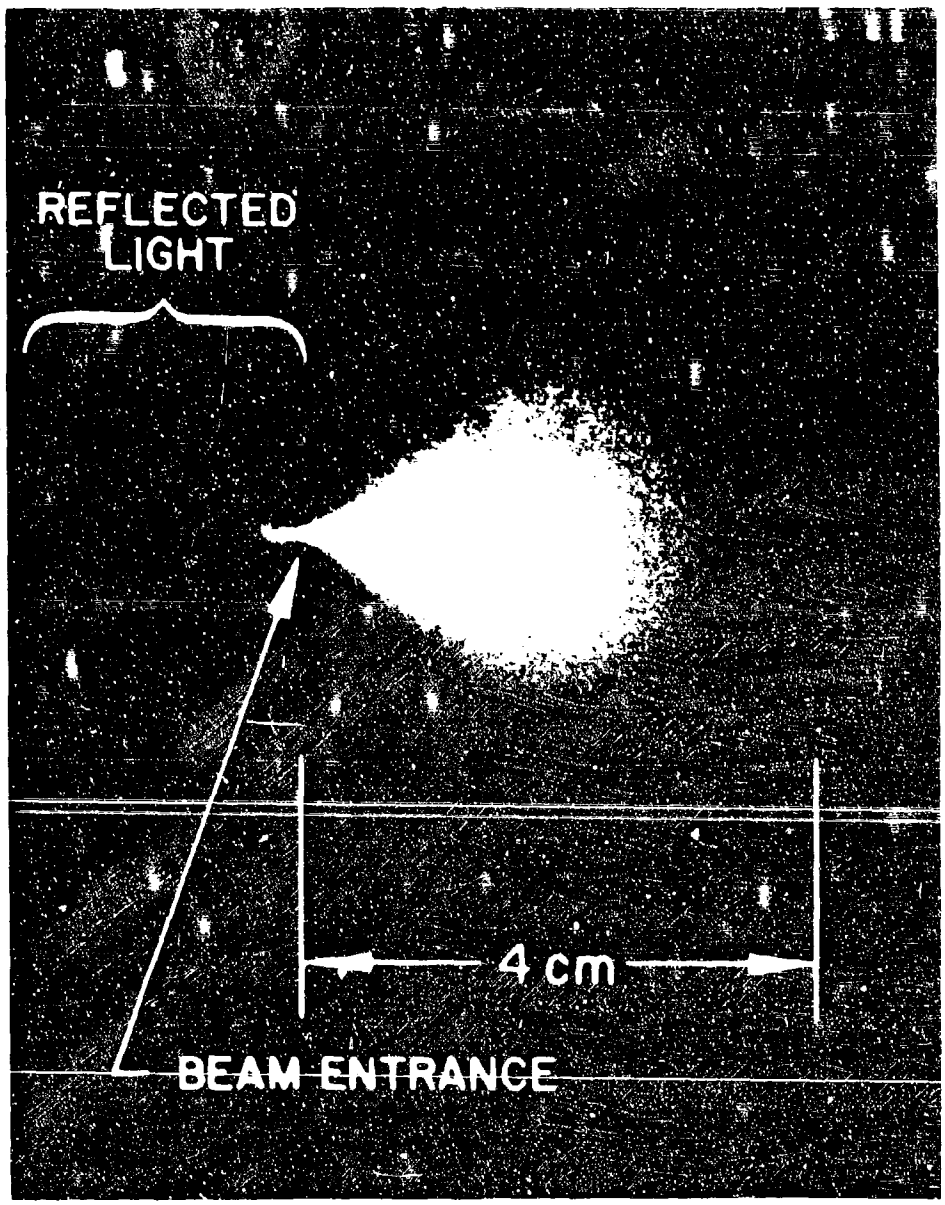

AY-0353

Figure 5

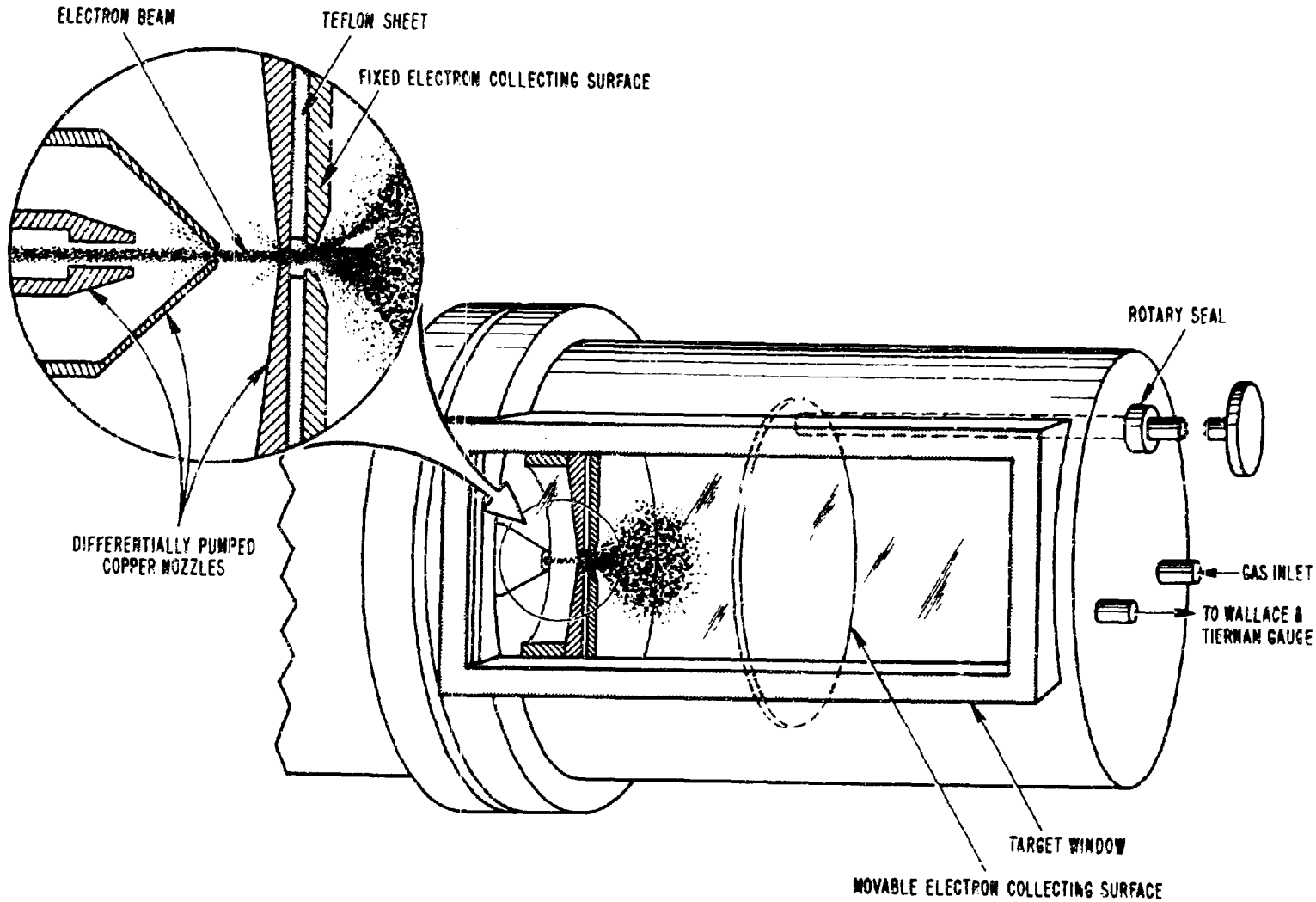

Figure 6

TARGET CHAMBER FOR THICK TARGET CASE

the electron range and also the target gas. For the 50 kev, 600 Torr case the difference in the total measured beam current with the movable plate in its extreme positions is approximately a factor of two. In the recent measurements, with the movable plate beyond the electron range about half the incident electrons are lost either to the differentially pumped plate or through the opening. The total measured beam current is essentially constant for a given energy from thin target (range of the electron very large compared to the target chamber dimensions) to thick target (range of the electron less than 10 cm) conditions. All surfaces within the target chamber were painted black to minimize reflections such as observed on the unpainted surfaces in Figure 5. The constant relative intensities of the band systems recorded before and after the paint was applied ensured the paint was ineffective as a target gas contaminant.

3.2 Procedure

3.2.1 Recording Spectra

The spectra presented from 2,000 Å to 11,000 Å were recorded with the monochromator aligned with the center of the fluorescing volume. The f/10 monochromator was positioned such that the field of view was slightly underfilled. This ensured that the total fluorescing region was observed with a slight sacrifice in solid angle collecting efficiency. The 2,000 to 11,000 Å spectra were recorded in three segments. The 3,200 to 6,000 Å region was recorded with an RCA 6199 photomultiplier with S-11 response and the 5,000 to 11,000 Å region with a liquid nitrogen cooled RCA 7102 photomultiplier with S-1 response. The low wavelength limit was extended to 2000 Å by using an S-13 EMI 6256 photomultiplier with a 1200 line/mm Bausch and Lomb grating blazed at 3000 Å. The wavelength region observed with this grating-photomultiplier combination ranged from 2,000 to 5,000 Å. The 1200 line/mm Bausch and Lomb gratings used in the monochromator with 2.0 mm slits resulted in an effective spectral slit width of 18 Å. The relative spectral response of each detection system was measured with a

standard tungsten filament lamp. For wavelengths below 3200 Å the system spectral response is less certain due to an increasing uncertainty in the standard lamp intensity. Below 2500 Å, the lower limit of the standard lamp calibration, the system response was based on a calibration technique using sodium salicylate as a constant quantum detector.

3.2.2 Ultraviolet Calibration Technique

The experimental set up for the ultraviolet calibration procedure is shown in Figure 7. The ultraviolet source, a discharge tube producing the hydrogen continuum, illuminated the entrance slit of the calibration monochromator. In effect, the ultraviolet source-calibration monochromator system functioned as a continuously variable monochromatic source with a line width of approximately 20 Å. A beam splitter at the exit slit of the calibration monochromator divided the emerging beam between a sodium salicylate coated photomultiplier and the entrance slit of the system to be calibrated. The beam splitter consisted of two front surface aluminum mirrors. The intensities of the split effective line source were recorded by a dual channel strip chart for a series of wavelengths from 2,000 to 3,000 Å. The relative response of the system to be calibrated was calculated based on the relative intensity of the effective source as measured by the coated photomultiplier, assuming constant quantum efficiency for the sodium salicylate phosphor. However, the ultraviolet radiation incident on the MacPherson monochromator may have been partially polarized. Polarization may occur both in the calibration grating monochromator and at the beam splitter. In addition, the degree of polarization is a function of wavelength. Since the grating efficiency of the system under calibration is a function of the degree of polarization of the incident radiation, the measured relative response is a unique case for the given calibrating source polarization. Grating polarizing effects are conventionally described by intensity magnitudes in two orthogonal directions, parallel and perpendicular to the grating rulings. However, rotating the MacPherson monochromator ninety degrees about its entrance slit optic axis, reverses the intensity vectors of

EXPERIMENTAL ARRANGEMENT TO MEASURE UV SYSTEM SPECTRAL RESPONSE

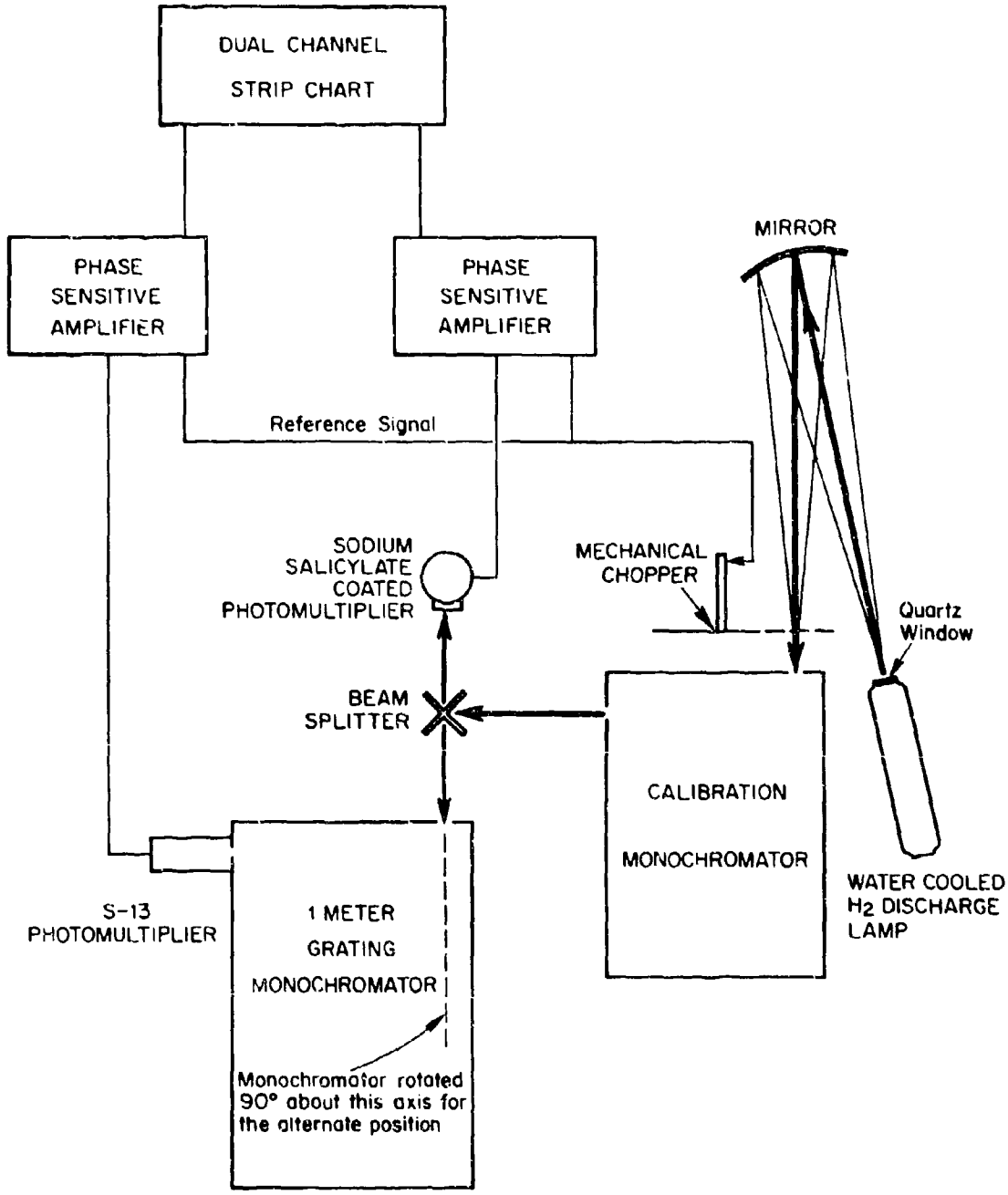

Figure 7

1602

the incident polarized radiation with respect to the MacPherson grating rulings. In Figure 8, A and B are defined as the relative system response in the two mutually orthogonal monochromator positions to the same partially polarized source. The relative response in position A and B differ by as much as 35%. Also shown in Figure 8 is the relative response of the system above 2500 Å as measured with the standard tungsten lamp. The relative responses for these three cases have been arbitrarily normalized at 2800 Å. The relative system response to unpolarized radiation, C, may be described by

$$[\ (K_1 A)^2 + B^2\ ]^{1/2} = C = K_2 D$$

where D is the relative response measured by the standard tungsten lamp and K_1 and K_2 are constants to correct for the arbitrary normalization at 2800 Å. Since A, B and D are known for several wavelengths K_1 and K_2 may be found by simultaneous equations. The relative system response to an isotropic source measured directly with the standard lamp and indirectly with the partially polarized effective line source show maximum discrepancies of the order of 15 percent.

3.2.3 Absolute Fluorescent Efficiency

The relative integrated intensity of each resolvable spectral feature was determined from the relative intensity data by graphical integration with a polar planimeter. Determining the absolute fluorescent efficiency for a single transition defined the absolute fluorescent efficiencies for all spectra from 2,000 to 11,000 Å since the relative integrated intensities were known. An intense section of the fluorescing spectra was observed with a bandpass interference filter mounted on a photomultiplier. The photomultiplier was positioned several meters from the fluorescing gas to approximate conditions of point source illumination. The absolute responsivity of the photomultiplier and filter was measured with a standard tungsten lamp calibrated by the National Bureau of Standards. Knowing the transmission of the filter to the observed spectra, incident electron energy and electron beam current and assuming the radiating gas approximated an

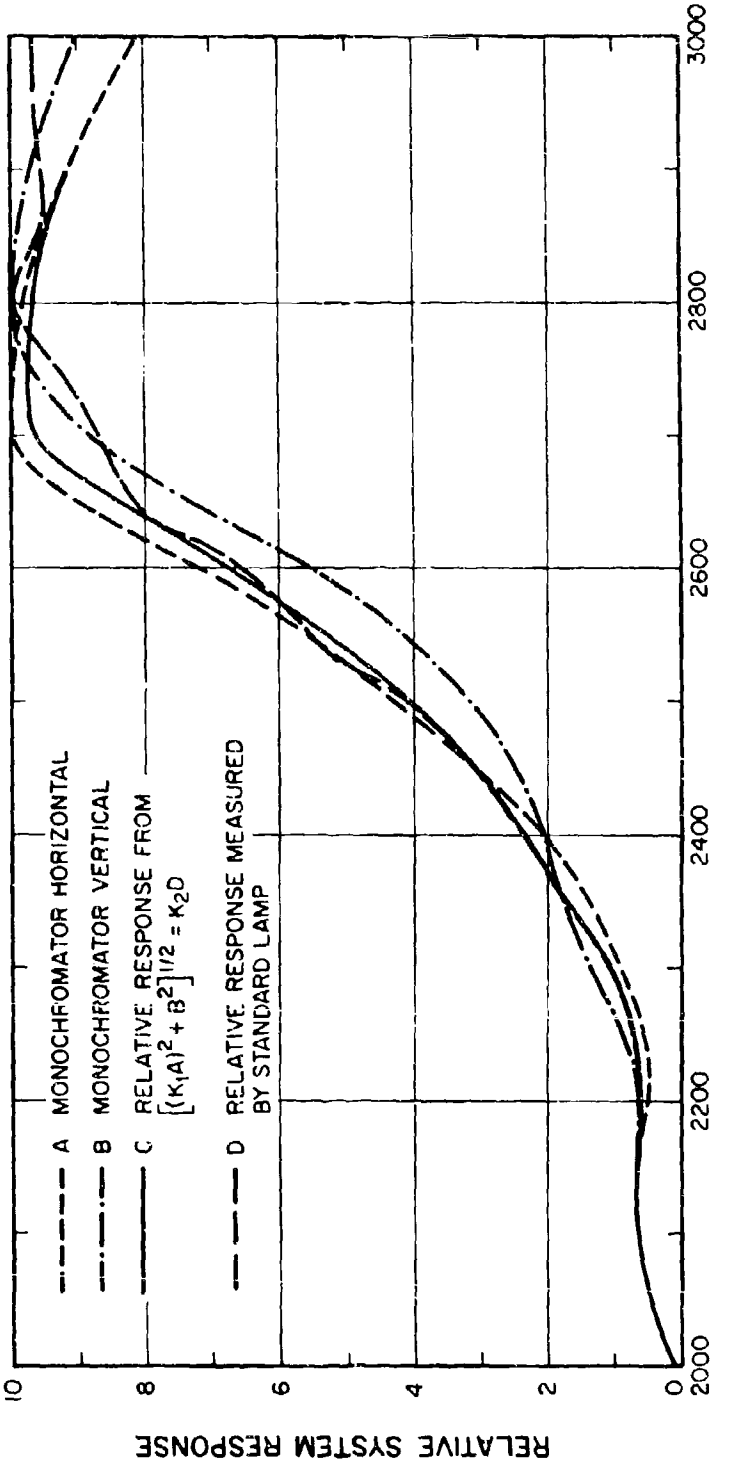

ULTRAVIOLET SYSTEM RESPONSE

Figure 8

isotropic point source, the absolute fluorescent efficiency was calculated.

3.3 Results and Discussion

The spectra observed from 2,000 to 10,600 Å in the four experimental cases considered are presented in Figures 9 through 12. The spectra were observed with an effective spectral slit width of 18 Å with a scan speed of 100 Å/minute. The relative intensity profiles have been normalized to a maximum intensity of 10^4 in each case.

Absolute fluorescent efficiencies are presented in Table 1 for each resolved spectral feature from 3,200 to 10,600 Å. Absolute fluorescent efficiencies are not presented for the 2,000 to 3,200 Å region. The intensity of the NO γ bands, the dominant radiator in this wavelength region, is a complex function of several parameters. Until the relationships of these several parameters are established in a controlled experiment, absolute fluorescent efficiencies are of little value.

3.3.1 NO γ System

The NO γ bands were readily observed in nitrogen (O_2 present as an impurity) and air at both target pressures studied. The manufacturer's analysis of the N_2 supply, Airco prepurified tagged nitrogen, showed an O_2 impurity of 0.9 PPM and a dew point of -70°C. Previously, an independent analysis of a similar cylinder from the same manufacturer showed an O_2 impurity level of less than 4 PPM. In addition, a sample from the target chamber showed no measurable difference from a sample taken directly from the cylinder. Thus the O_2 impurity level of the target gas appears to be limited by the gas supply.

Of the spectra observed, this band system is unique in that the intensity is not directly proportional to the electron beam current. Figures 13 and 14 show that in both air and nitrogen the NO γ intensity, I (NO γ), may be described by the expression

$$I\ (NO\ \gamma) = KJ^{1.5}$$

where K is a constant and J is the electron beam current. Figure 14 indicates

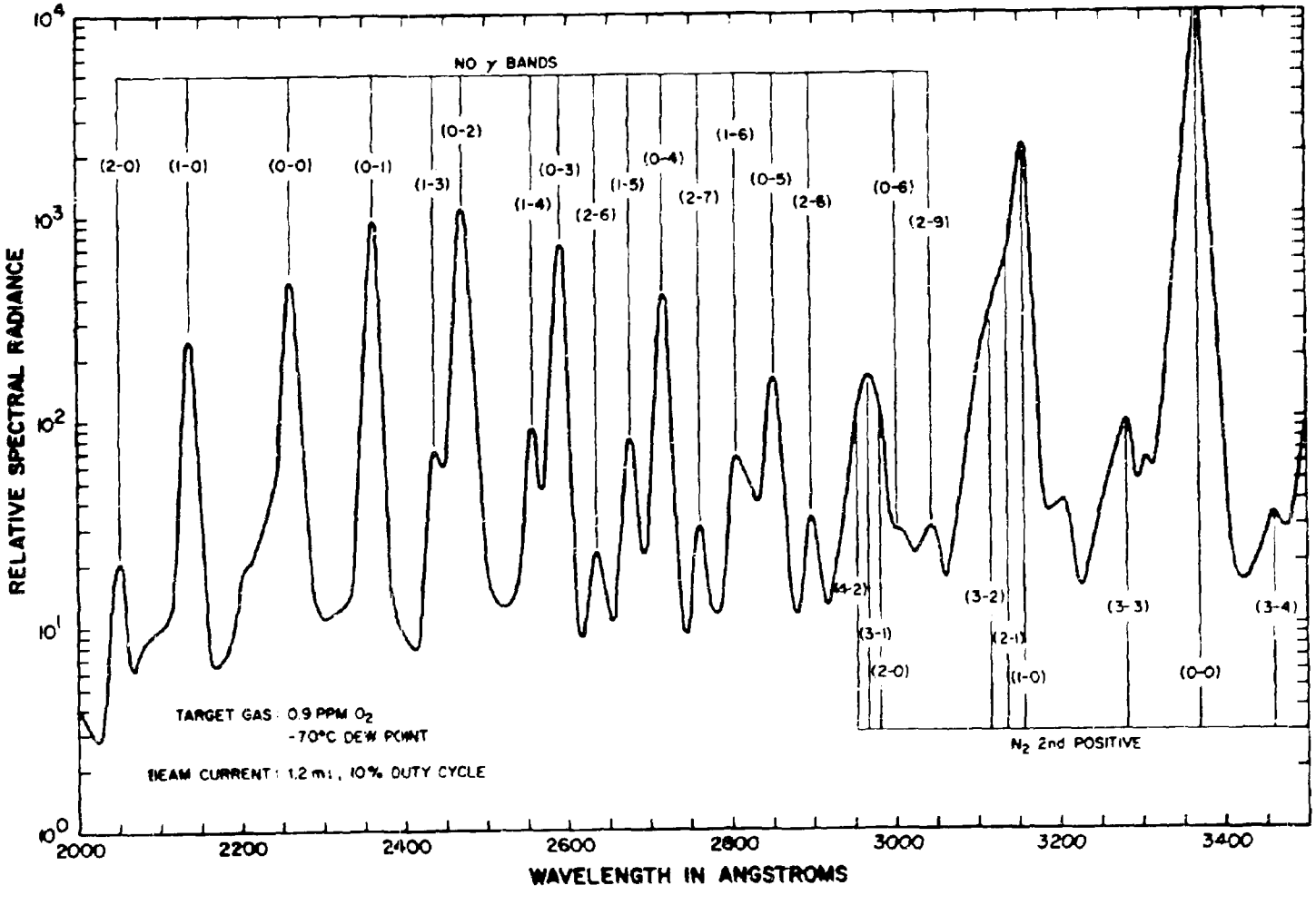

Figure 9a

FLUORESCENCE OF N_2 AT 600 TORR EXCITED BY 50 keV ELECTRONS

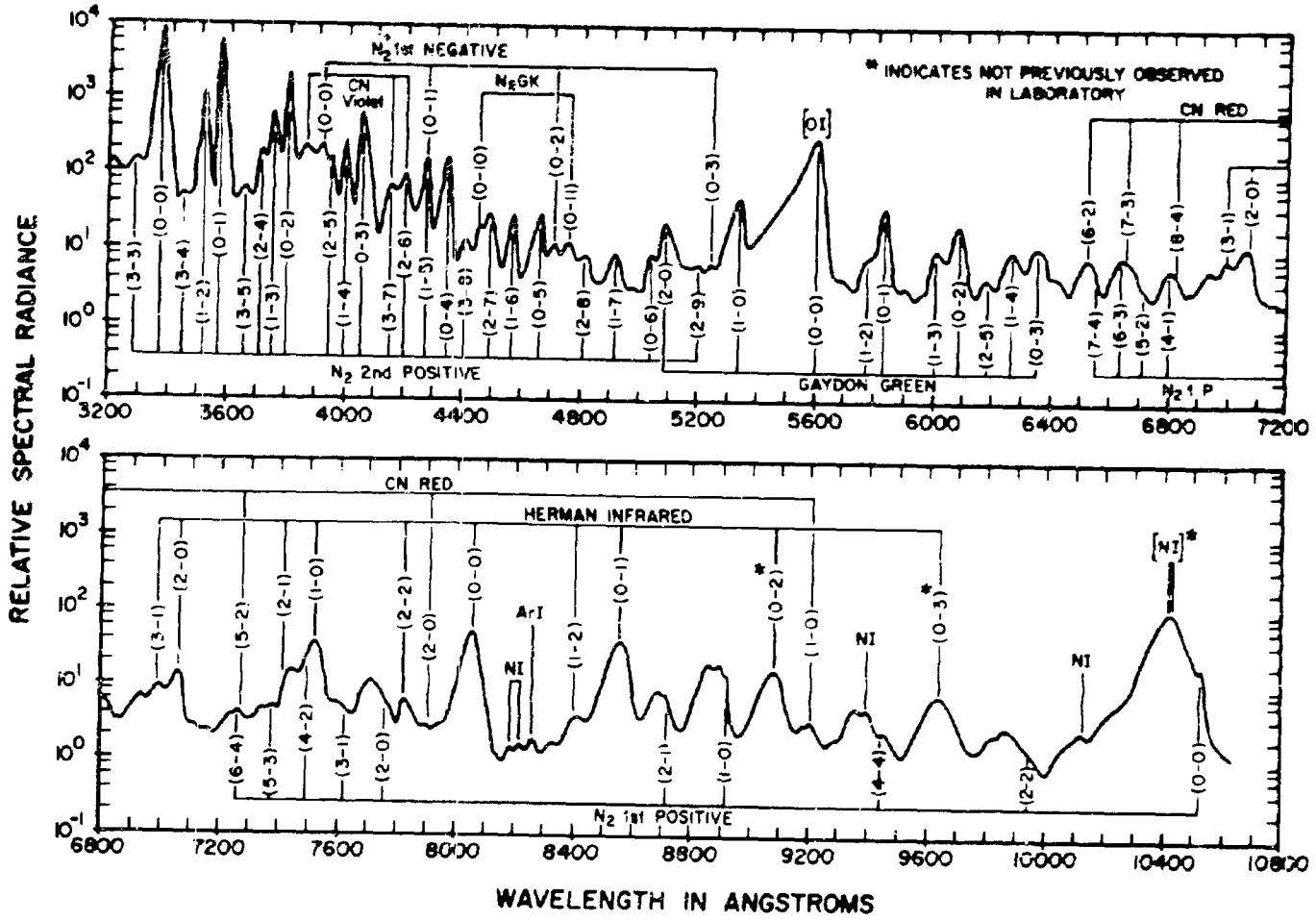

Figure 9b

22

FLUORESCENCE OF N_2 AT 600 TORR EXCITED BY 50 keV ELECTRONS

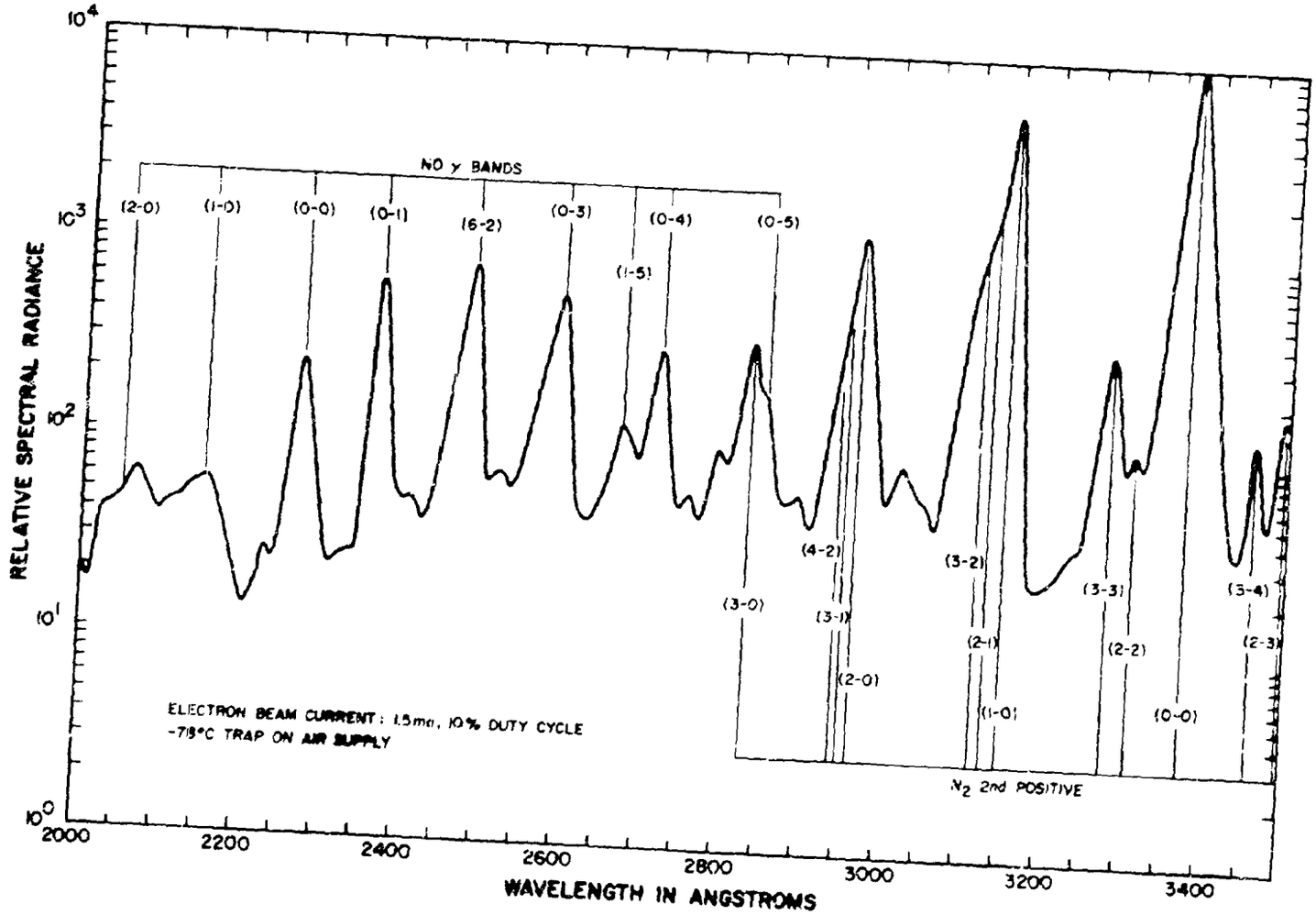

Figure 10a

FLUORESCENCE OF AIR AT 600 TORR EXCITED BY 50 keV ELECTRONS

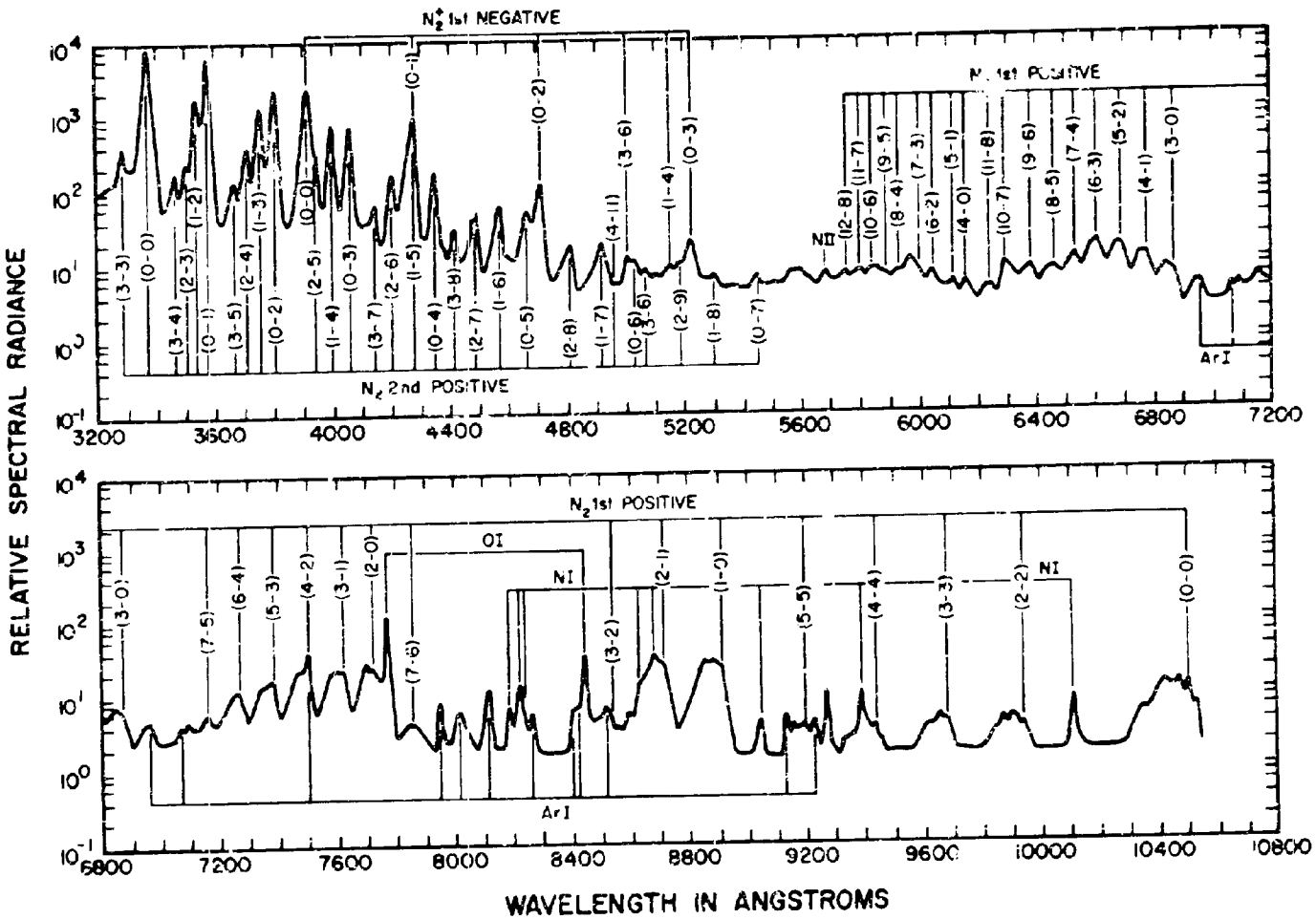

Figure 10b

FLUORESCENCE OF AIR AT 600 TORR EXCITED BY 50 keV ELECTRONS

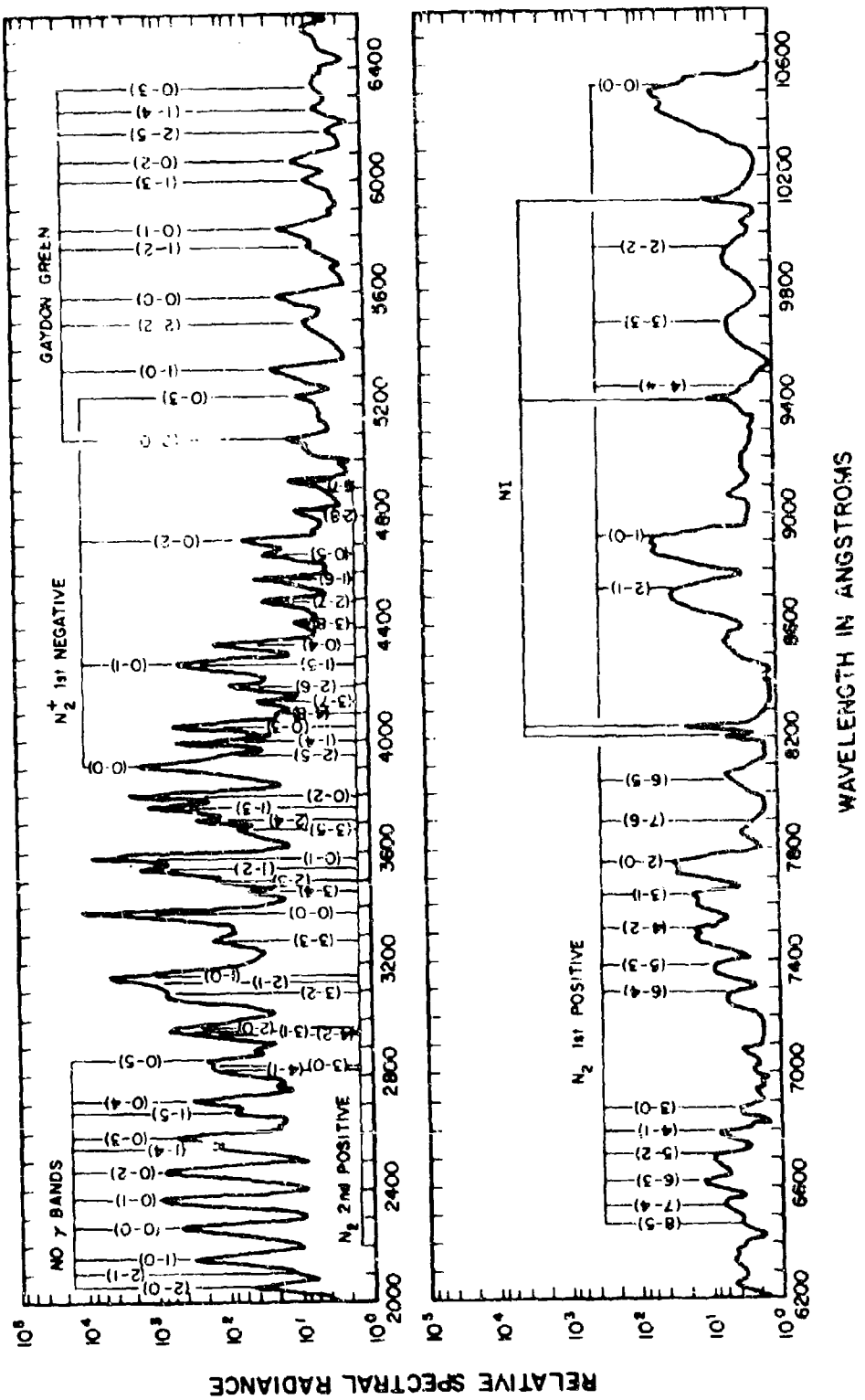

FLUORESCENCE OF N_2 AT 22 TORR EXCITED BY 10 keV ELECTRONS

Figure 11

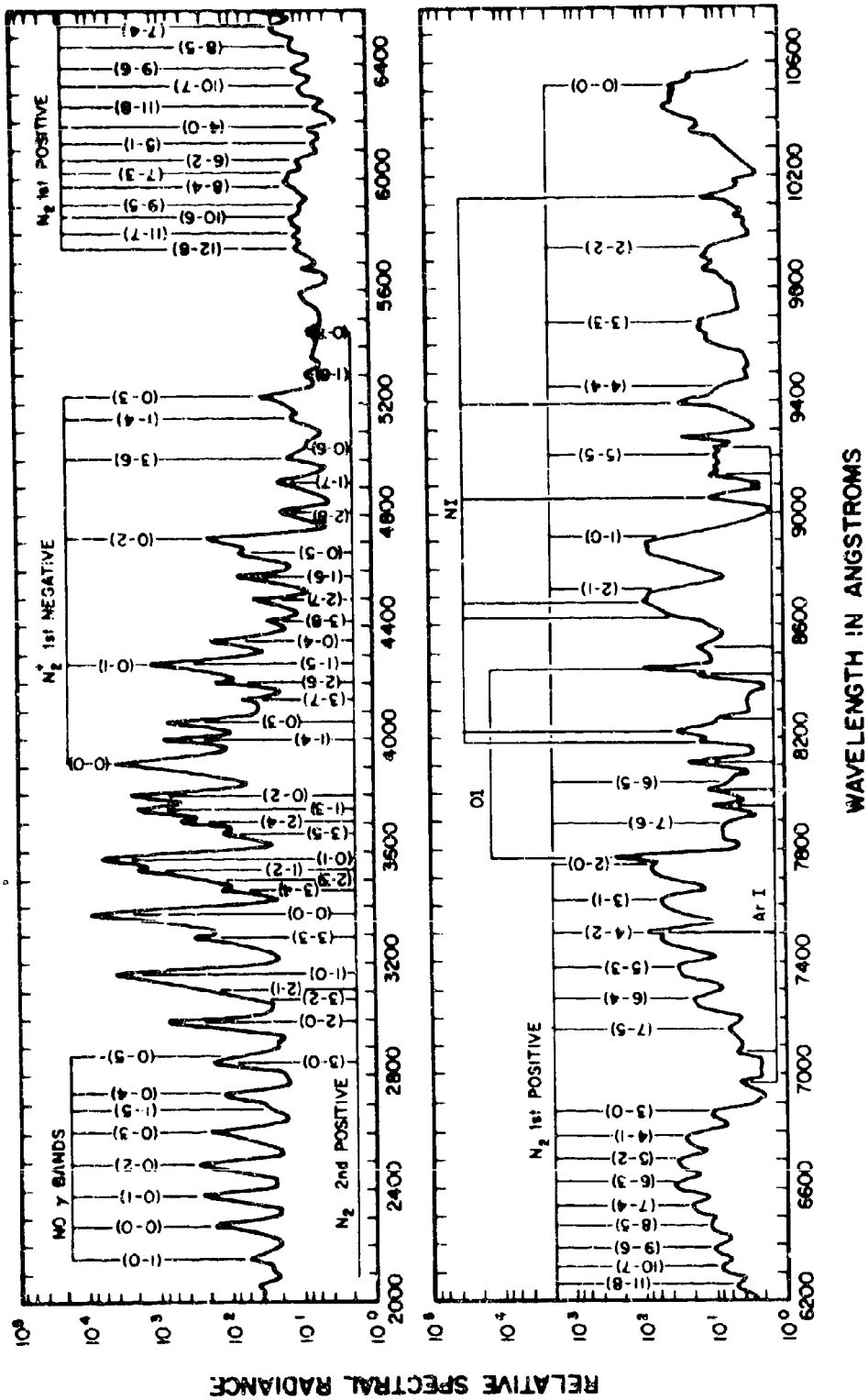
FLUORESCENCE OF AIR AT 22 TORR EXCITED BY 10 keV ELECTRONS
RELATIVE SPECTRAL RADIANCE
WAVELENGTH IN ANGSTROMS
N2+ 1st NEGATIVE
N2 1st POSITIVE
N2 2nd POSITIVE
NO γ BANDS
NI
OI
Ar I

Figure 12

TABLE I

Spectral Fluorescent Efficiencies of Nitrogen and Air

λ (Å)[a]	Molecule or Atom	Band or line (s)[b]	600 Torr Excited by 50 keV Electrons				22 Torr Excited by 10 keV Electrons			
			N_2		Air		N_2		Air	
			x 10^{-7}	Remarks	x 10^{-7}	Remarks	x 10^{-7}	Remarks	x 10^{-7}	Remarks
3285	N_2	2P (3-3)	44	SO	6.4	I			140	SO
3371	N_2	2P (0-0)	4300	I	210	I	14600	I	3600	I
3469	N_2	2P (3-4)	11	PO	2.6	SO			35	PO
3501	N_2	2P (2-3)			2.0	PO				
3537	N_2	2P (1-2)	440	SO	30	SO	2600	PO	730	PO
3577	N_2	2P (0-1)	3000	I	140	I	10400	I	2600	I
3672	N_2	2P (3-5)	17	PO	1.9	SO	140	PO	40	PO
3711	N_2	2P (2-4)	72	SO	7.7	I	480	SO	150	SO
3756	N_2	2P (1-3)	340	I	31	I	2000	I	690	I
3805	N_2	2P (0-2)	1180	I	53	I	3900	I	1000	I
	CN violet Main system	(4-4) (3-3) (2-2) (1-1) (0-0)	200	SO						
3914	N_2^+	1N (0-0)	120	I	70	I	3280	I	1900	I
3943	N_2	2P (2-5)	80	PO	4.8	PO	400	I	130	I
3998	N_2	2P (1-4)	180	I	18	I	1100	I	350	I
4059	N_2	2P (0-3)	360	I	18	I	1180	I	310	I
4142	N_2	2P (3-7)			1.3	SO	76	SO	29	SO

TABLE I

Spectral Fluorescent Efficiencies of Nitrogen and Air

λ (Å)[a]	Molecule or Atom	Band or line (s)[b]	600 Torr Excited by 50 keV Electrons				22 Torr Excited by 10 keV Electrons			
			N_2		Air		N_2		Air	
			x 10^{-7}	Remarks	x 10^{-7}	Remarks	x 10^{-7}	Remarks	x 10^{-7}	Remarks
4142	CN violet	(5-6) (4-5)	38	SO						
4201	CN violet Main system N_2	(3-4) (2-3) 2P (2-6)	90	SO	3.5	I	240	SO	77	SO
4270	N_2	2P (1-5)	(56)[e]	(SO)[e]						
4278	N_2^+	1N (0-1)	98 (40)[e]	I (SO)[e]	28	I	1320	I	700	SO
4344	N_2	2P (0-4)	96	I	4.6	I	310	I	95	I
4417	N_2	2P (3-8)	7	SO	.6	SO	38	SO	11	SO
4432	N_2	GK (0-10)	14	SO						
4490	N_2	2P (2-7)	18	SO	1.1	I	94	I	29	I
4574	N_2	2P (1-6)	19	I	1.6	I	116	I	40	I
4667	N_2	2P (0-5)	19	I	1.0	SO	106	PO	31	PO
4709	N_2^+	1N (0-2)	8	SO	3.5	I	174	SO	104	I
4728	N_2	GK (0-11)	9	SO						
4815	N_2	2P (2-8)	4	SO	.6	SO	32	SO	11	I
4917	N_2	2P (1-7)	4.2	I	.46	I	38	I	11.2	I
5011	N_2^+	1N (3-6)			.28	I	28	PO	7.9	

TABLE I

Spectral Fluorescent Efficiencies of Nitrogen and Air

			600 Torr Excited by 50 keV Electrons				22 Torr Excited by 10 keV Electrons			
			N_2		Air		N_2		Air	
λ (Å)[a]	Molecule or Atom	Band or line (s)[b]	x 10^{-7}	Remarks	x 10^{-7}	Remarks	x 10^{-7}	Remarks	x 10^{-7}	Remarks
5032	N_2	2P (0-6)	5.4	SO						
5066	N_2	2P (3-10)			.08	SO				
5073	N_2	GG (2-0)	18	I			52	SO		
5149	N_2^+	IN (1-4)			.07	PO			3.7	PO
							22	HO		
5179	N_2	2P (2-9)	1.8	PO	.06	PO				
5228	N_2^+	IN (0-3)	2.2	PO	.5	I	28	SO	18	SO
5272	N_2	GG (2-1)	48	I			94	I		
5309	N_2	GG (1-0)								
5309	N_2	2P (1-8)			.062	SO			2.9	PO
5376	unidentified				.026	SO				
5412	N_2	2P (0-7)			.055	I			1.7	PO
5435	N_2	GG (3-3)	430	I			44	SO		
5480	N_2	GG (2-2)								
5574	N_2	GG (0-0)					62	I		

TABLE I

Spectral Fluorescent Efficiencies of Nitrogen and Air

			600 Torr Excited by 50 keV Electrons				22 Torr Excited by 10 keV Electrons			
			N_2		Air		N_2		Air	
λ (Å)[a]	Molecule or Atom	Band or line (s)[b]	x 10^{-7}	Remarks	x 10^{-7}	Remarks	x 10^{-7}	Remarks	x 10^{-7}	Remarks
5577	O I	Auroral								
Continuum										
5591	unidentified several bands present				.19	I				
5681	N II				.06	I	3.4	SO	2.2	PO
5755	N_2	GG (1-2)	7	PO			18	HO		
5755	N_2	IP (12-8)			.07	SO				
5804	N_2	IP (11-7)			.05	SO				
5815	N_2	GG (0-1)	40	I			66	SO		
5854	N_2	IP (10-6)			.12	PO			N_2IP $\Delta v = 4$ progression	
5878	CN	Red (7-2)	3	HO						
5906	N_2	IP (9-5)			.08	PO			81	I
5959	N_2	IP (8-4)			.26					
6014	N_2	IP (7-3)								
5995	N_2	GG (1-3)	11.6	I			40	SO		
6069	N_2	GG (0-2)	11.6	I			44	I		
6070	N_2	IP (6-2)			.15	SO				

TABLE I

Spectral Fluorescent Efficiencies of Nitrogen and Air

λ (Å)[a]	Molecule or Atom	Band or line (s)[b]	600 Torr Excited by 50 keV Electrons				22 Torr Excited by 10 keV Electrons			
			N_2		Air		N_2		Air	
			x 10^{-7}	Remarks	x 10^{-7}	Remarks	x 10^{-7}	Remarks	x 10^{-7}	Remarks
6127	N_2	IP (5-1)			.086	PO				
6161	N_2	GG (2-5)	4.8	PO			130	PO		
6187	N_2	IP (4-0)			.046	PO			5.3	PO
6246	N_2	GG (1-4)	9	SO			22	PO		
6253	N_2	IP (11-8)			.09	PO			4.8	PO
6323	N_2	IP (10-7)			.05	SO			8.4	PO
6336	N_2	GG (0-3)	12.4	I						
6355	CN	Red (5-1)					44	HO		
6395	N_2	IP (9-6)	4.3	HO	.42	SO			10	PO
6469	N_2	IP (8-5)			.46	PO	18	HO	13	HO
6502	CN	Red (6-2)	10.8	I						
6545	N_2	IP (7-4)			.64	SO	44	SO	21	SO
6624	N_2	IP (6-3)			1.0	I	70	SO	37	SO
6656	CN	Red (7-3)	19.8	I						
6705	N_2	IP (5-2)			.88	I	54	SO	35	SO
6789	N_2	IP (4-1)	8.2	I	.66	I	42	SO	26	SO

TABLE I

Spectral Fluorescent Efficiencies of Nitrogen and Air

			600 Torr Excited by 50 keV Electrons				22 Torr Excited by 10 keV Electrons			
			N_2		Air		N_2		Air	
λ (Å)[a]	Molecule or Atom	Band or line (s)[b]	x 10^{-7}	Remarks	x 10^{-7}	Remarks	x 10^{-7}	Remarks	x 10^{-7}	Remarks
6818	CN	Red (8-4)								
6875	N_2	IP (3-0)			.48	SO	20	SO	12	SO
6954	CN	Red (3-0)	8.2	SO						
6948	unidentified				.2	SO			1.8	SO
6965	Ar I									
7001	N_2	HIR (3-1)	9	SO						
7062	N_2	HIR (2-0)	14	I						
7067	Ar I				.046	PO				
7091	unidentified				.073	PO				
7158	unidentified				.075	SO				
7165	N_2	IP (7-5)								
7274	N_2	IP (6-4)	3.6	I	.79	I	36	I	24	I
7282	CN	Red (5-2)								
7387	N_2	IP (5-3)	4.2	SO	1	I	56	I	40	I
7435	N_2	HIR (2-1)	8.2	PO						

TABLE I

Spectral Fluorescent Efficiencies of Nitrogen and Air

			600 Torr Excited by 50 keV Electrons				22 Torr Excited by 10 keV Electrons			
			N_2		Air		N_2		Air	
λ (Å)[a]	Molecule or Atom	Band or line (s)[b]	x 10^{-7}	Remarks	x 10^{-7}	Remarks	x 10^{-7}	Remarks	x 10^{-7}	Remarks
7505	N_2	IP (4-2)					140			
7504	Ar I				2	I			88	I
7521	N_2	HIR (1-0)	40	I						
7627	N_2	IP (2-1)	4.8	PO	1.5	I	128	I	73	I
7754	N_2	IP (2-0)	16.6	I	1.7	I	226	I	73	SO
7774	O I				2.3	I			112	SO
7829	N_2	HIR (2-2)	7.6	I						
7897	N_2	IP (7-6)			.29	SO	22	PO	11.4	SO
7915	CN	Red (2-0)	2.4	HO						
7948	Ar I				.15	I			3.7	I
8010	Ar I	8006 8015			.12	SO			8.1	SO
8047	N_2	IP (6-5)					38	PO		
8058	N_2	HIR (0-0)	55	I						
8110	Ar I	8104 8115			.26	I			9.5	I
		8185	.3	PO	.09		7	PO		

TABLE I

Spectral Fluorescent Efficiencies of Nitrogen and Air

λ (Å)[a]	Molecule or Atom	Band or line (s)[b]	600 Torr Excited by 50 keV Electrons				22 Torr Excited by 10 keV Electrons			
			N_2		Air		N_2		Air	
			x 10^{-7}	Remarks	x 10^{-7}	Remarks	x 10^{-7}	Remarks	x 10^{-7}	Remarks
8186	N I	8188								
8219	N I	8216–8223	.4	PO	.03	SO	11	PO	26	I
8265	Ar I		.5	PO	.06	SO				
8397	N_2	HIR (1-2)	4.2	SO						
8408	Ar I				.12	SO				
8425	Ar I				.6	I			25	I
8446	O I									
8521	Ar I				.24	SO			11	PO
8542	N_2	IP (3-2)					66	PO		
8549	N_2	HIR (0-1)	60	I						
8685	N I	8680–8683			2.4	I	270	I	134	I
8723	N_2	IP (2-1)	15.6	I						
8912	N_2	IP (1-0)	36	I	2.6	I	500	I	143	I

TABLE I

Spectral Fluorescent Efficiencies of Nitrogen and Air

λ (Å)[a]	Molecule or Atom	Band or line (s)[b]	600 Torr Excited by 50 keV Electrons				22 Torr Excited by 10 keV Electrons			
			N_2		Air		N_2		Air	
			x 10^{-7}	Remarks	x 10^{-7}	Remarks	x 10^{-7}	Remarks	x 10^{-7}	Remarks
9050	N I	9046, 9049, 9050			.12	SO			5.9	I
9071	N_2	HIR (0-2)	28	I						
9123	Ar I				.066	PO				
9198	CN	Red (1-0)	3.2	SO						
9202	N_2	IP (5-5)			.18	PO	30	HO	18	I
9225	Ar I				.07	PO				
9266	unidentified				.16	I			10.8	I
9390	N I	9387, 9393	10.8	I	.19	SO	22	PO	9.7	SO
9435	N_2	IP (4-4)			.29	PO	22	HO	13	PO
9436	CN	Red (2-1)								
9629	N_2	HIR (0-3)	16.6	I						
9682	N_2	IP (3-3)			.40	PO	38	HO	24	I
9942	N_2	IP (2-2)	8.0	SO	.27	PO	60	PO	21	SO

TABLE I

Spectral Fluorescent Efficiencies of Nitrogen and Air

λ (Å)[a]	Molecule or Atom	Band or line (Å)[b]	600 Torr Excited by 50 keV Electrons				22 Torr Excited by 10 keV Electrons			
			N_2		Air		N_2		Air	
			x 10^{-7}	Remarks	x 10^{-7}	Remarks	x 10^{-7}	Remarks	x 10^{-7}	Remarks
10 114	N I	10 105 10 109 10 112 10 115	.8	PO	.17	SO	20	PO	9.3	I
10 395	N I		200	I						
10 404	N I									
10 508	N_2	IP (0-0)			1.6	SO	690	I	95	I
Total Fluorescence Efficiency			1.2×10^{-4}		6.8×10^{-5}		4.6×10^{-3}		14×10^{-4}	

[a] The wavelength listed is for the most intense band head of the identified bands and the position of maximum intensity of the unidentified bands. The indentified band-head wavelengths are from L. Wallace, Astrophys. J. Suppl. Ser. 6, 445 (1962); 7, 165 (1962). The wavelengths of the permitted lines of the neutral nitrogen atom are from K. B. S. Eriksson, Arkiv Fysik. 13, 429 (1958). The monochromator wavelengths were calibrated to within $\pm$ 1 Å.

[b] For band identifications the following abbreviations are used: 2P, second positive; 1N, first negative; GK, Goldstein-Kaplan; GG, Gaydon green; 1P, first positive; HIR, Herman infrared. For the line identifications I indicates the neutral atom and II the singly ionized atom.

[c] Fluorescent efficiency of the given spectra exclusive of any adjacent or overlapping spectra indicates the given band or line was not observed.

TABLE I

Spectral Fluorescent Efficiencies of Nitrogen and Air

(d) When more than one identification is given the fluorescent efficiency refers to the identified source as a single spectral feature. The symbols indicate the estimated accuracy of the relative fluorescent efficiencies as follows: I, isolated $\pm$ 10 ; SO, slightly overlapped, $\pm$ 20%; PO, partially overlapped, $\pm$ 35%; HO, heavily overlapped, $\pm$ 100%. The error in the absolute measurement is estimated to be an additional $\pm$ 15%.

(e) The 4270-Å $^2\Sigma_u^+$, 2P (1-5) and 4278-Å $^1\Sigma_2^+$ + IN (0-1) bands appear as a single band using an 18-Å effective spectral slitwidth. A higher-resolution spectrogram was used to isolate the bands.

NO γ (0-3) INTENSITY IN AIR

~10 PPM H_2O, 10% ELECTRON BEAM DUTY CYCLE

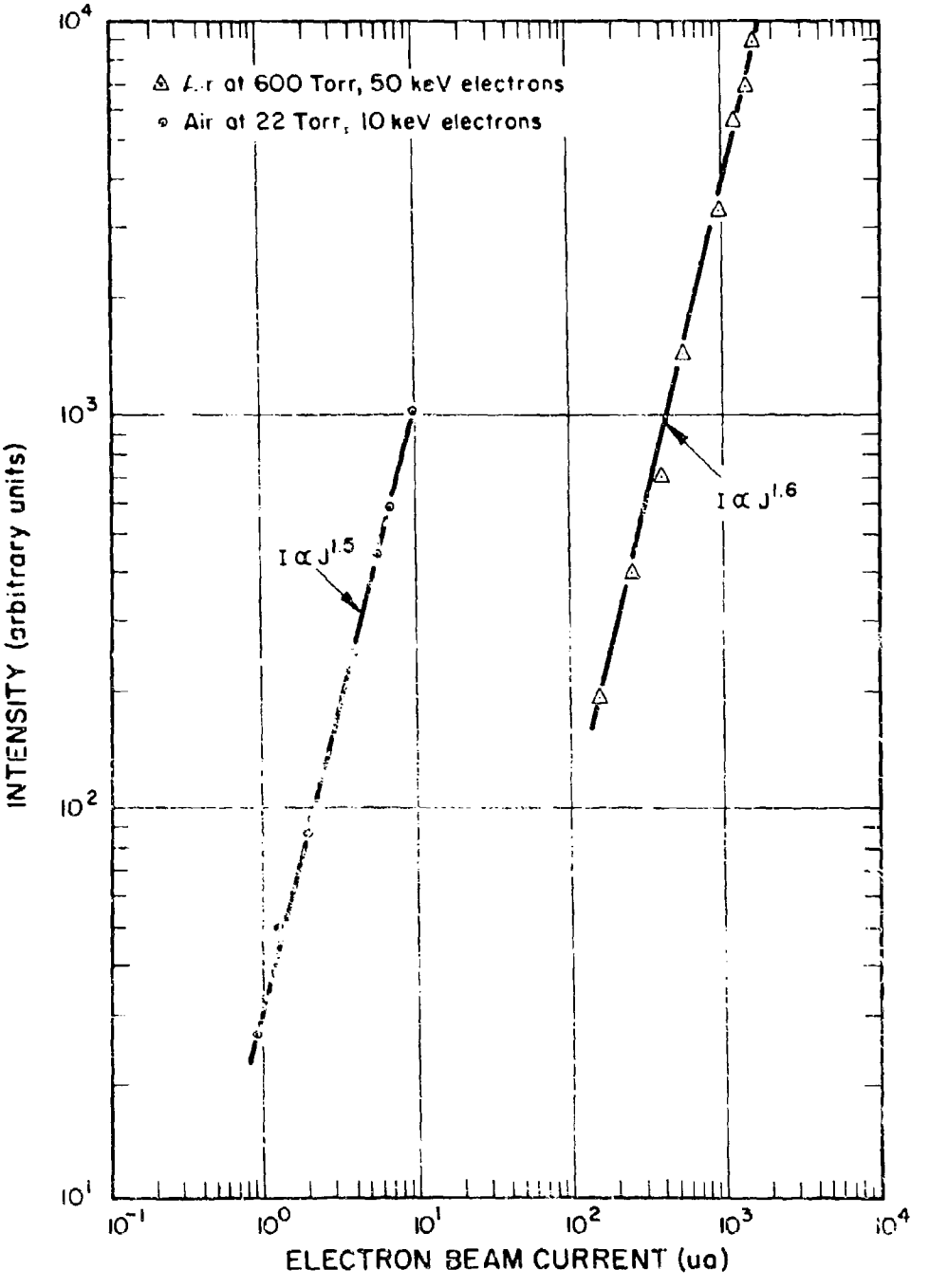

Figure 13

1602

NO γ (0-3) INTENSITY IN N_2

0.9 PPM O_2, 3 PPM H_2O, 10% ELECTRON BEAM DUTY CYCLE

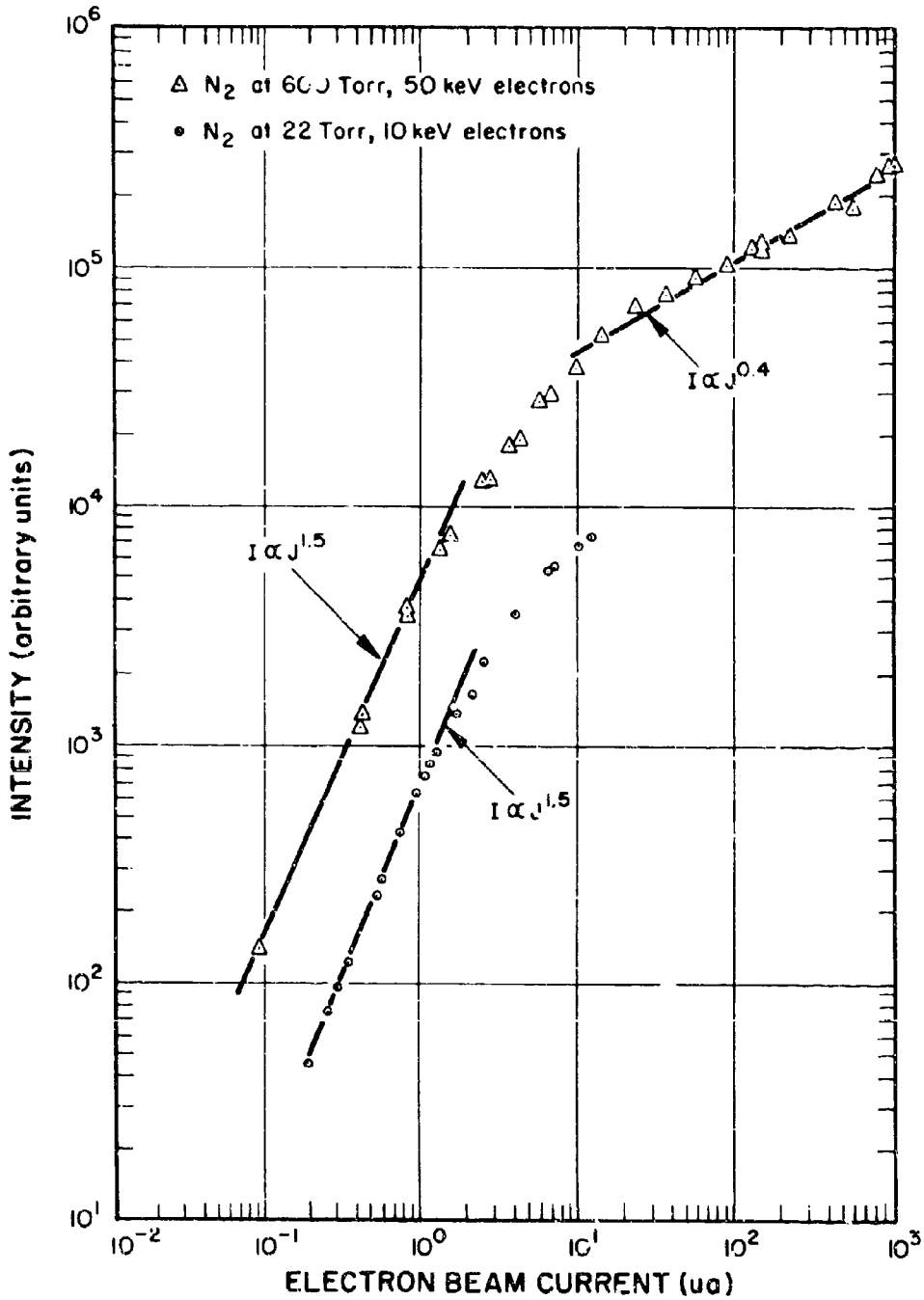

Figure 14

that above several microamps of electron beam current the NO γ intensity in nitrogen increases at a less than linear rate with electron beam current. An order of magnitude calculation suggests this effect is due to the limited O_2 available.

Figure 15 compares the intensity of the NO γ (0-3) band and the N_2 2P (2-0) band in air as a function of the electron beam duty cycle. Measurements indicate the intensity of the second positive bands is directly proportional to the electron beam current. The intensity of the second positive band has been used as a measure of the amplitude of the fundamental harmonic (signal measured by the narrow band phase sensitive amplifier) of the pulsed electron beam. Thus comparing the NO γ band as a function of duty cycle to the N_2 2P band, in effect is a measure of the ratio of the amplitudes of the fundamental frequency of the NO γ emission and the electron beam. The slope of Figure 15 supports the beam current dependence established in Figure 13.

When the emission in air was observed, the addition of a -78°C cold trap on the gas supply increased the intensity of the NO γ emission. The cold trap was located close to the gas supply and after cooling the target gas passed through a 20 foot length of copper tubing to allow the gas to revert to room temperature. This ensured that the effects of the cold trap were due to the removal of a condensable impurity, presumably water vapor, rather than gas kinetics due to a reduced molecular velocity. The addition of a water bubbler to the air supply line reduced the NO γ emission. Thus at pressures of from 22 to 600 Torr, water vapor is an effective quencher of the NO γ bands. In order to control the water vapor present, the air spectra were recorded with a -78°C cold trap on the gas supply. Assuming the target gas approached the temperature of the cold trap, water vapor was present in the target gas with a concentration of 1 - 10 PPM.

In order to compare the intensity of NO γ bands in the four cases, Figures 13 and 14 were used to reduce the intensity to a standard electron beam current arbitrarily established as one microamp. Table II presents the relative intensity of the NO γ (0-n) progression for the four experimental cases.

NO γ VS N_2 2P RELATIVE INTENSITY AS A FUNCTION OF ELECTRON BEAM DUTY CYCLE

AIR AT 600 TORR, 50 keV ELECTRONS

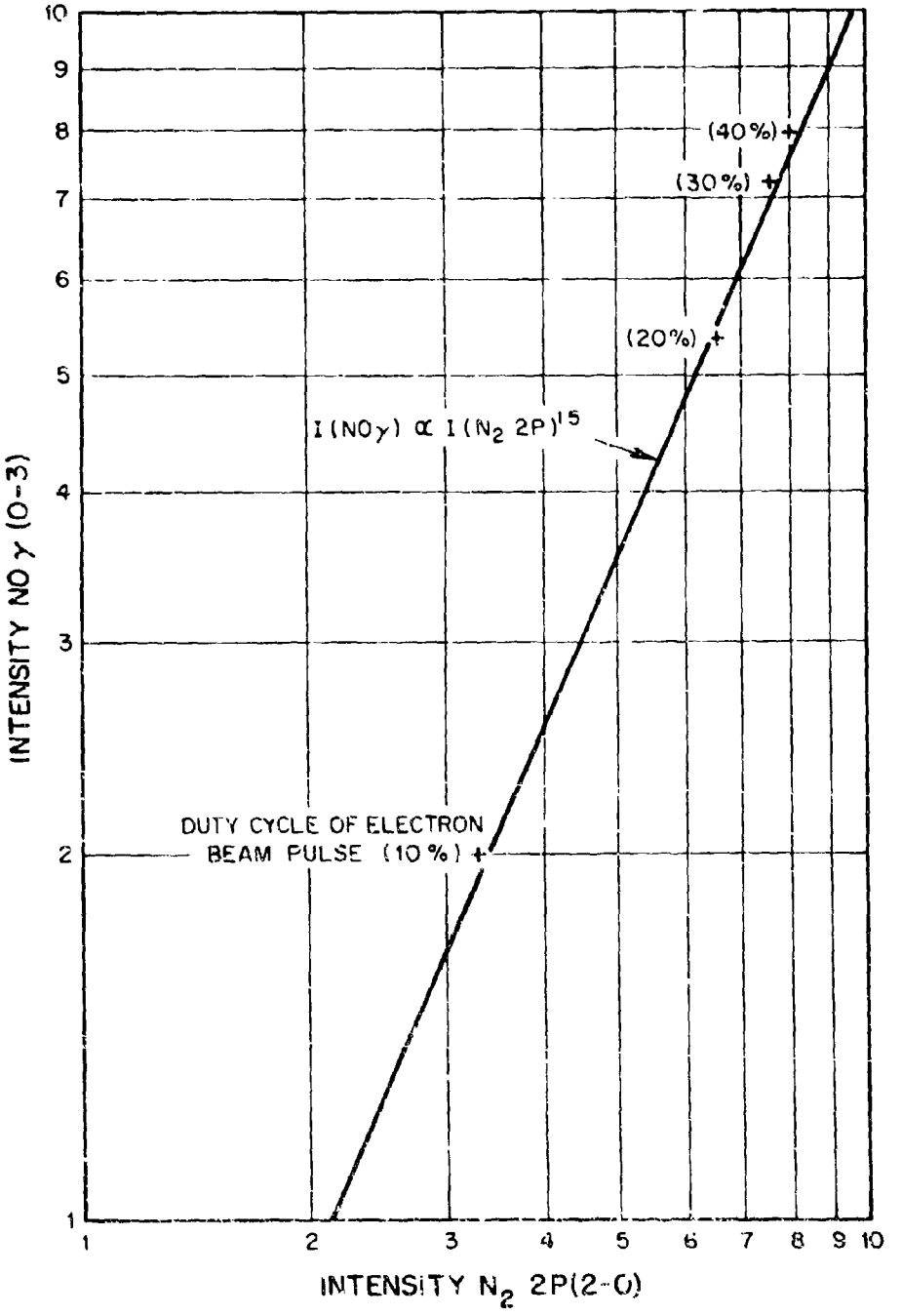

Figure 15

1602

TABLE II

NO γ (0-n) RELATIVE INTENSITIES FOR 1 μa BEAM CURRENT

Target Gas	Electron Energy, Gas Pressure	
	10 kev, 22 Torr	50 kev, 600 Torr
N_2 (0.9 PPM O_2, 3 PPM H_2O)	3×10^4	2×10^5
Air (1-10 PPM H_2O)	4×10^2	1

The intensities of the NO γ bands in air are reduced by the quenching effect of several atmospheric constituents in addition to water vapor. Dondes, Hartech and Kunz[5] have observed NO γ emission excited by alpha particles in nitrogen at atmospheric pressure with varying O_2 concentrations. They conclude NO γ emission is maximized when the O_2 concentration is 500 PPM and above this level O_2 acts as an effective quencher. Young and Sharpless[6] have determined that the atmospheric constituents CO_2 and N_2O quench NO γ emission in accord with the Stern-Volmer mechanism. Stern-Volmer quenching assumes that the excitation process is independent of pressure and collisional deactivation is described by an expression of the form:

$$I = I_o (1 + K \bar{v} \tau \sigma P)^{-1}$$

where I is the intensity of emitted radiation, I_o the intensity at a pressure low enough to exclude quenching, K a proportionally constant, $\bar{v}$ the average velocity of the colliding molecules, τ the lifetime of the excited species, σ the cross section of the quenching molecule and P the partial pressure of the quenching molecule. Comparing the NO γ intensity of Table 2 in air at 22 and 600 Torr indicates the intensity increases by a factor of 4×10^2 in going to the lower pressure. Since the Stern-Volmer two body mechanism implies a maximum increase of 27 (600/22), this expression does not describe the NO γ quenching in air. The increase in intensity of a factor of 400 is in fair agreement with the square of the pressure ratio ($27^2 = 720$). The decrease in intensity from N_2 to air by a factor of 2×10^5 at 600 Torr is also in reasonable agreement with a quadratic pressure effect. This suggests the dominant quenching mechanism in air in this pressure range may be three body collisions.

3.3.2 N_2^+ First Negative System

In addition to the fluorescent efficiencies presented in Table I, values have been determined for many combinations of incident electron energy and nitrogen gas pressure from 10 to 60 kev and 22 to 300 Torr. The data points presented in Figure 16 summarize and indicate the range of many more experimental points. For a given electron energy the fluorescent efficiency was measured with the target gas pressure varied to change the

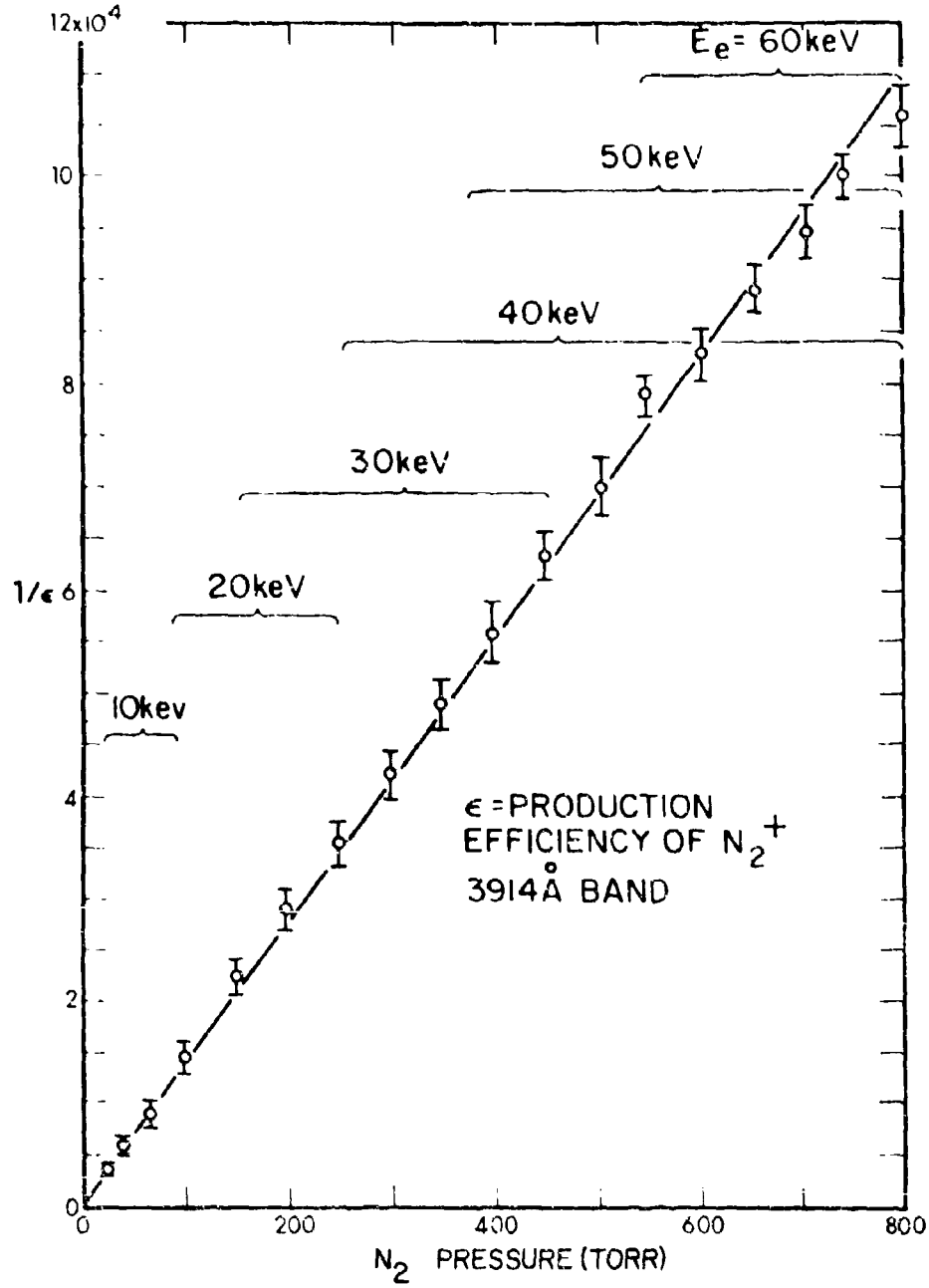

Figure 16 Production Efficiency of N_2^+ (3914 Å) Emission by Electrons

electron range from approximately 3 to 10 cm. The linear relationship of Figure 16 suggests that both the fluorescent efficiency is independent of electron energy and the Stern-Volmer mechanism describes the quenching process of the 3914 Å emission. Figure 14 may be analyzed in terms of the Stern-Volmer expression of the form

$$\frac{1}{\epsilon} = \frac{1}{\epsilon_o} \left(1 + 2.2 \times 10^{21} \sigma \tau P \right)$$

where ϵ is the fluorescent efficiency at any pressure, ϵ_o the fluorescent efficiency at low pressure where quenching is an insignificant depopulating process, σ the deactivation cross section of the neutral nitrogen molecule in cm^2, τ the lifetime of the 3914 Å band in seconds and P the pressure in Torr. As discussed in the thin target results, electron excitation cross section measurements of the 3914 Å band together with other experimental evidence indicate that in nitrogen ϵ_o is $(6.0 \pm 1.0) \times 10^{-3}$ for excitation by electrons with an energy of several hundred ev or more. The lifetime of the 3914 Å band has been measured by Bennett and Dalby[7]; Fink and Welge[8]; Sebacher[9]; Jeunehomme[10]; Fowler and Holzberlein[11] and Hesser and Dressler.[12] The experimental results are summarized in Table III. The value of Bennett and Dalby has been used to calculate collisional deactivation cross sections. With these values for ϵ_o and τ, Figure 16 results in a N_2 collisional deactivation cross section of $5.9 \pm 1.4 \times 10^{-15}$ cm^2.

Measurements similar to those presented in Figure 16 have been made in air. In the pressure range of 20 to 800 Torr the efficiency for production of the 3914 Å band in air is reduced by a constant factor of 1.7 from the value at the corresponding pressure in nitrogen. Quenching of the 3914 Å band is examined in air by an expression of the form

$$\frac{1}{\epsilon \text{ (air)}} = \frac{1}{\epsilon_{o(air)}} \left[1 + 2.2 \cdot 10^{21} \tau \left(\sigma_{N_2} P_{N_2} + \sigma_{O_2} P_{O_2} \right) \right]$$

where it is assumed deactivation in air is caused by collisions with either N_2 or O_2. The value of ϵ_o in air is estimated to be 0.75 the value in N_2. This estimate implies O_2 and N_2 are almost equally efficient in absorbing the kinetic energy of the high energy primary electron as well as the less

TABLE III

N_2^+ FIRST NEGATIVE (0-0) BAND LIFETIME MEASUREMENTS

Experimenter	Lifetime
Bennett & Dalby	$6.58 \pm 0.35 \times 10^{-8}$ seconds
Fink & Welge	$4.5 \pm 0.4 \times 10^{-8}$ seconds
Sebacher	$6.5 \pm 0.2 \times 10^{-8}$ seconds
Jeunehomme	$7.15 \pm 0.4 \times 10^{-8}$ seconds
Fowler & Holzberlein	$8.2 \pm 0.8 \times 10^{-8}$ seconds
Hesser and Dressler	$5.9 \pm 0.6 \times 10^{-8}$ seconds

energetic higher order electrons. This interpretation is supported by the total ionization cross sections for O_2 and N_2 under electron impact. Tate and Smith[13] present total ionization cross sections for O_2 and N_2 that differ by less than 5 percent for electrons with energy of up to 750 ev. The more recent results of Schram et al[14] reporting a 15 percent larger ionization cross section for O_2 than N_2 have been used to estimate ϵ_o in air. With a value of ϵ_o in air of 4.6×10^{-3} and using $(5.9 \pm 1.4) \times 10^{-15}$ cm^2 for the N_2 quenching cross section, the air fluorescent efficiencies result in an O_2 quenching cross section of $1.4 \pm 1.0 \times 10^{-14}$ cm^2.

The quenching cross sections of N_2 and in some cases O_2 for the 3914 Å band have been measured by Brocklehurst and Downing[15], Jeunehomme[10], Hirsh et al[16] and Brocklehurst[17]. The summarized results, presented in Table IV, show reasonable agreement with the exception of Jeunehomme's value. In Jeunehomme's experiment the quenching cross section was measured by observing the decrease of the apparent lifetime of the 3914 Å fluorescence with increasing pressure in a modulated rf discharge. Jeunehomme has suggested that the unusually large collisional deactivation cross section might be due to quenching by species in the discharge other than ground state N_2.[18]

The rotational temperature of the 3914 Å band has been measured in nitrogen and air at target gas pressures ranging from approximately 3×10^{-2} to $6 \times 10^{+2}$ Torr. The data presented in Figure 17 summarize and indicate the range of the experimental results. For a given pressure there was no measurable difference in the rotational temperatures in air and nitrogen. At a target gas pressure of 10 Torr the rotational temperature was measured as a function of the electron beam current and monochromator field of view. With a beam current of several milliamps and the field of view limited to a volume less than 1 cm from the electron beam entrance hole, an effective rotational temperature of approximately $375^{o}K$ was observed. When the field of view was shifted to exclude this region of maximum current density the measured rotational temperature decreased to approximately

TABLE IV

COLLISIONAL DEACTIVATION CROSS SECTIONS FOR THE

N_2^+ FIRST NEGATIVE (0-0) BAND

Experimenter[a]	Quenching Molecule	
	N_2	O_2
	($\times 10^{-15}$ cm^2)	($\times 10^{-15}$ cm^2)
Jeunehomme	34	
Brocklehurst & Downing	5.9 ± 2.2	
Hirsh et. al.	6.9 ± 1.0	12.3 ± 2.1
Brocklehurst	6.0 ± 3.0	5.6 ± 2.8
This experiment	5.9 ± 1.4	14 ± 10

[a]In calculating the collisional deactivation cross section, all experimenters have used a value of $6.58 \pm 0.35 \times 10^{-8}$ seconds for the 3914 Å band lifetime.

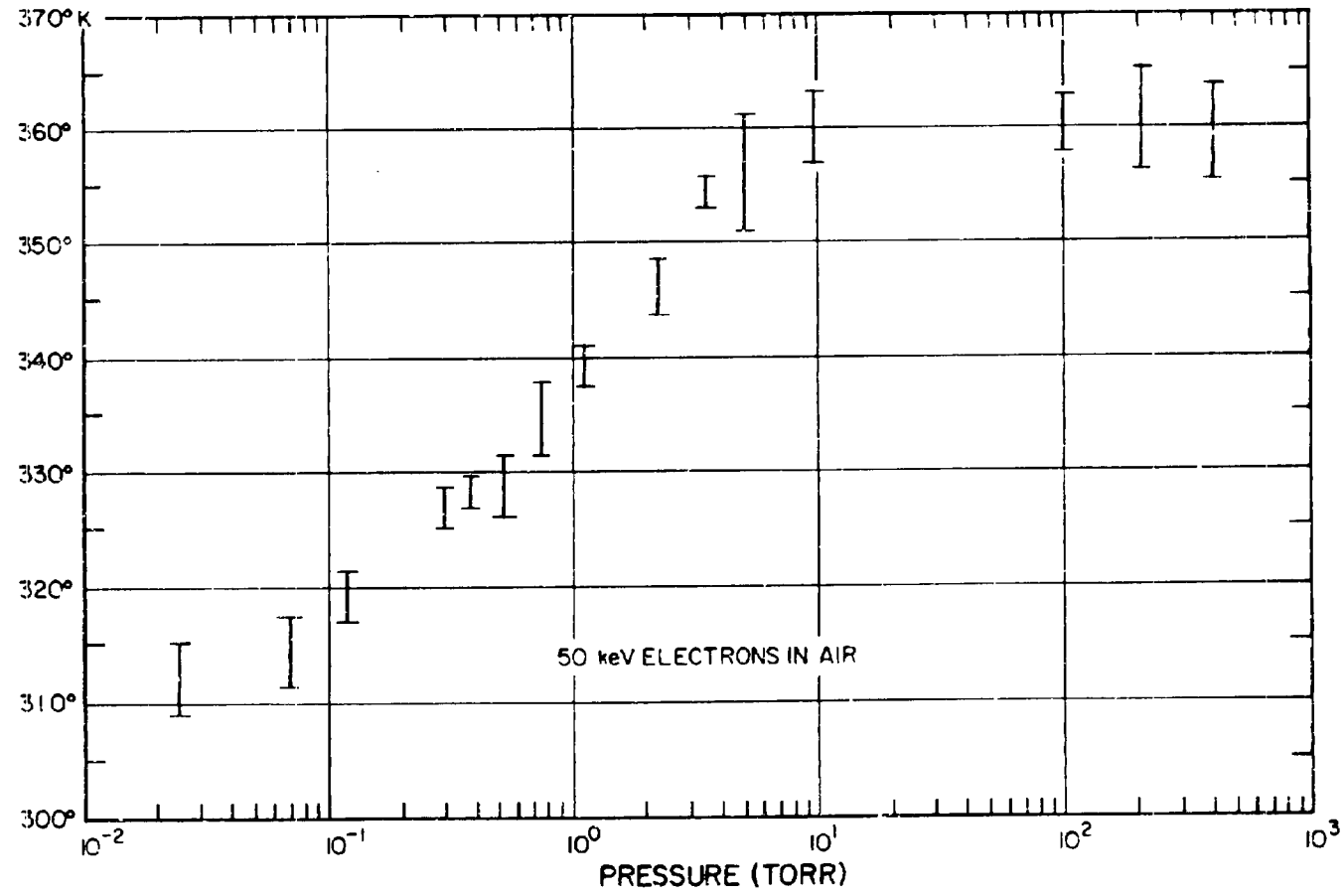

ROTATIONAL TEMPERATURE OF N_2^+ (3914Å)

Figure 17

360°K. Decreasing the beam current by an order of magnitude resulted in a 360°K rotational temperature both in the field of view restricted to the region of the beam entrance aperture and the larger field of view excluding the entrance aperture. Thus, a slight thermal heating effect was detectable at the beam entrance aperture with high (ma) beam currents.

The increase in rotational temperature observed in Figure 17 occurs over a pressure range where the excitation conditions shift from a thin to a thick target. In the low pressure thin target case the excitation is due to high energy (50 kev) electrons contrasting with a much lower average energy of the excitation electrons in the thick target case. The observed pressure dependence of Figure 17 may reflect an energy dependence of the 3914 Å band rotational temperature. Culp and Stair[19] have recently measured the rotational temperature of the 3914 Å band with electron energy from threshold to 300 ev. Their measurements indicate a rotational temperature of 310°K from 300 to approximately 30 ev. Below 30 ev as threshold (18.7 ev) is approached, the rotational temperature increases to a maximum of approximately 350°K. The authors interpret the increase in rotational temperature, as a momentum transfer at excitation energies near threshold. The reported increase is too small in magnitude and occurs over too small an energy range to fully explain the increase in rotational temperature observed in Figure 17.

The rotational temperature dependence fits a collisional model of the form

$$\text{No collision } T_{rot} = 312^{\circ}K$$
$$\text{collision } T_{rot} = 360^{\circ}K$$
$$P = 1 - e^{-2.2 \times 10^{21} \sigma \tau P}$$

where P_c is the probability of collision, σ the cross section of the colliding molecule, P the pressure in Torr, and τ the 3914 Å band lifetime (6.58×10^{-8} seconds). The data of Figure 17 fits this model with a collision cross section of from 3 to 8 x 10^{-15} cm^2. Herzberg[20] discusses the effect on the rotational temperature of the 3914 Å band excited by electrons when the pressure increases such that collisions occur before the excited species decays to

the ground state. For electron excitation Herzberg interprets the rotational temperature as an accurate description of the kinetic temperature providing the appropriate value of the rotational constant is used. At low pressures where collisions of the excited state are unlikely, the distribution of rotational states is described by the rotational constant of the N_2 ground state. At high pressures where collisions are probable the rotational constant of the $N_2^+ B^2 \Sigma_u^+$ state should describe the population of rotational states. Because of the similar magnitude of the rotational constants this explanation accounts for only a 4% (12^oK) increase in rotational temperature from the low pressure to the high pressure case. Since the quenching cross section of N_2 for the 3914 Å band has been measured to be $(5.9 \pm 1.4) \times 10^{-15}$ cm^2 in good agreement with the collisional process described by Figure 17, it appears the higher rotational temperature at higher pressures is due to a preferential quenching of lower rotational states.

In the recent publications of both Fink and Welge[8] and Jeunehomme[10], the authors suggest two excitation processes populate the $N_2^+ B^2 \Sigma_u^+$ level. Fink and Welge observe a decrease in the 3914 Å band lifetime for excitation by electrons of less than 50 ev. The authors interpret this effect as a cascade population of the $N_2^+ B^2 \Sigma_u^+$ state from an undetermined higher energy level. Extrapolating the observed energy dependence of the 3914 Å band to excitation threshold, Fink and Welge conclude the lifetime of the 3914 band is $4.5 \pm 0.4 \times 10^{-8}$ seconds. Bennett and Dalby observed a similar effect in their earlier measurements but assumed the decrease in lifetime at low energies was due to overlapping by the N_2 second positive bands. Fink and Welge had sufficient resolution to eliminate this possibility. Jeunehomme, exciting the 3914 Å band in an rf discharge with an average electron energy of from 20 - 28 ev, supports the lifetime of the 3914 Å band given by Bennett and Dalby (Table III). Jeunehomme also observes a dual lifetime fluorescence decay which is interpreted as a direct and indirect population of the $N_2^+ B^2 \Sigma_u^+$ level. The indirect process which accounts for 10 to 20 percent of the 3914 Å photons, decays with a

3.6 to 4.4 x 10^{-7} second lifetime. However, like the unusually large N_2 deactivation cross section measured by Jeunehomme (Table IV), the observed indirect populating mechanism may be unique to the rf discharge source rather than a general electron impact mechanism. Sebacher[9] has observed that metastable helium states can excite the 3914 Å band and cause a dual fluorescence decay in N_2 -He gas mixtures.

A dual excitation process could explain the rotational temperature effect of Figure 17. For example, at higher pressures the population of rotational states from the cascade mechanism might be collisionally redistributed. The higher rotational temperature of Figure 17 could thus reflect a larger rotational constant of the level from which cascading originates. Although the recent results of Fink and Welge and of Jeunehomme indicate an indirect exciting mechanism for the 3914 Å band, these results also propose values for other parameters (the radiative lifetime and the N_2 quenching cross section) that are not consistent with other experimental results. Until these discrepancies are resolved, the indirect populating process of the 3914 Å band is not assured as a general electron impact mechanism.

3.3.3 N_2 Second Positive System

As shown in Figures 9 through 12, the N_2 second positive bands are the most intense radiators for the thick target cases considered. A previous study[1] presented the relative integrated intensities of the emission from 3,200 to 10,800 Å in air and nitrogen at 600, 200 and 5 Torr excited by 50 kev electrons. However, in the 200 and 5 Torr cases only a fraction of the total range of the 50 kev electrons was observed. As discussed in the N_2^+ first negative section, the absolute fluorescent efficiency for the 3914 Å band excited by energetic electrons incident on air and nitrogen is independent of electron energy and a function of only the number density of the target gas molecules. The relative integrated intensities of the second positive bands of the earlier results were converted into absolute fluorescent efficiencies by a conversion factor based on the known absolute fluorescent

efficiency of the 3914 Å band at the given target pressure. In the cases where only a fraction of the total range was observed, this technique assumes the relative intensities of the 3914 Å band and the second positive bands are typical of the ratio of the intensities integrated over the total range. With this assumption, the fluorescent efficiencies are known for the second positive bands excited by 50 kev electrons incident on N_2 at 600, 200 and 5 Torr as well as for excitation by 10 kev electrons incident on N_2 at 22 Torr. Figure 18 presents the four values for the (0-0) and (0-1) transitions in the form of a Stern-Volmer plot. The data at 600 and 22 Torr are directly measured fluorescent efficiencies (Table I). The values at 5 and 200 Torr are based on the intensity relative to the 3914 Å band in a spectrogram where a fraction of the total electron range is observed. The linear relationship of Figure 18 indicates that both the inherent assumption is accurate within experimental error and Stern-Volmer quenching describes the pressure dependence.

The evidence that the fluorescence of the first negative and second positive system have a similar spatial distribution over the range of an energetic electron is not surprising. Since the excitation of the N_2 second positive system from the ground state involves a forbidden signlet-triplet transition, direct excitation is accomplished by electron exchange. This mechanism is reflected in the electron excitation function by a strong velocity dependence. The absolute electron excitation cross sections presented by Stewart and Gabathuler[21] and more recently by Jobe, Sharpton and St. John[22] show a sharp maximum at 15 ev and a rapid decrease at higher electron energies. The low energy electrons that are most efficient at exciting the N_2 second positive bands are produced by ionization of the target gas. Valentine and Curran[23] in a review article present experimental evidence that indicates electrons with energy greater than 100 ev lose an average of 35 ev per ion pair produced in both N_2 and air. As discussed in the thin target results, electron excitation cross section measurements show that for electrons with energy greater than approximately 100 ev the ratio

FLUORESCENT EFFICIENCY OF N_2 2P BANDS BY ELECTRON BOMBARDMENT OF N_2

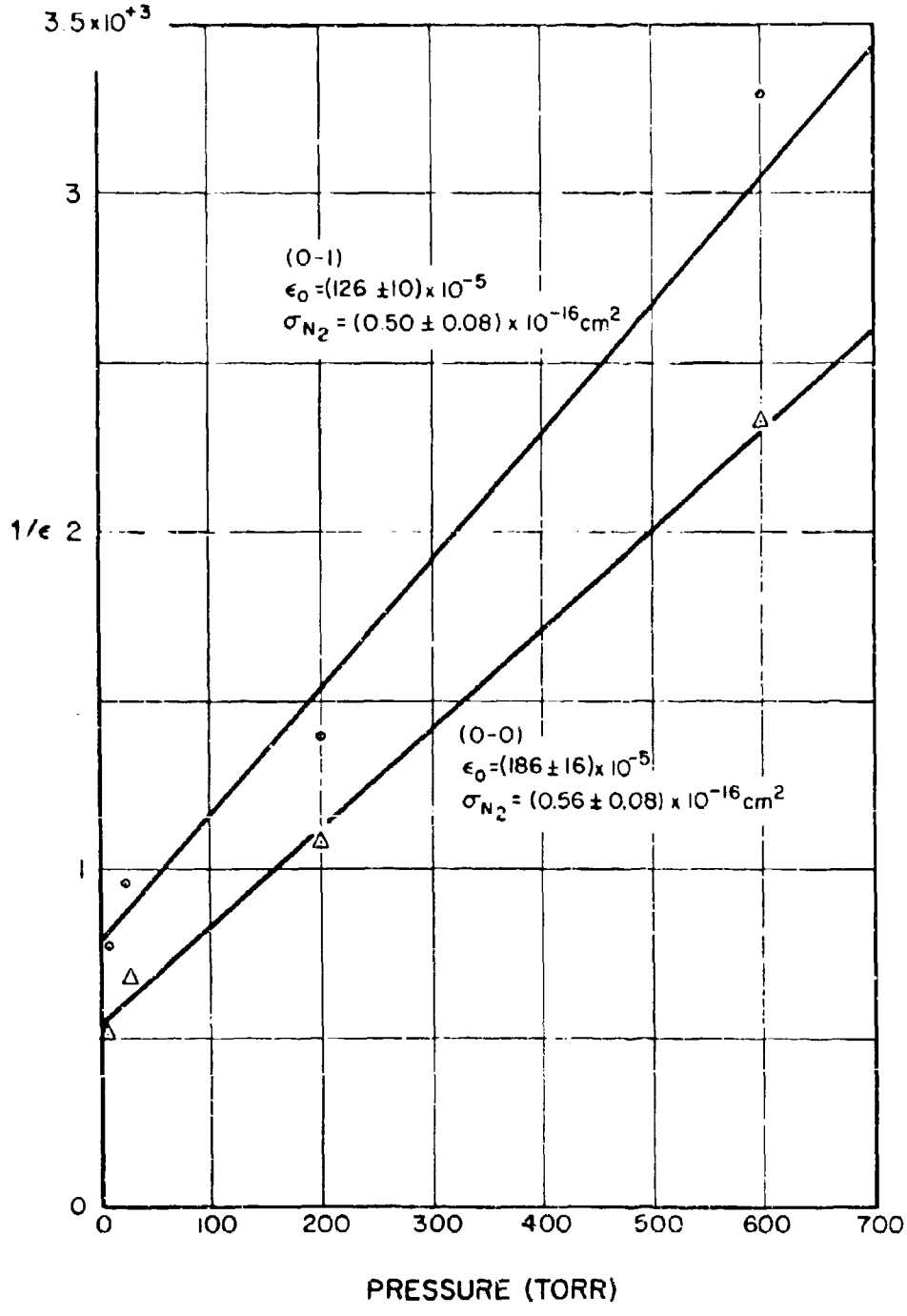

1802

Figure 18

of the total ionization cross section of N_2 to the excitation cross section of the 3914 Å band is constant. Since both the low energy secondary electrons and the 3914 Å band are produced at a rate that is directly proportional to the rate of ionization, the second positive and the 3914 Å emission are proportional. At the gas pressures used in the thick target studies (5 Torr or greater) the range of the secondary electrons is very small. Thus the relative intensities of the 3914 Å and second positive emission should be spatially congruent over the energetic electron's range.

The lifetime of the second positive bands has been measured by Bennett and Dalby[7], Fink and Welge[8], and Jeunehomme.[10] The lifetime measurements indicate that a multiple excitation process exists, presumably a direct and an indirect cascade process. In calculating a value for ϵ_o and σ (see first negative discussion) from the Stern-Volmer plots, Bennett and Dalby's value for the radiative lifetime for the lowest vibrational level was used for all transitions.

The values for ϵ_o and σ with their probable errors as determined by a weighted least square analysis are presented in Figure 18 for the (0-0) and (0-1) second positive bands. Figures 19 through 38 present analogous data for other transitions in N_2 and air. Table V summarizes the collisional deactivation cross sections of N_2 and air for the transitions considered. A weighted average of the quenching cross sections for each upper vibrational level is also given in Table V where the weight of a given transition is proportional to the inverse square of its probable error. Using the average values of the N_2 and air quenching cross sections, an O_2 quenching cross section calculated from

$$\sigma_{air} = 0.79\,\sigma_{N_2} + 0.21\,\sigma_{O_2}$$

is given in Table VI. Table VI compares the quenching cross sections of N_2 and O_2 measured in this experiment with the values presented by Brocklehurst and Downing[15], Hirsh et al[16], and Brocklehurst.[17] The values of ϵ_o, the fluorescent efficiency at pressures low enough to exclude quenching,

FLUORESCENT EFFICIENCY OF N_2 2P BANDS BY ELECTRON BOMBARDMENT OF N_2

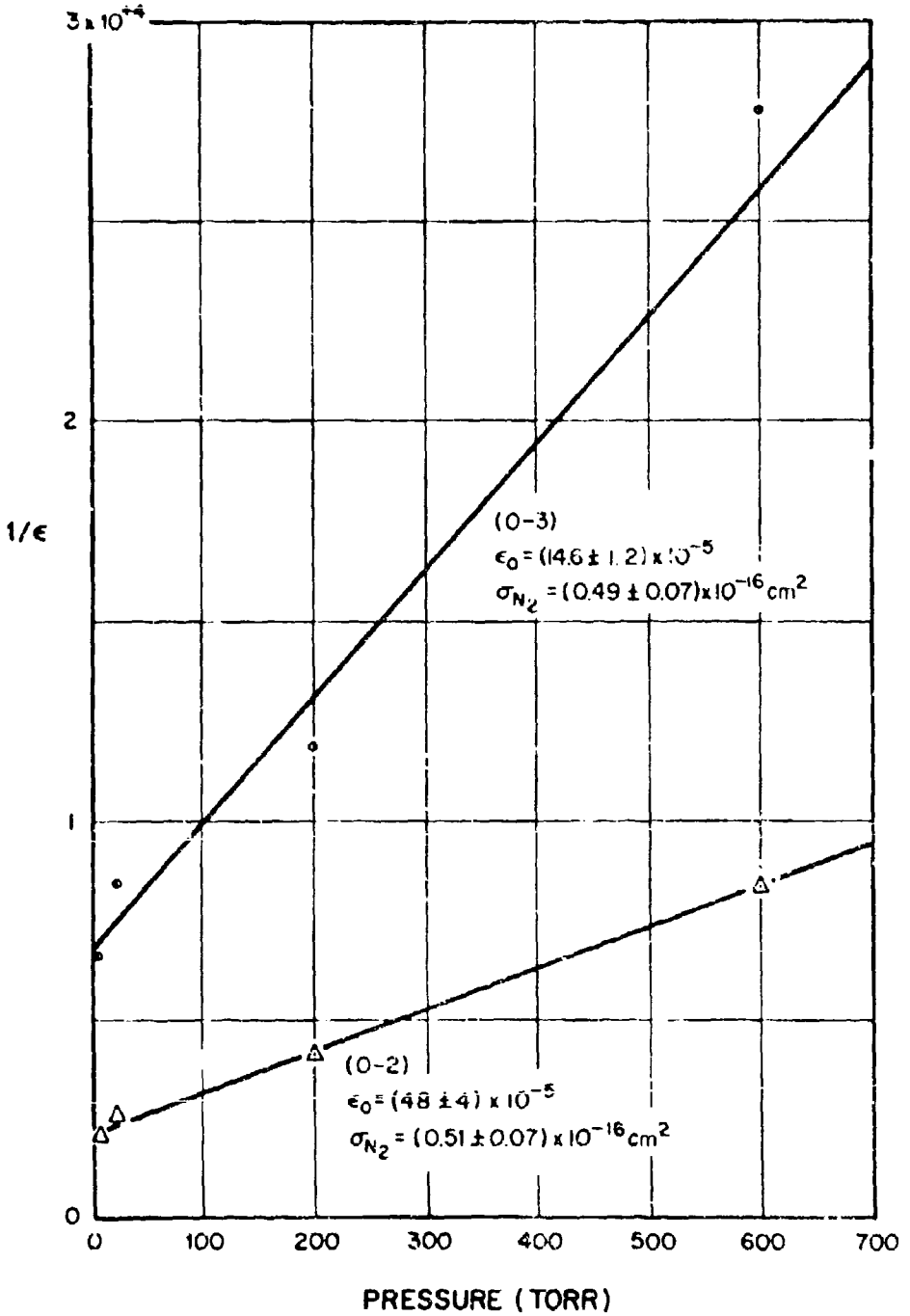

Figure 19

1602

FLUORESCENT EFFICIENCY OF N_2 2P BANDS BY ELECTRON BOMBARDMENT OF N_2

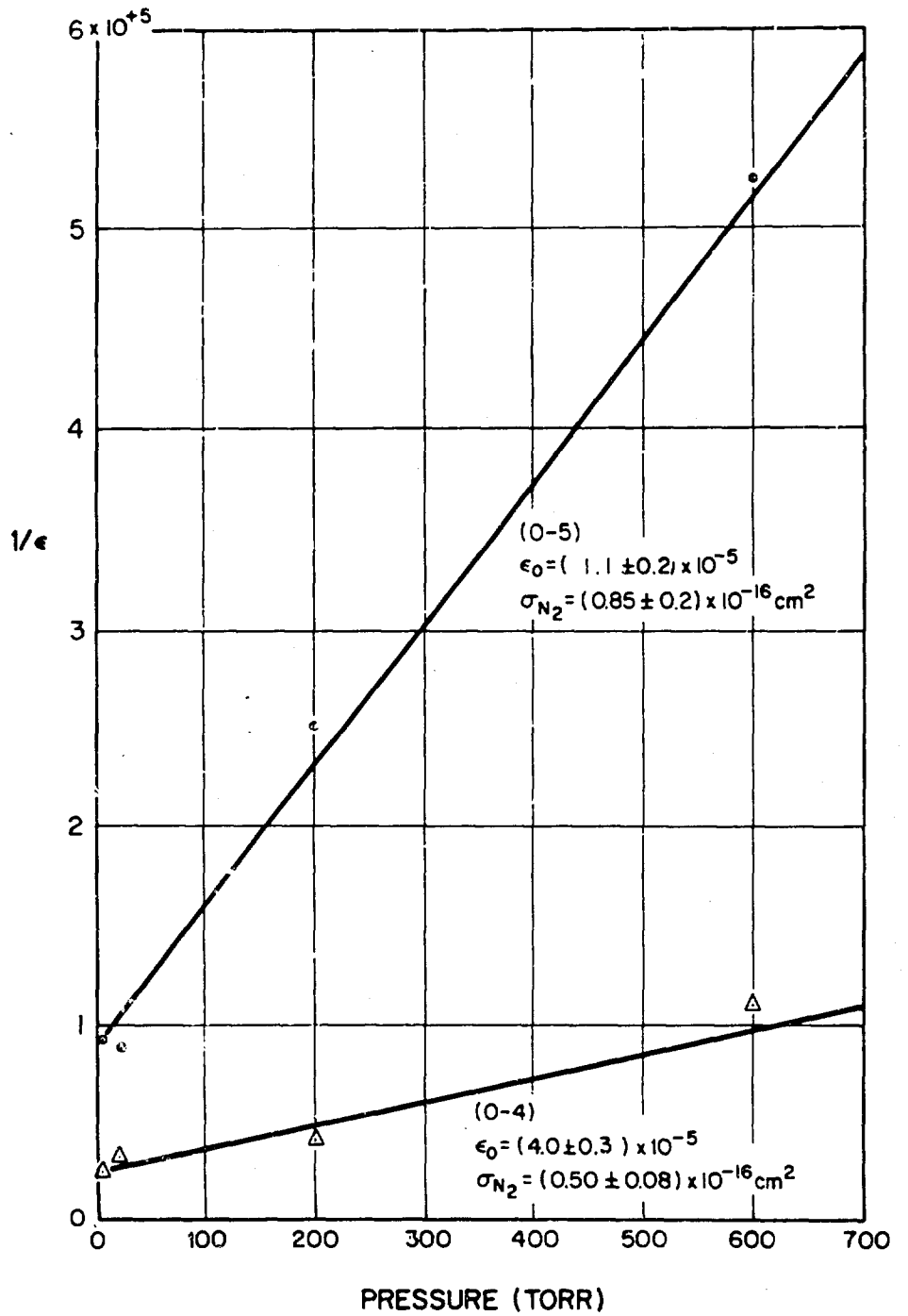

Figure 20

FLUORESCENT EFFICIENCY OF N_2 2P BANDS BY ELECTRON BOMBARDMENT OF N_2

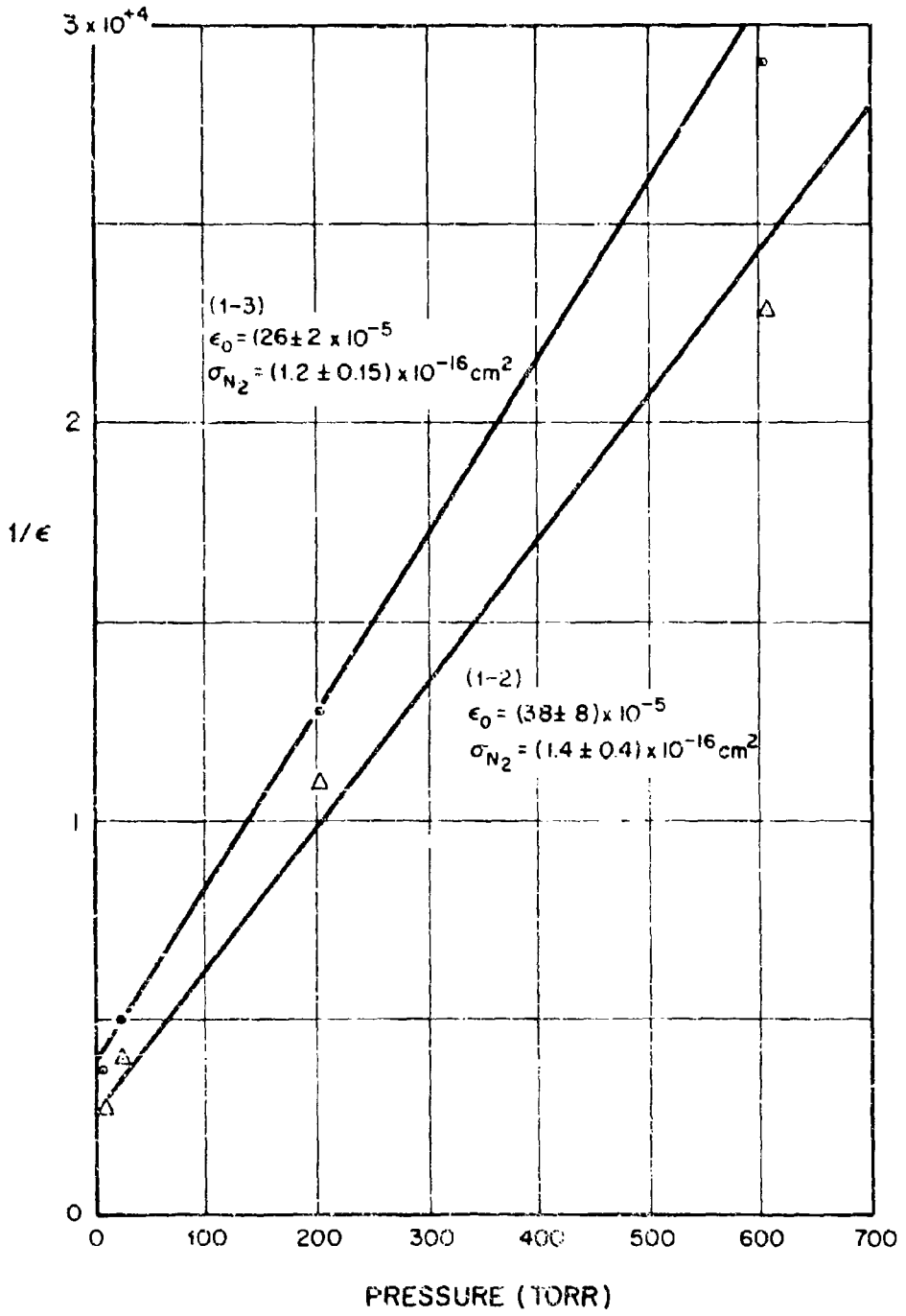

Figure 21

1602

FLUORESCENT EFFICIENCY OF N_2 2P BANDS BY ELECTRON BOMBARDMENT OF N_2

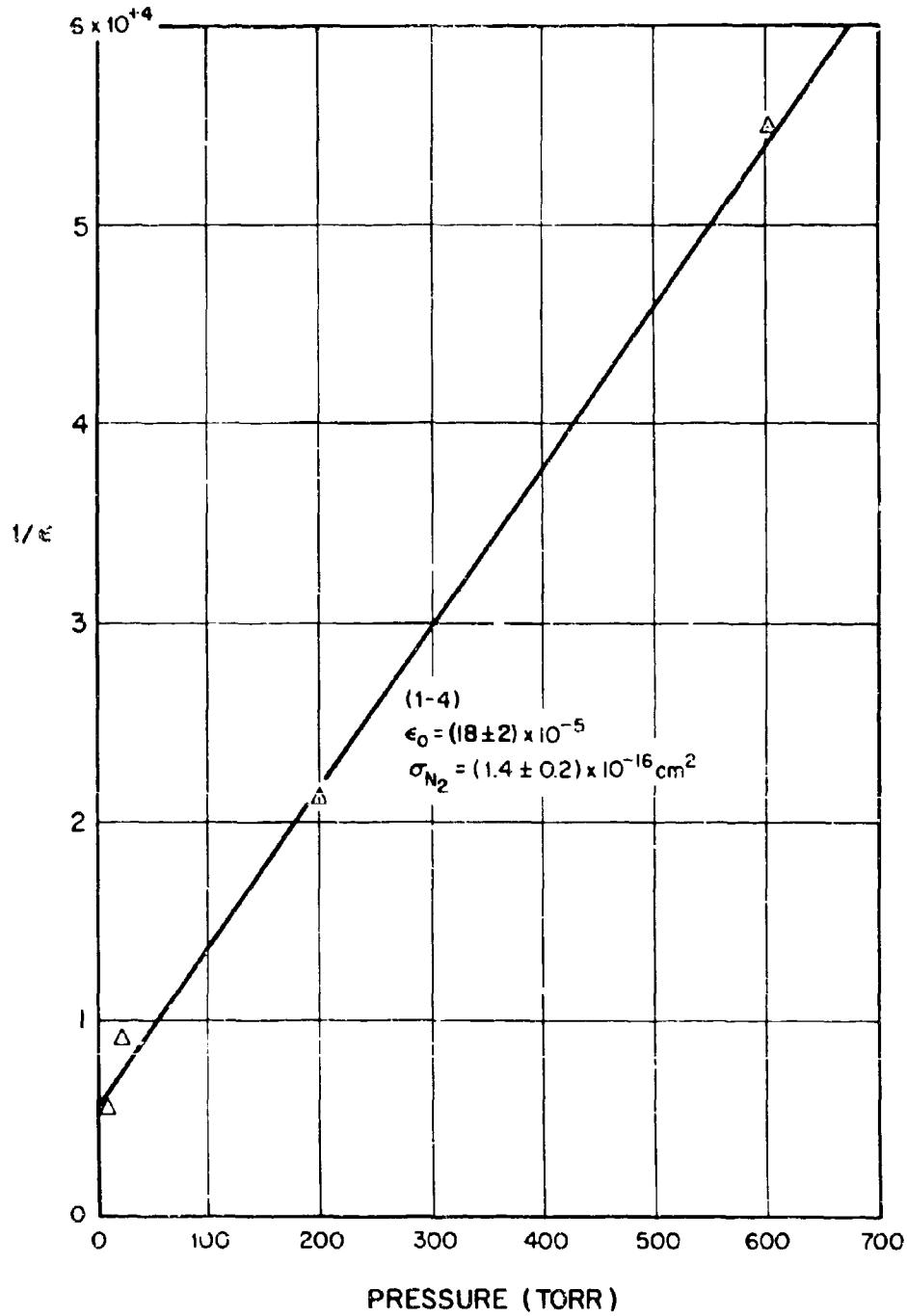

Figure 22

FLUORESCENT EFFICIENCY OF N_2 2P BANDS BY ELECTRON BOMBARDMENT OF N_2

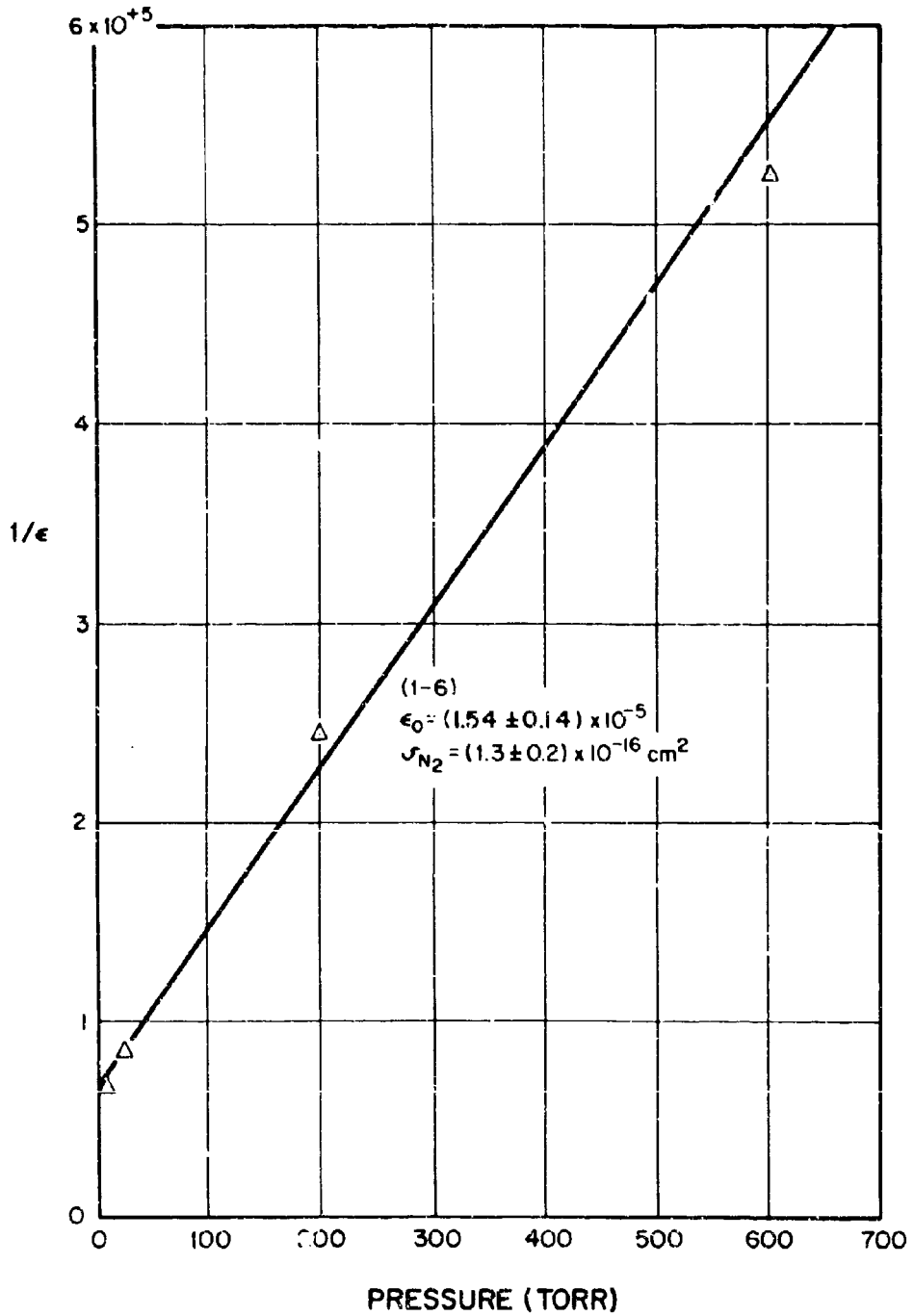

Figure 23

1602

FLUORESCENT EFFICIENCY OF N_2 2P BANDS BY ELECTRON BOMBARDMENT OF N_2

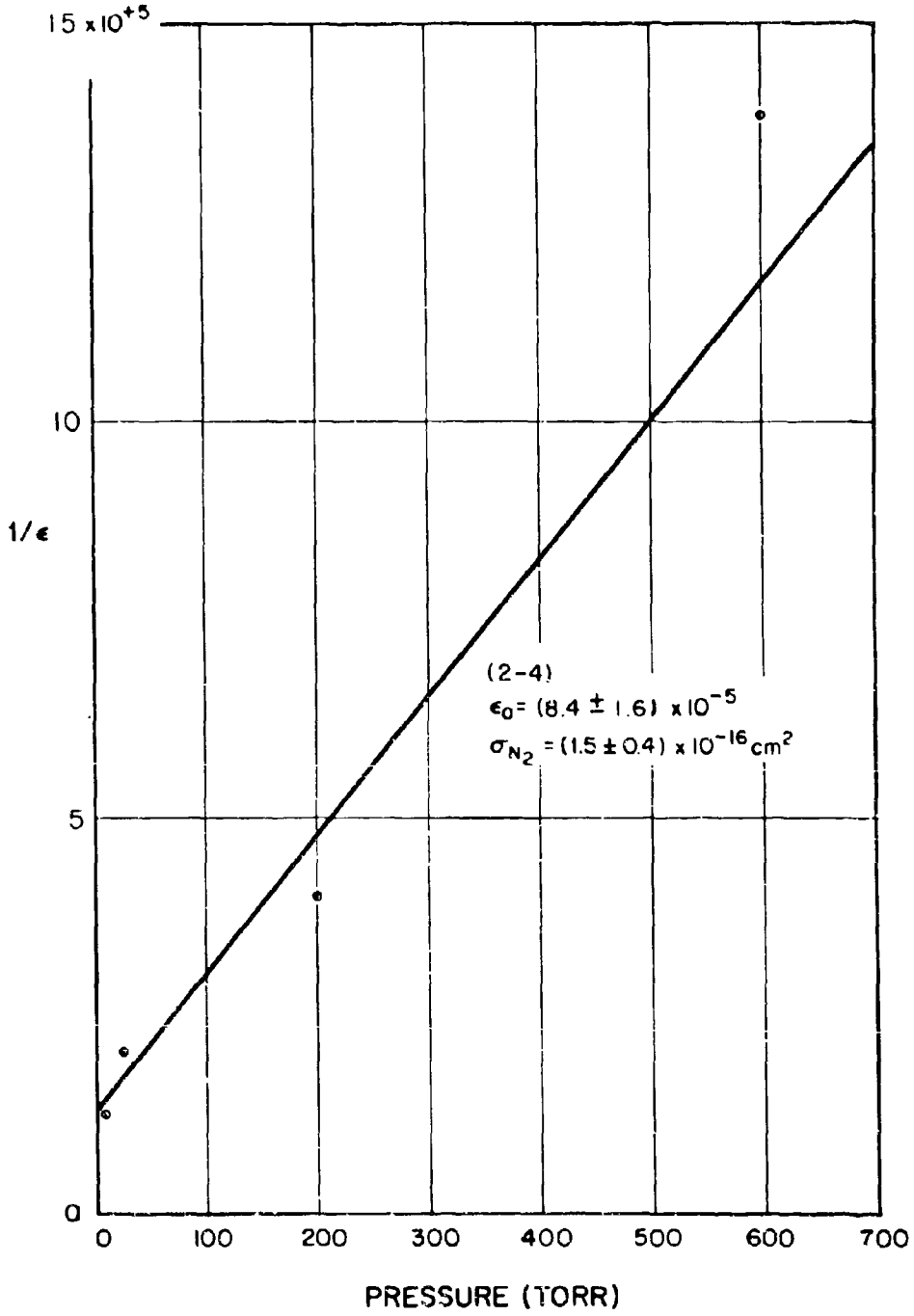

Figure 24

FLUORESCENT EFFICIENCY OF N_2 2P BANDS BY ELECTRON BOMBARDMENT OF N_2

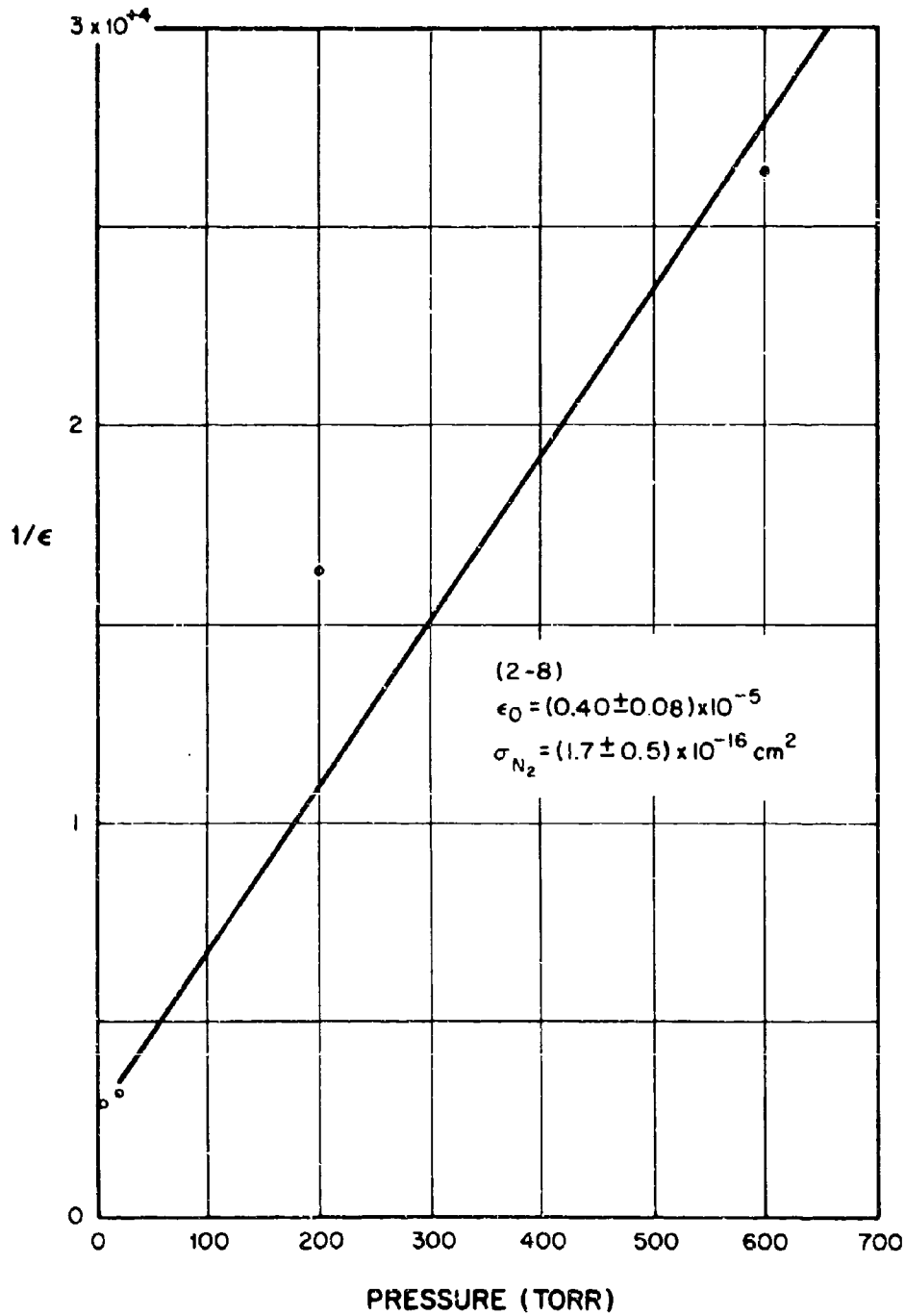

Figure 25

FLUORESCENT EFFICIENCY OF N_2 2P BANDS BY ELECTRON BOMBARDMENT OF N_2

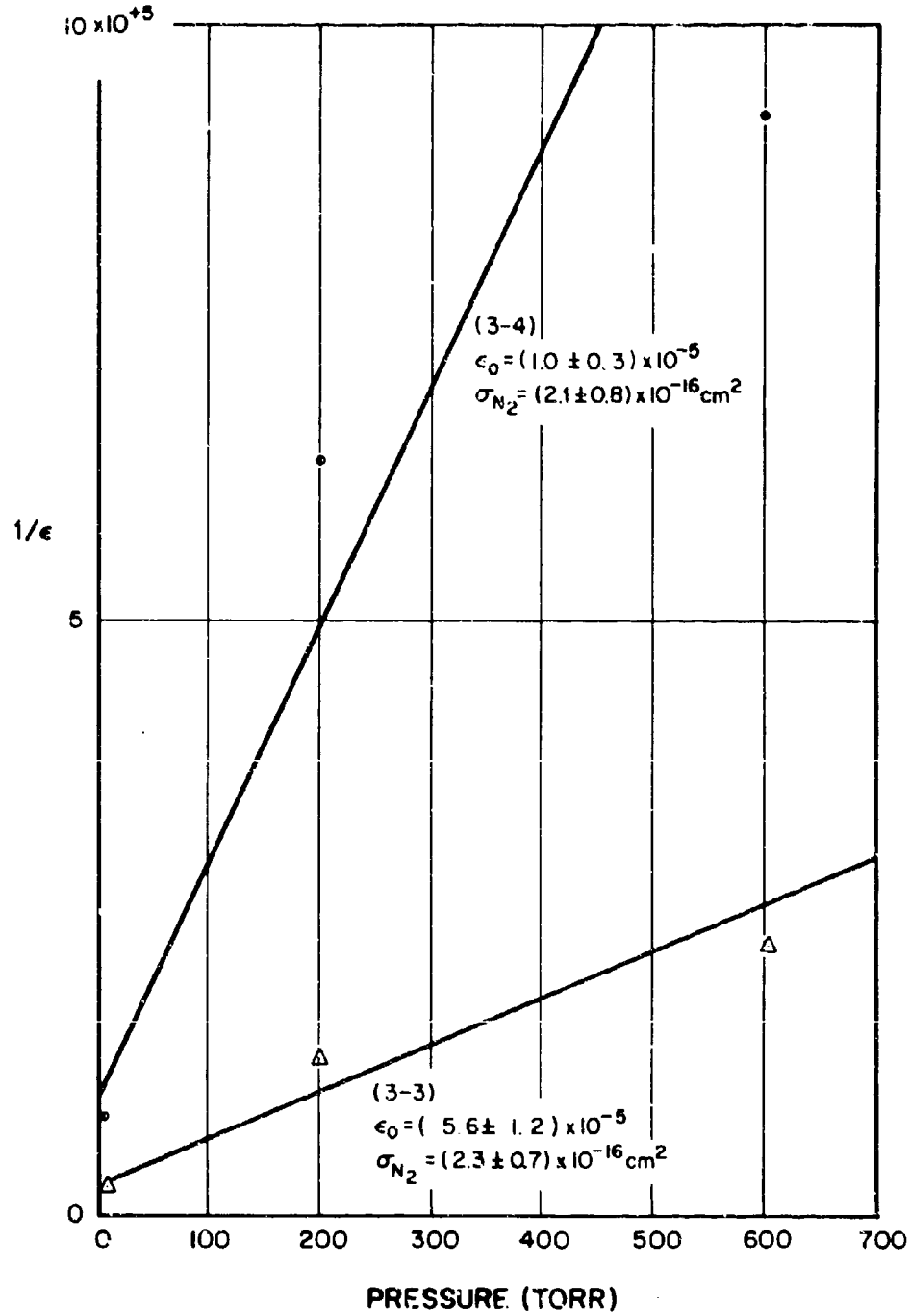

Figure 26

1502

FLUORESCENT EFFICIENCY OF N_2 2P BANDS BY ELECTRON BOMBARDMENT OF N_2

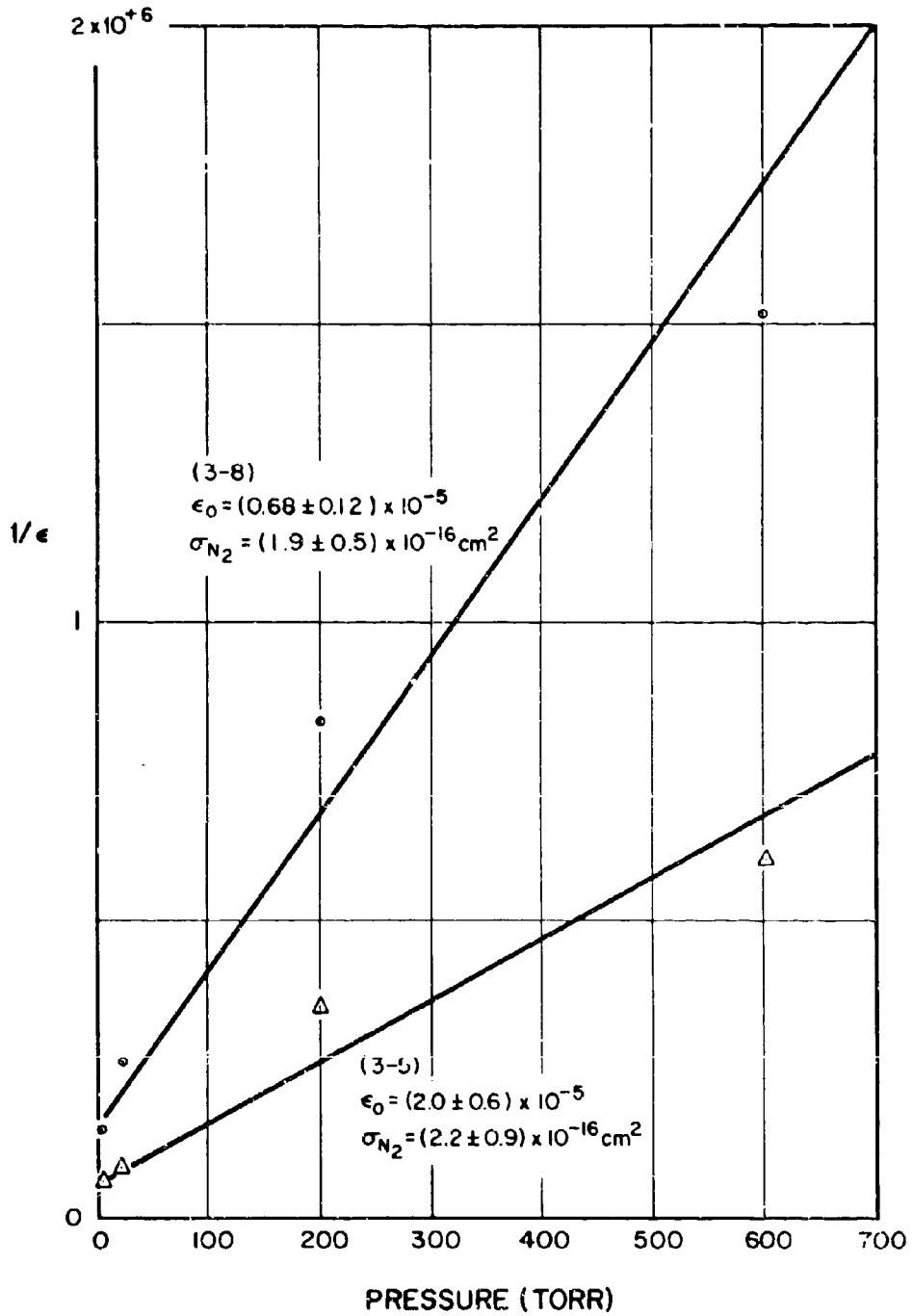

Figure 27

1602

FLUORESCENT EFFICIENCY OF N_2 2P BANDS BY ELECTRON BOMBARDMENT OF AIR

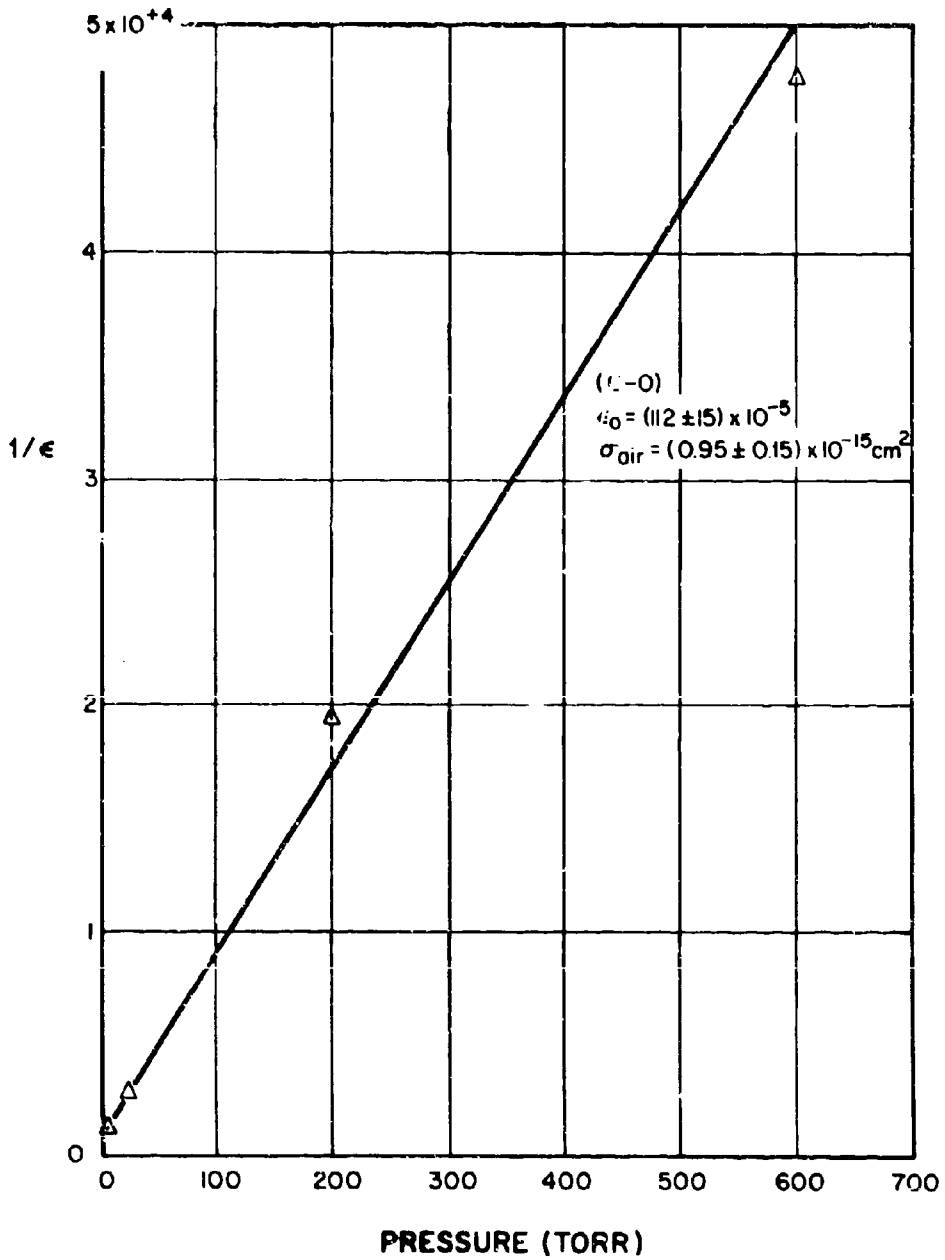

Figure 28

FLUORESCENT EFFICIENCY OF N_2 2P BANDS BY ELECTRON BOMBARDMENT OF AIR

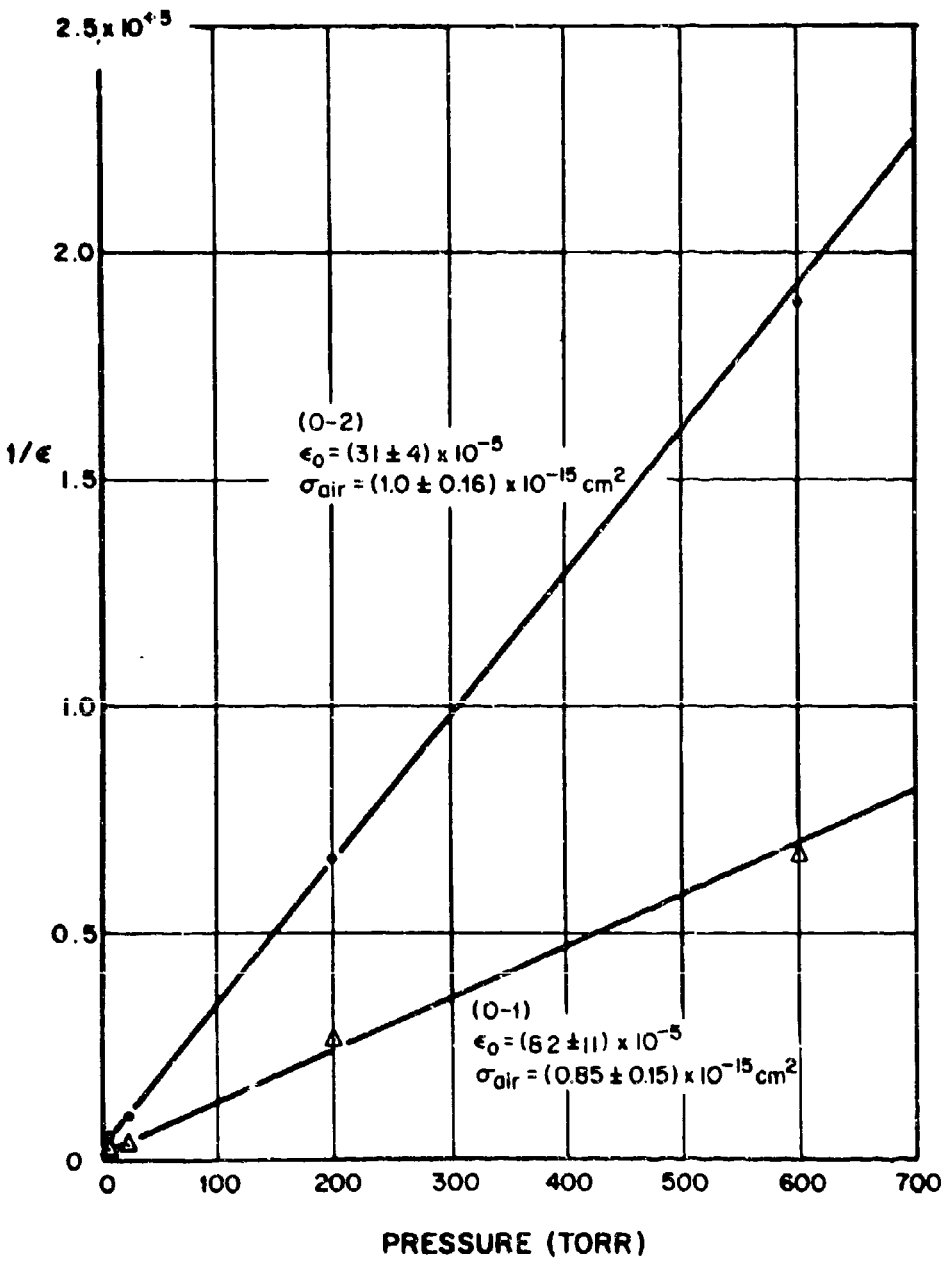

Figure 29

FLUORESCENT EFFICIENCY OF N_2 2P BANDS BY ELECTRON BOMBARDMENT OF AIR

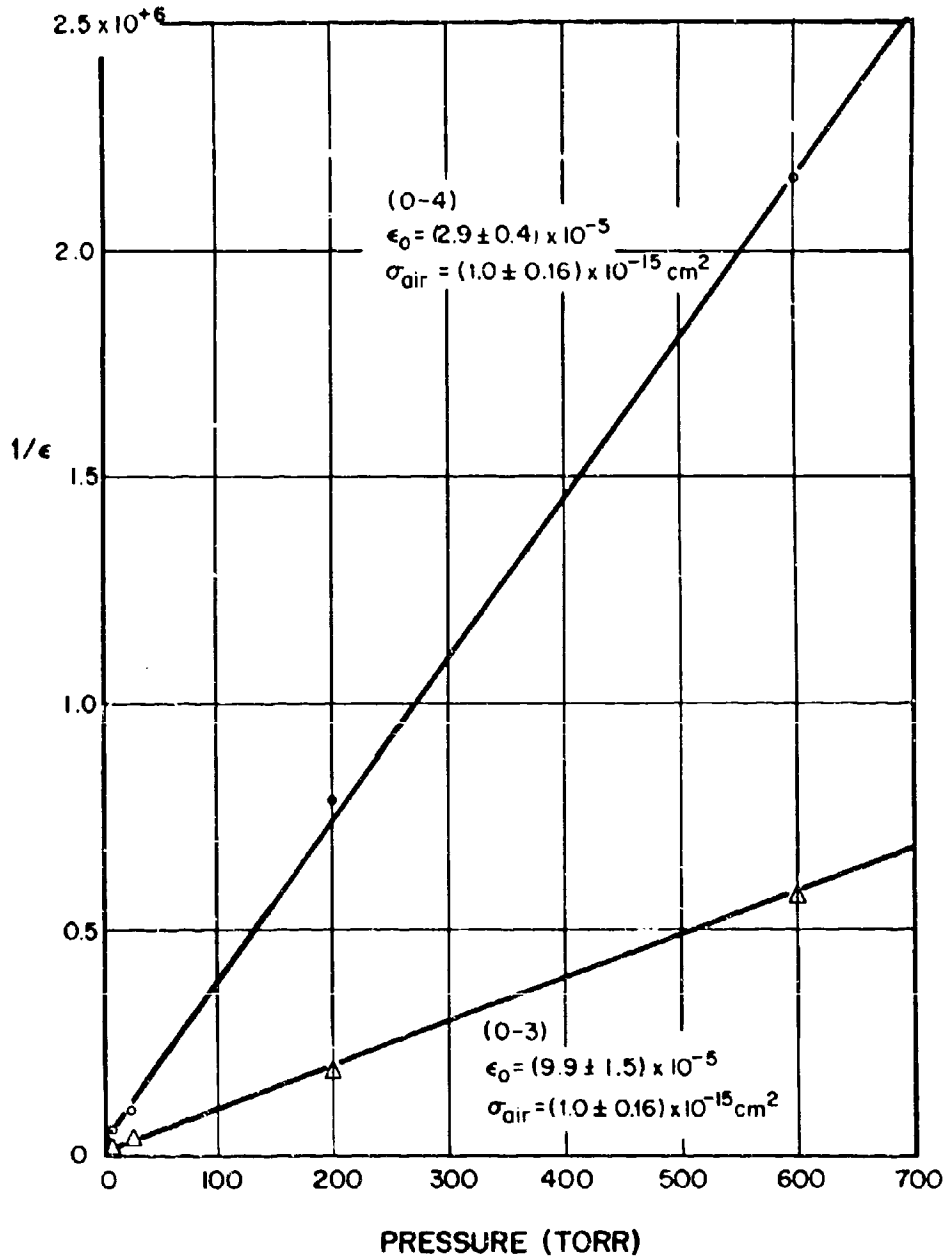

Figure 30

FLUORESCENT EFFICIENCY OF N_2 2P BANDS BY ELECTRON BOMBARDMENT OF AIR

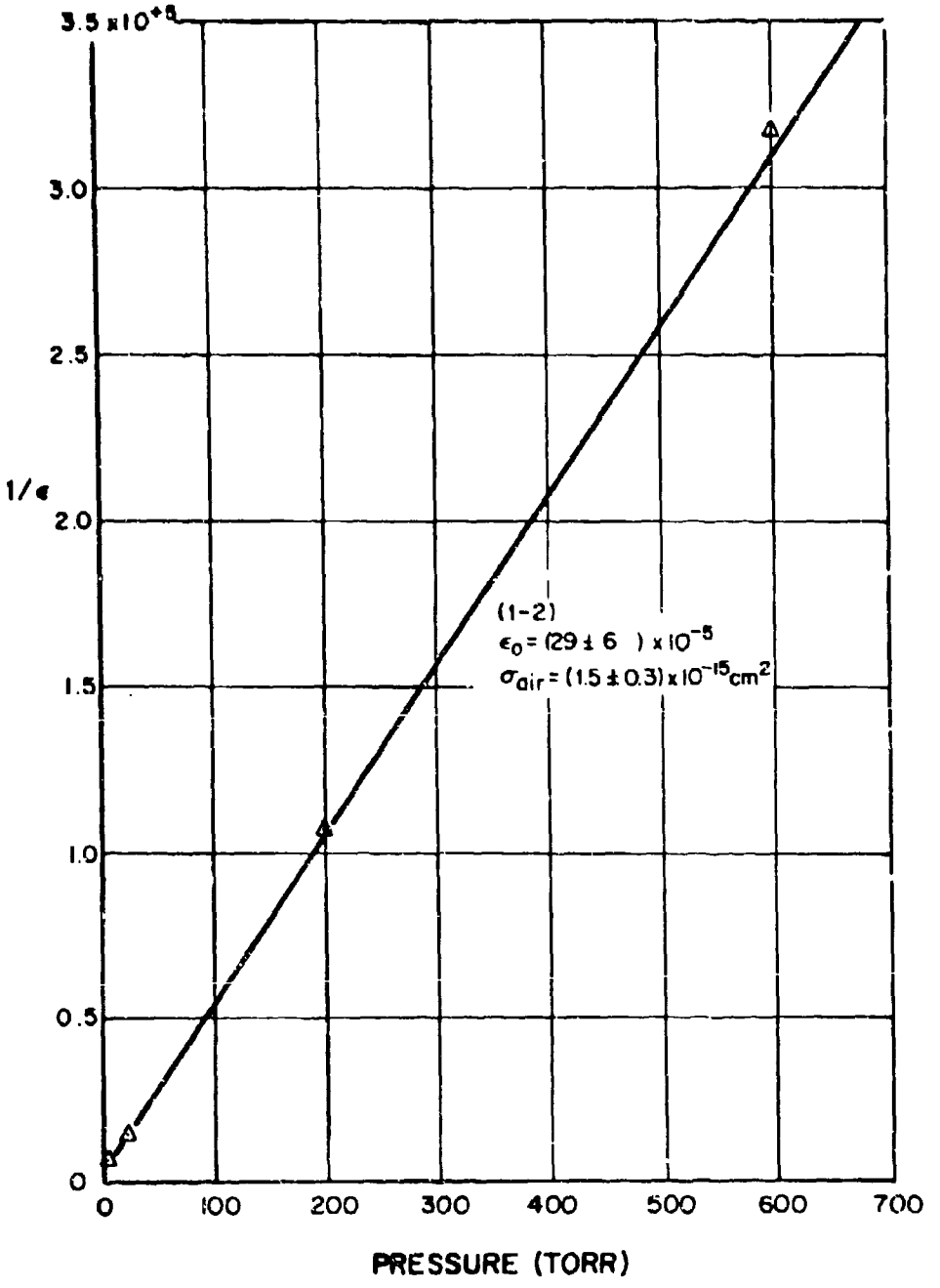

Figure 31

FLUORESCENT EFFICIENCY OF N_2 2P BANDS BY ELECTRON BOMBARDMENT OF AIR

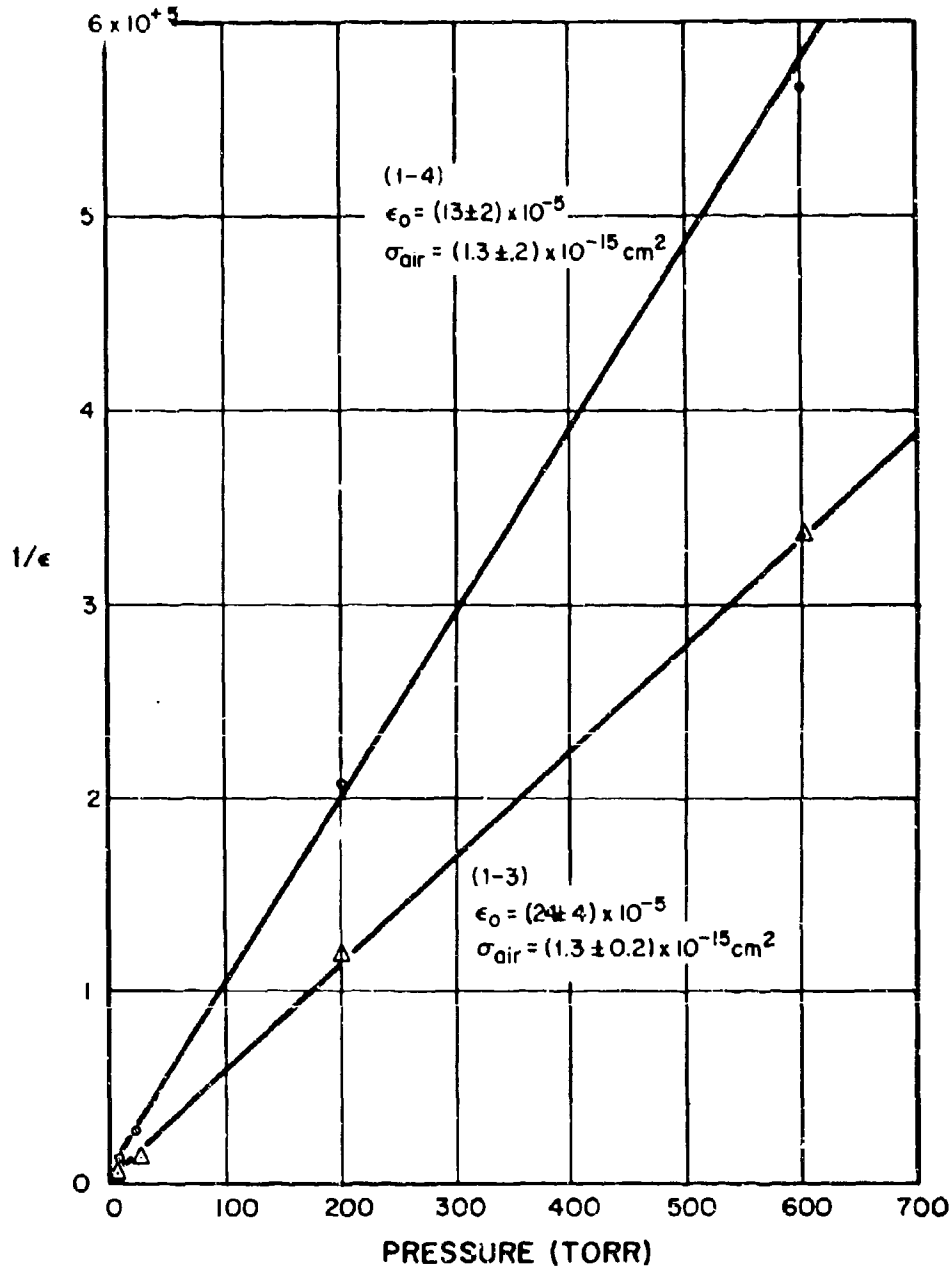

Figure 32

1602

FLUORESCENT EFFICIENCY OF N_2 2P BANDS BY ELECTRON BOMBARDMENT OF AIR

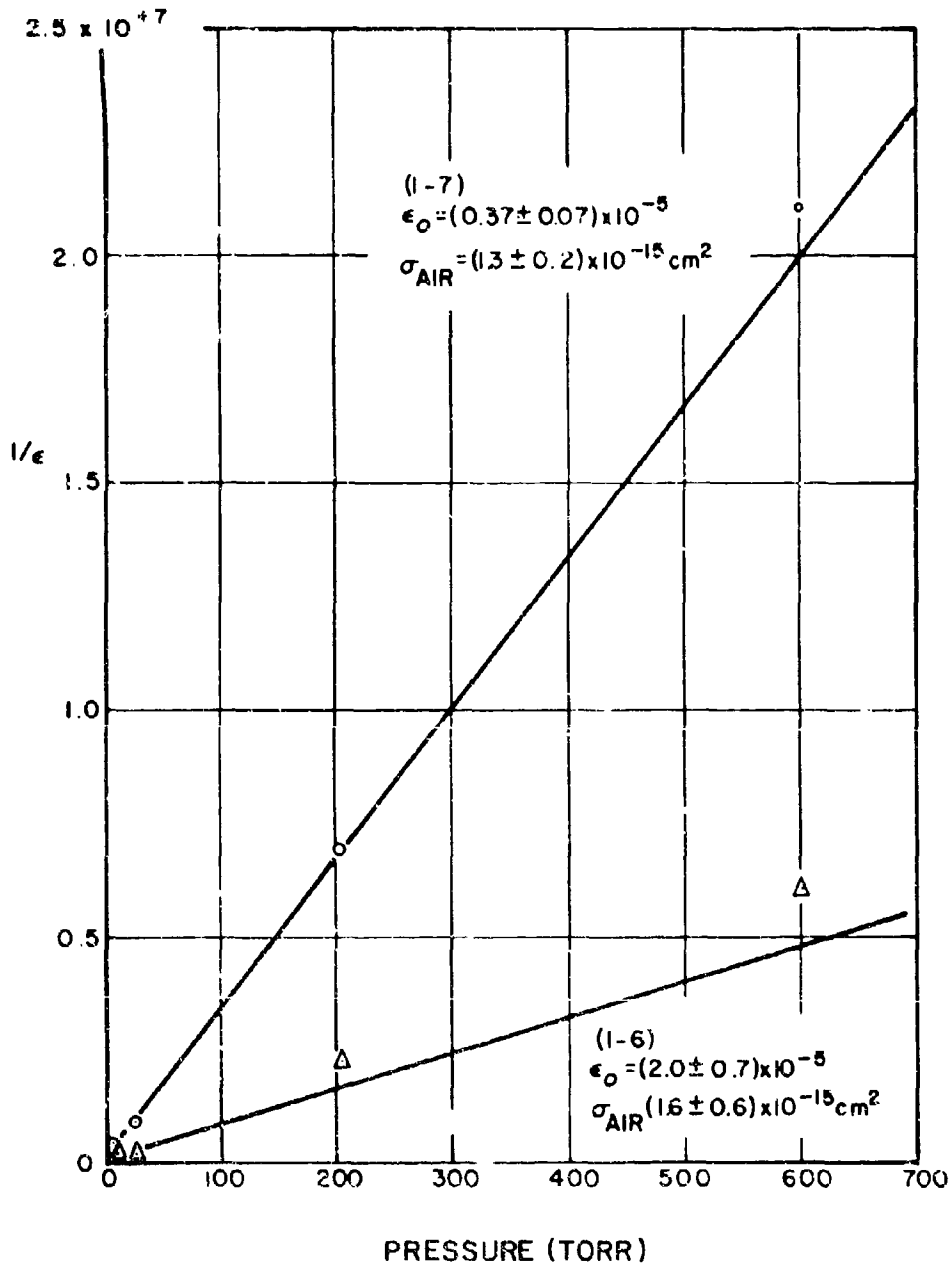

Figure 33

FLUORESCENT EFFICIENCY OF N_2 2P BANDS BY ELECTRON BOMBARDMENT OF AIR

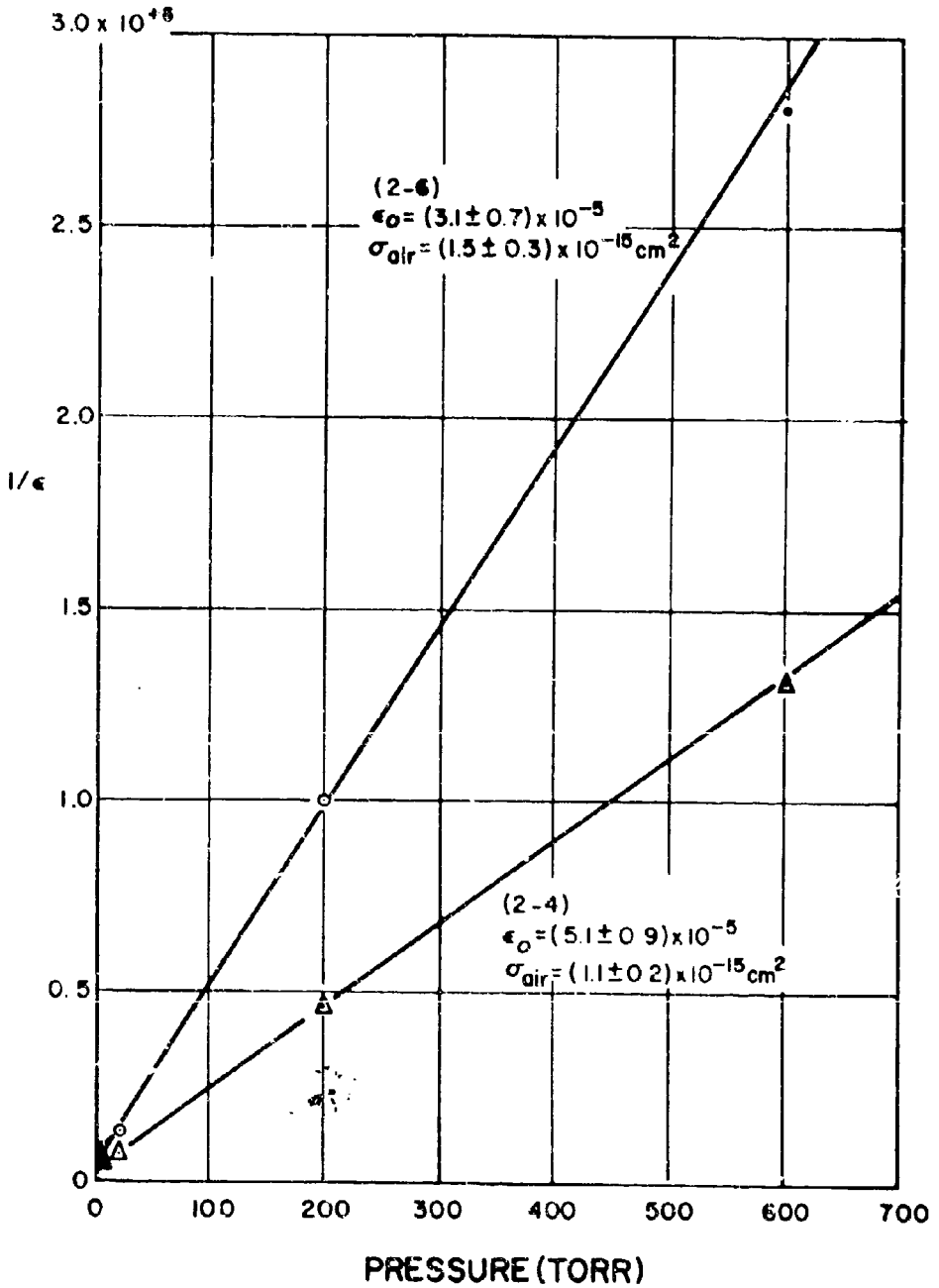

Figure 34

FLUORESCENT EFFICIENCY OF N_2 2P BANDS BY ELECTRON BOMBARDMENT OF AIR

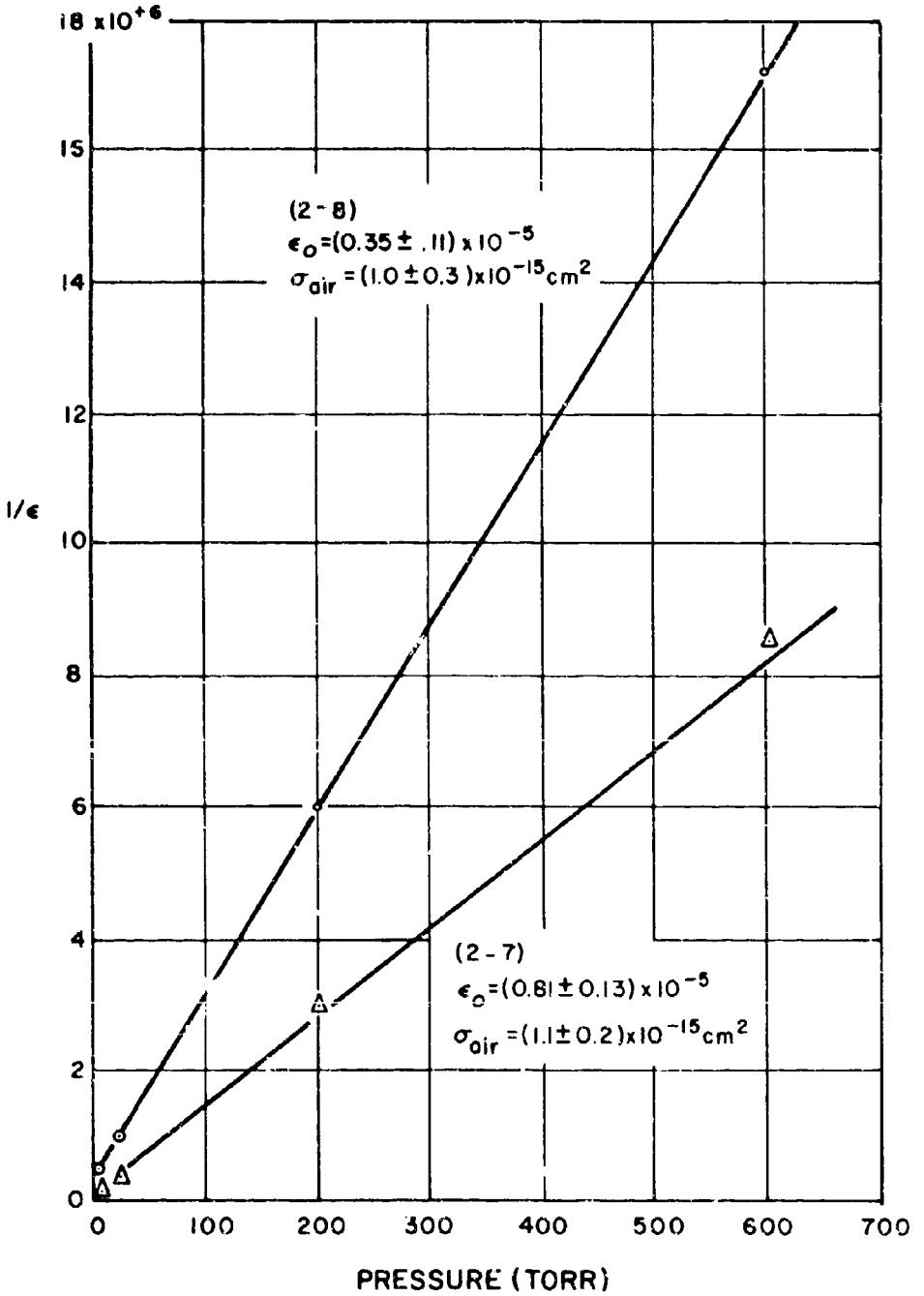

Figure 35

FLUORESCENT EFFICIENCY OF N_2 2P BANDS BY ELECTRON BOMBARDMENT OF AIR

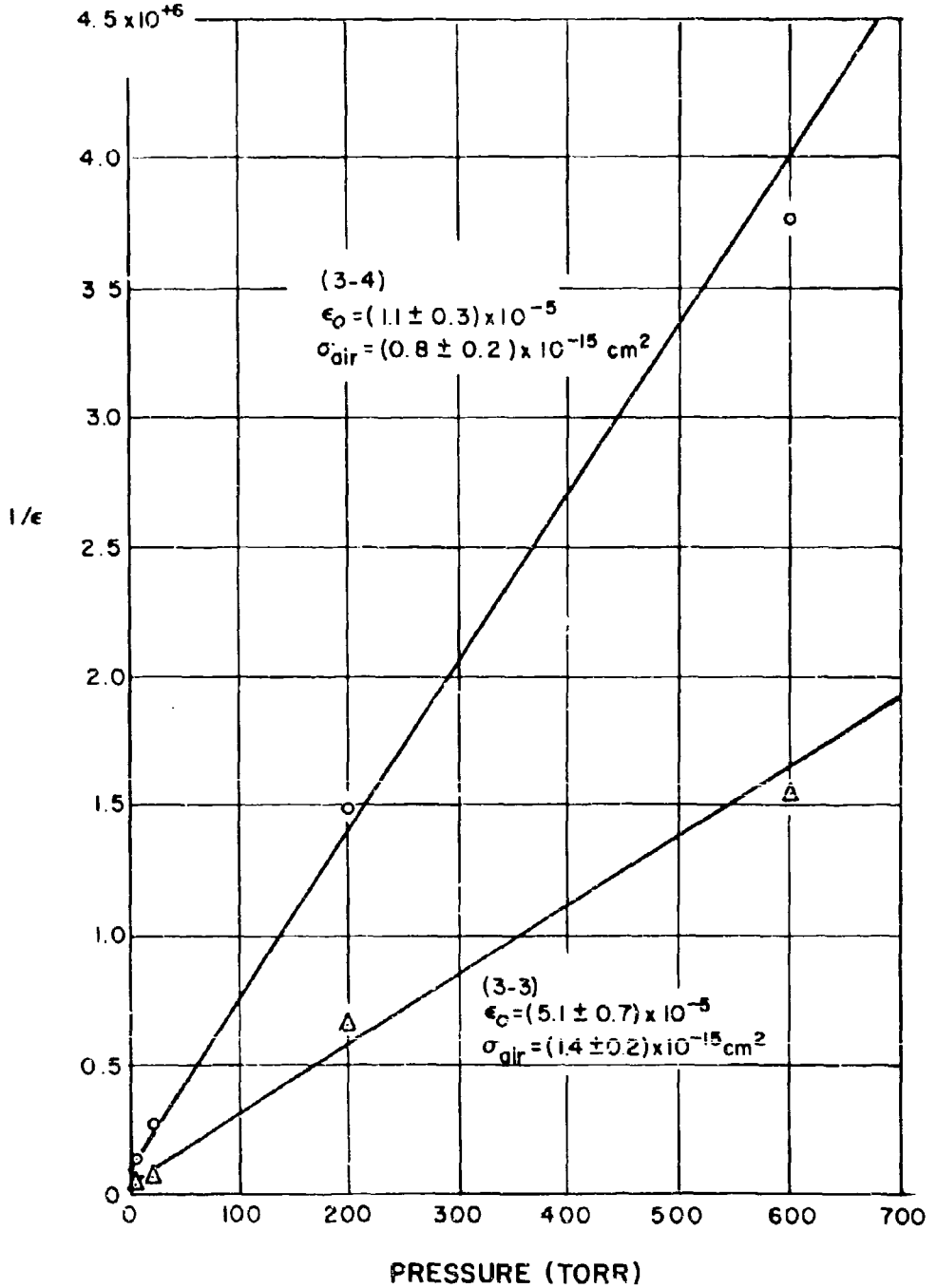

Figure 36

FLUORESCENT EFFICIENCY OF N_2 2P BANDS BY ELECTRON BOMBARDMENT OF AIR

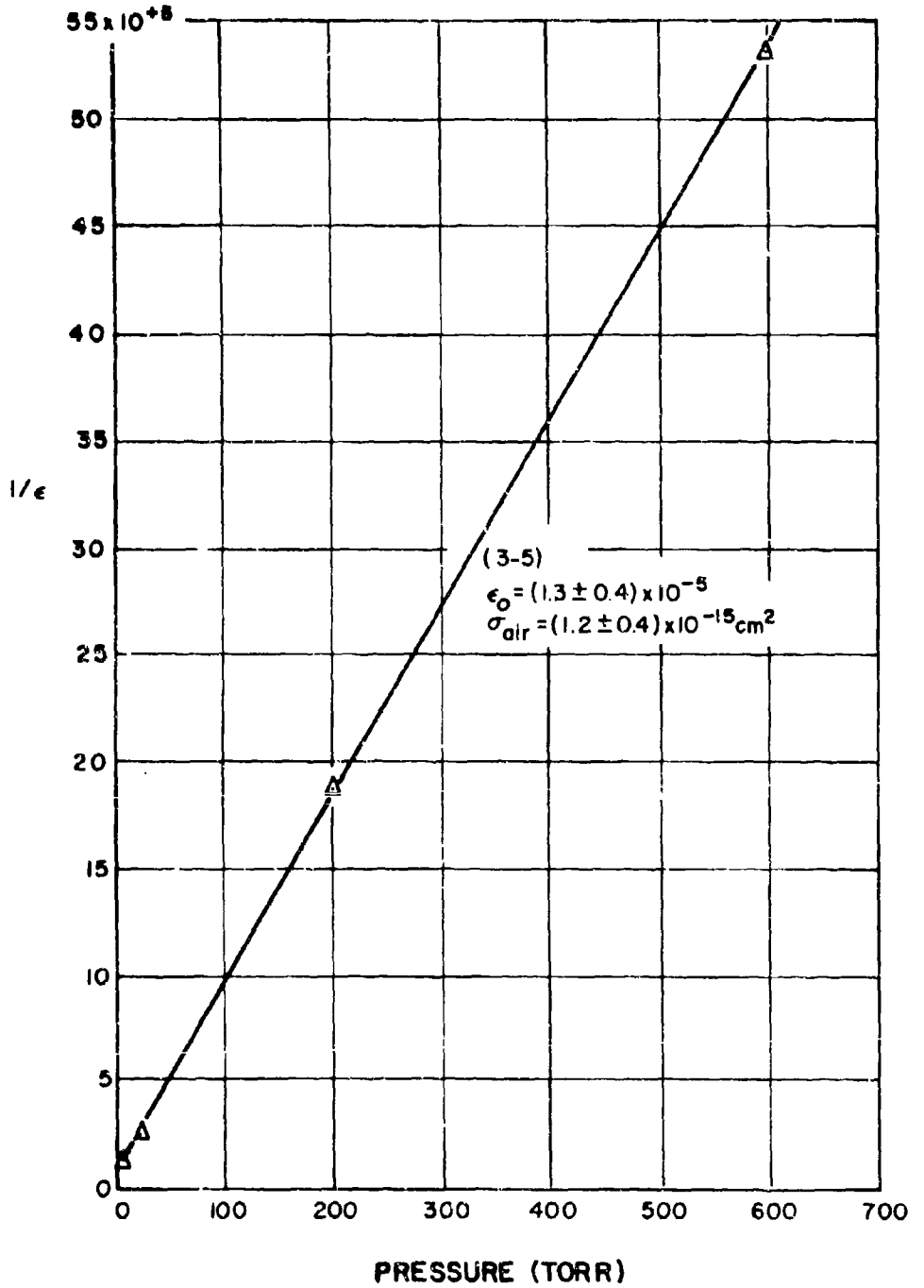

Figure 37

FLUORESCENT EFFICIENCY OF N_2 2P BANDS BY ELECTRON BOMBARDMENT OF AIR

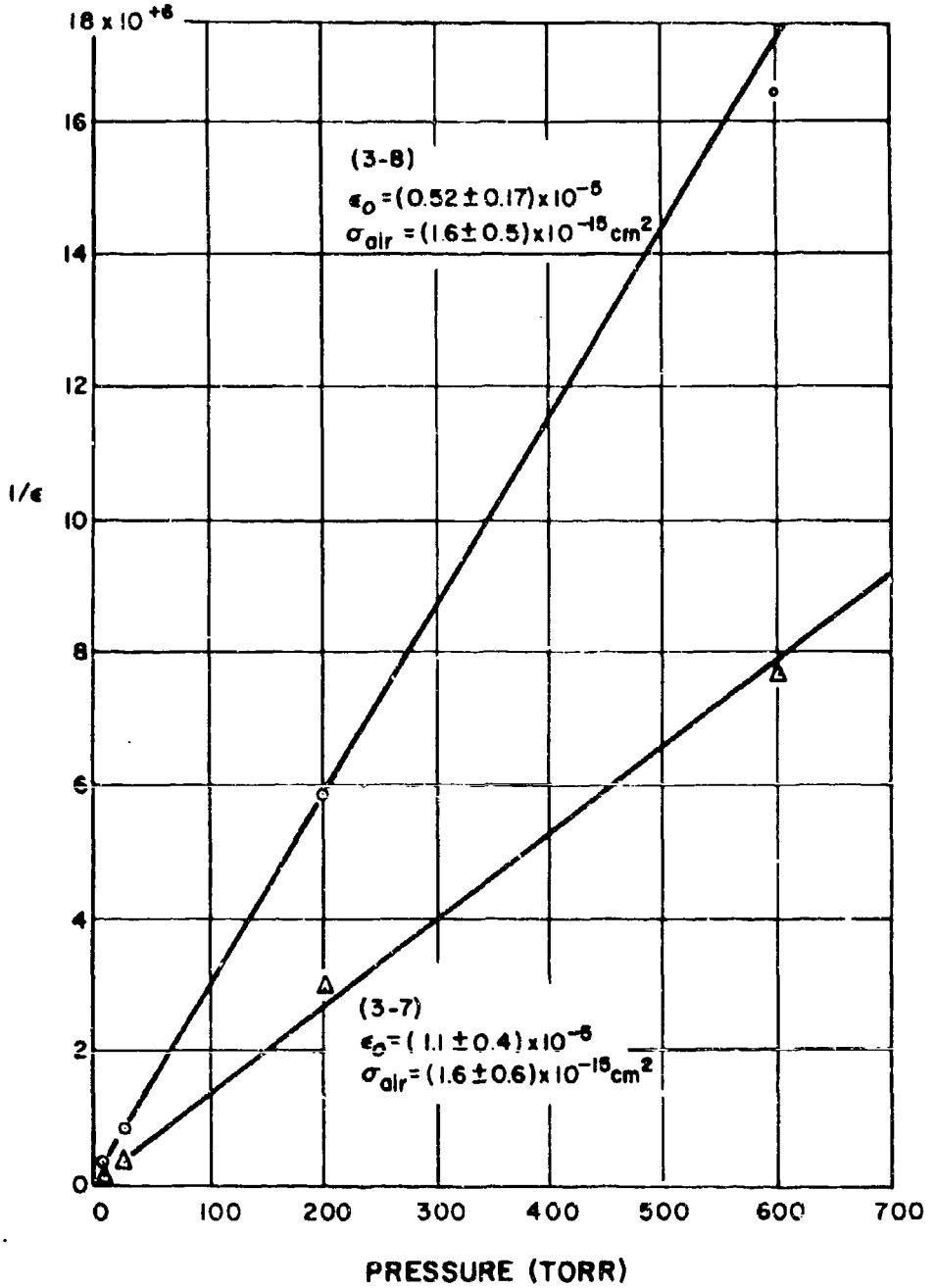

Figure 38

TABLE V

COLLISIONAL DEACTIVATION CROSS SECTIONS OF N_2 AND AIR FOR THE SECOND POSITIVE BANDS OF N_2

Transition	Quenching Gas		Weighted Average for Progression	
	N_2	Air	N_2	Air
	($\times 10^{-16}$ cm^2)	($\times 10^{-15}$ cm^2)	($\times 10^{-16}$ cm^2)	($\times 10^{-15}$ cm^2)
0-0	0.56 ± 0.08	0.95 ± 0.15		
0-1	0.50 ± 0.08	0.85 ± 0.13		
0-2	0.51 ± 0.07	1.0 ± 0.16	0.52 ± 0.03	0.95 ± 0.07
0-3	0.49 ± 0.07	1.0 ± 0.16		
0-4	0.50 ± 0.08	1.0 ± 0.16		
0-5	0.85 ± 0.20			
1-2	1.4 ± 0.4	1.5 ± 0.3		
1-3	1.2 ± 0.15	1.4 ± 0.3		
1-4	1.4 ± 0.2	1.3 ± 0.2	1.4 ± 0.1	1.4 ± 0.12
1-6	1.3 ± 0.2	1.6 ± 0.6		
1-7		1.3 ± 0.2		
2-4	1.5 ± 0.4	1.1 ± 0.2		
2-6		1.5 ± 0.3	1.6 ± 0.2	1.2 ± 0.11
2-7		1.1 ± 0.2		
2-8	1.7 ± 0.5	1.0 ± 0.3		
3-3	2.3 ± 0.7	1.4 ± 0.2		
3-4	2.1 ± 0.8	0.8 ± 0.2		
3-5	2.2 ± 0.9	1.2 ± 0.4	2.0 ± 0.3	1.2 ± 0.14
3-7		1.6 ± 0.6		
3-8	1.9 ± 0.5	1.6 ± 0.5		

TABLE VI

COLLISIONAL DEACTIVATION CROSS SECTIONS OF N_2 AND O_2 FOR THE VIBRONIC LEVELS OF THE SECOND POSITIVE BANDS OF N_2

Progression[a]	Brocklehurst	Hirsh et al	Brocklehurst Downing	This Experiment[b]
	N_2 ($\times 10^{-16}$ cm^2)			
0-n	1.5 ± 0.4	1.2 ± 0.6	1.8 ± 0.3	0.52 ± 0.03
1-n	4.2 ± 0.9		4.1 ± 0.5	1.4 ± 0.1
2-n	4.8 ± 1.4		5.3 ± 0.8	1.6 ± 0.2
3-n			6.2 ± 1.3	2.0 ± 0.3
	O_2 ($\times 10^{-16}$ cm^2)			
0-n	48 ± 20	39 ± 11		44 ± 4
1-n		52 ± 18		59 ± 6
2-n		81 ± 32		49 ± 6
3-n				50 ± 7

[a] All quenching cross sections are based on the radiative lifetime, $(4.45 \pm 0.6) \times 10^{-8}$ seconds, measured by Bennett and Dalby for the (0-n) transitions.

[b] The probable errors of this experiment do not include the error in the radiative lifetime.

TABLE VII

FLUORESCENT EFFICIENCIES FOR THE N_2 SECOND POSITIVE BANDS EXCITED BY ENERGETIC ELECTRONS INCIDENT ON N_2 AND AIR

Transition	$\epsilon_o (\times 10^{-5})$[a]		Ratio	Weighted Average of Ratio for each progression
	N_2	Air	$\epsilon_o(N_2)/\epsilon_o$(Air)	
0-0	186 ± 16	112 ± 15	1.7 ± 0.3	
0-1	126 ± 10	82 ± 11	1.5 ± 0.2	
0-2	48 ± 4	31 ± 4	1.5 ± 0.2	1.6 ± 0.1
0-3	14.6 ± 1.2	9.9 ± 1.5	1.5 ± 0.3	
0-4	4.0 ± 0.3	2.9 ± 0.4	1.5 ± 0.3	
0-5	1.1 ± 0.2			
1-2	38 ± 8	29 ± 6	1.3 ± 0.4	
1-3	26 ± 2	24 ± 4	1.1 ± 0.2	1.1 ± 0.1
1-4	18 ± 2	13 ± 2	1.4 ± 0.3	
1-6	1.54 ± 0.14	2.0 ± 0.7	$.8 \pm 0.3$	
1-7		0.37 ± 0.07		
2-4	8.4 ± 1.6	5.1 ± 0.9	1.6 ± 0.4	
2-6		3.1 ± 0.7		
2-7		0.81 ± 0.13		1.4 ± 0.3
2-8	0.40 ± 0.08	0.35 ± 0.11	1.1 ± 0.4	
3-3	5.6 ± 1.2	5.1 ± 0.7	1.1 ± 0.3	
3-4	1.0 ± 0.3	1.1 ± 0.3	0.9 ± 0.4	
3-5	2.0 ± 0.6	1.3 ± 0.4	1.5 ± 0.6	1.1 ± 0.2
3-7		1.1 ± 0.4		
3-8	0.68 ± 0.12	0.52 ± 0.17	1.3 ± 0.5	

[a]The fluorescent efficiencies are based on measurements in N_2 and Air extrapolated to low pressure where collisional deactivation is an insignificant depopulating process. The probable error does not include the error in the absolute measurement which is estimated to be an additional $\pm$ 15%.

derived from the Stern-Volmer plots of the second positive bands in air and N_2 are presented in Table VII. The ratio of the values in N_2 and air are calculated for each transition. For each upper vibrational level observed, a weighted average (based on the inverse square of the probable errors) is given in Table VII for the ratio of ϵ_o in N_2 and air. The values of ϵ_o for the lowest vibrational level is significantly higher in N_2 than air. This implies a unique excitation process populates the lowest vibrational level of the N_2 $C^3\Pi_u$ state in N_2 but is ineffective in air at the pressures used in these thick target studies (5 Torr or greater). At lower pressures (less than 5 Torr) presumably the values of ϵ_o would become equivalent, assuming competing inelastic electron collisions with O_2 and the other atmospheric constituents are negligible.

Brocklehurst and Downing[15] compare emission from nitrogen near atmospheric pressures excited by energetic electrons with the published[2] spectra of this experiment excited under similar conditions. The relative intensities of the band systems show reasonable agreement with the exception of the second positive bands which Brocklehurst and Downing estimate six times less intense in their results. Due to approximations in their measured integrated band intensities, it is suggested the experimental differences in the second positive system intensity is closer to a factor of three as indicated by the N_2 quenching cross sections of Table VI. The similar pressure ranges used in both experiments for the N_2 second positive quenching analysis and the general agreement in the magnitude of the O_2 quenching cross sections of Table VI, imply the differences in the second positive system intensities and the N_2 quenching cross sections are due to target gas impurities. Brocklehurst and Downing have measured relative band system intensities as a function of O_2 content in the N_2 supplied to the target chamber with only a slight increase in second positive system intensity when the estimated O_2 content decreased from 55 PPM to less than 4 PPM. Table VI indicates preferential quenching of the second positive system vibrational levels is strong for N_2 and slight for O_2. If a target gas impurity more than

triples the number of deactivating collisions in the experiment of Brocklehurst and Downing, the impurity depopulates the vibrational levels of the secon positive system in the same preferential ratio as nitrogen. This result in addition to the aforementioned measurements of Brocklehurst and Downing eliminates O_2 as a possible target gas impurity causing the experimental differences in the N_2 second positive system intensity.

When the gas flow through the target chamber of this experiment was decreased from an estimated 100 cm^3/sec to 10 cm^3/sec (maintaining the same target chamber pressure), the absolute intensity of the second positive system decreased by a factor of two while the first negative system remained unchanged. The change in second positive system intensity with gas flow is interpreted as collisional quenching from impurities originating in the vacuum system, possibly from leaks or outgassing products generated by electron collision with the chamber walls or other residual gases in the system that are reduced in partial pressure by increasing the gas flow. This tentative explanation is somewhat suspect in that it requires a surprisingly large combined partial pressure and quenching cross section for the impurity to produce an intensity change of two (different flow rates this experiment) or three (Brocklehurst and Downing and this experiment).

The electron induced fluorescence of air at pressures ranging from 10 to 600 Torr has been measured within a spectral bandpass of 3200 to 7000 Å by Grün.[24] The pressure dependence of the radiance was accurately described by a Stern-Volmer quenching process with the fluorescence reduced by a factor of two at 11.5 Torr. Figures 10 and 12 indicate the dominant radiator in air excited under these conditions is the lowest vibrational level of the second positive system of N_2. The quenching cross section of air measured in this experiment for the lowest second positive vibrational level (Table V) is equivalent to a half intensity air pressure of 10.9 Torr, in excellent agreement with the results of Grün. The similarity of these results is additional evidence supplementary to Table VI of the general agreement in the magnitude of the O_2 quenching cross section for

the second positive system.

3.3.4 N_2 First Positive System

The electron excitation conditions of the first positive bands are similar to the second positive bands. Direct excitation of the first positive system from the N_2 ground state, like the second positive system, involves a singlet-triplet transition. The electron excitation cross sections of Langstroth[25], Stewart[26], and Zapesochnyi and Skubenich[27] indicate a maximum at approximately 15 ev and a rapid decrease with increasing energy. In addition to direct excitation, the first positive system is populated by allowed transitions from higher triplet states (the second positive, Goldstein-Kaplan and fourth positive systems).

Jeunehomme[28] has recently measured the radiative lifetimes of the vibronic levels of the first positive system in a pulsed rf discharge. The fluorescence decay is described by the sum of three apparent lifetimes. The smallest value is interpreted as the natural radiative lifetime for direct excitation with the longer lifetimes due to cascading from longer lived states.

Using the analysis presented for the N_2 second positive bands, the collisional deactivation cross section and ϵ_o were calculated for the more intense transitions in nitrogen and air. The radiative lifetimes of Jeunehomme were used to determine the quenching cross sections. The number of isolated first positive transitions in the nitrogen spectra is limited because of overlapping emissions of the Gaydon-Green, Herman-Infrared and CN red systems as well as atomic nitrogen. Figures 39 through 46 illustrate the best fit of the data to a Stern-Volmer plot as determined by a weighted least squares analysis. Table VIII summarizes the results. The large probable errors are due to the poorly defined intercepts of the Stern-Volmer plots. An extension of the measurements to lower pressures is necessary to reduce the errors in the calculated parameters. In addition, the magnitude of the overlapping molecular spectra (observed with N_2 as the target gas) is reduced at lower target pressures.

FLUORESCENT EFFICIENCY OF N_2 1P BANDS BY ELECTRON BOMBARDMENT OF N_2

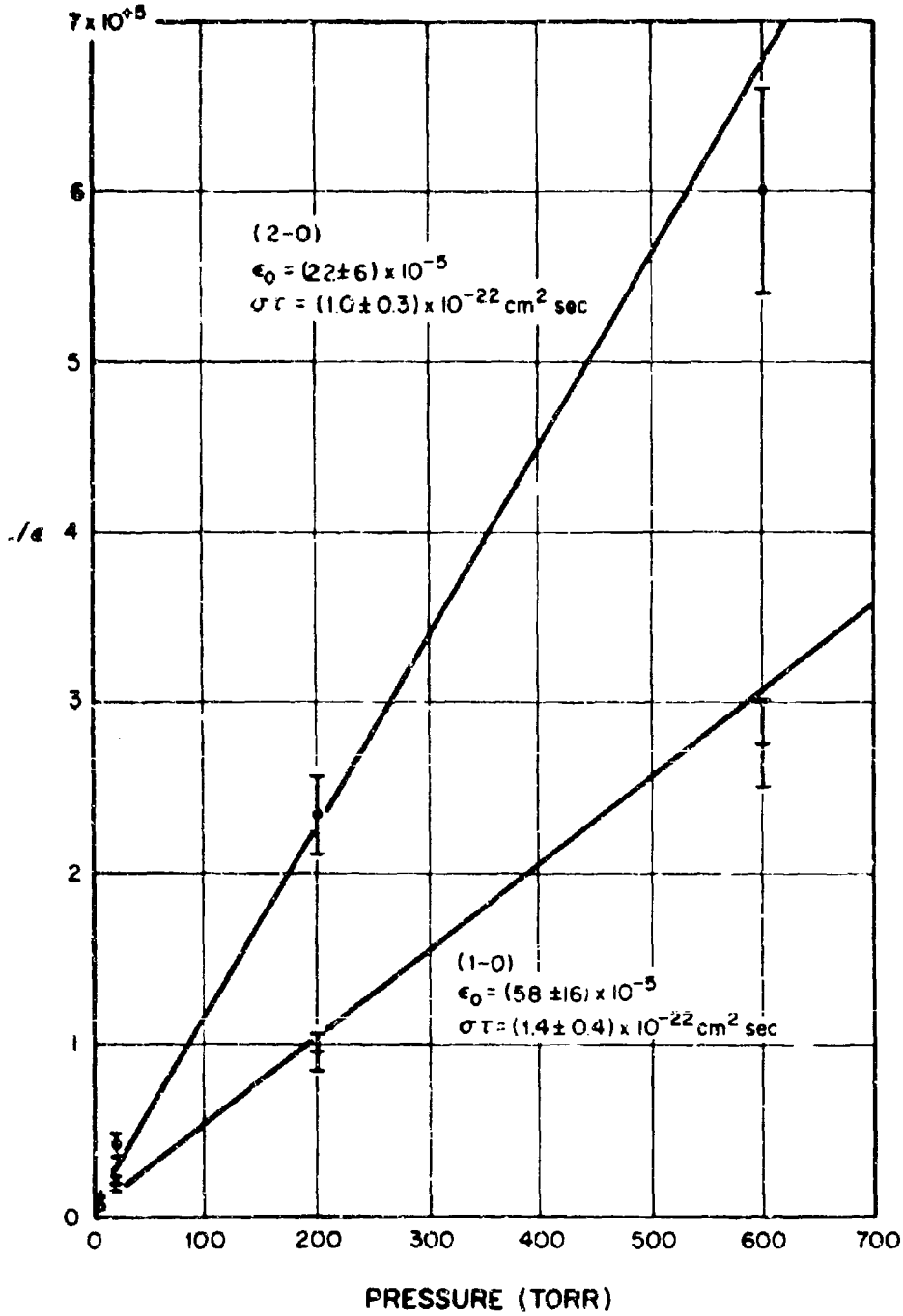

Figure 39

FLUORESCENT EFFICIENCY OF N_2 1P BANDS BY ELECTRON BOMBARDMENT OF N_2

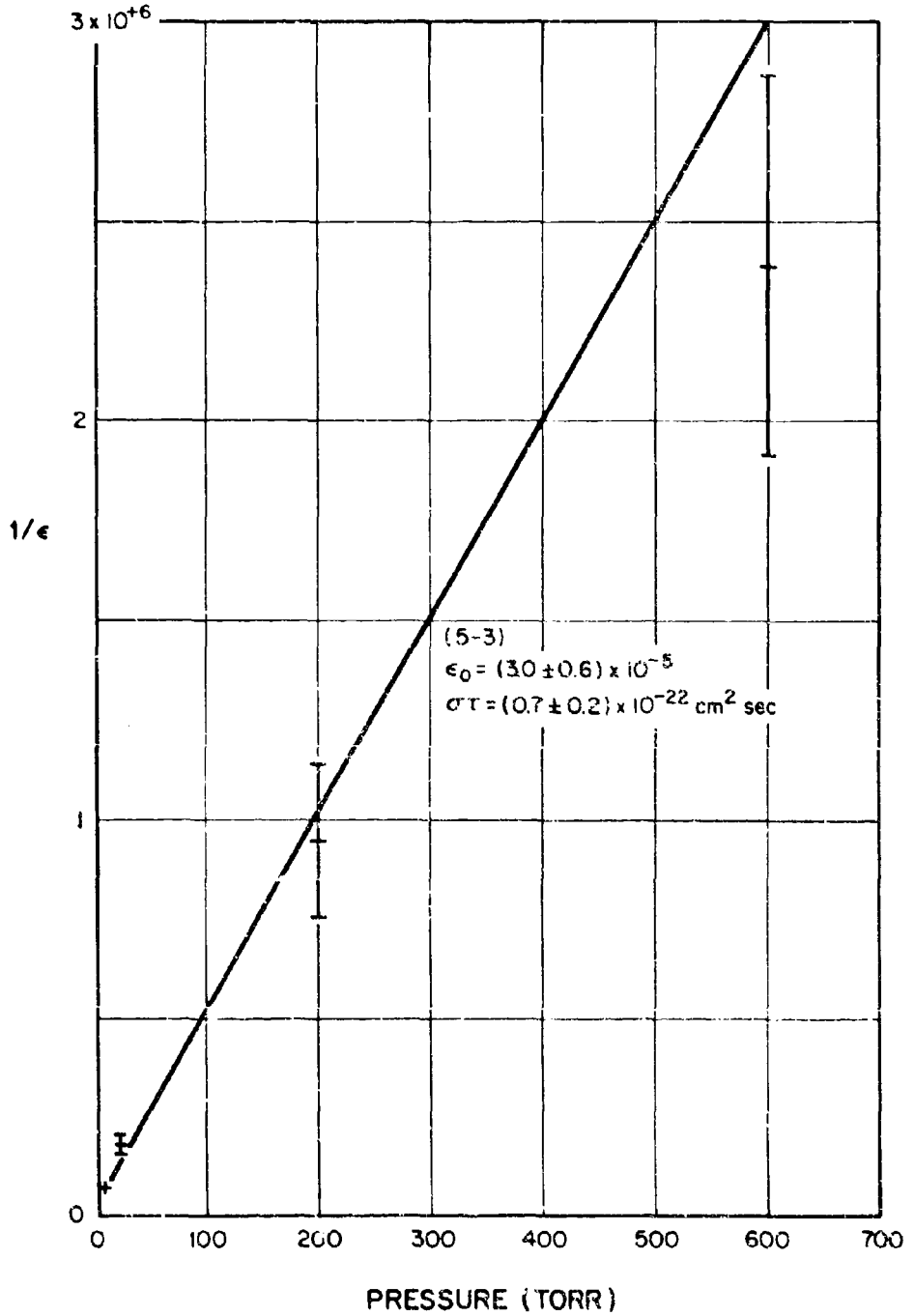

Figure 40

FLUORESCENT EFFICIENCY OF N_2 1P BANDS BY ELECTRON BOMBARDMENT OF AIR

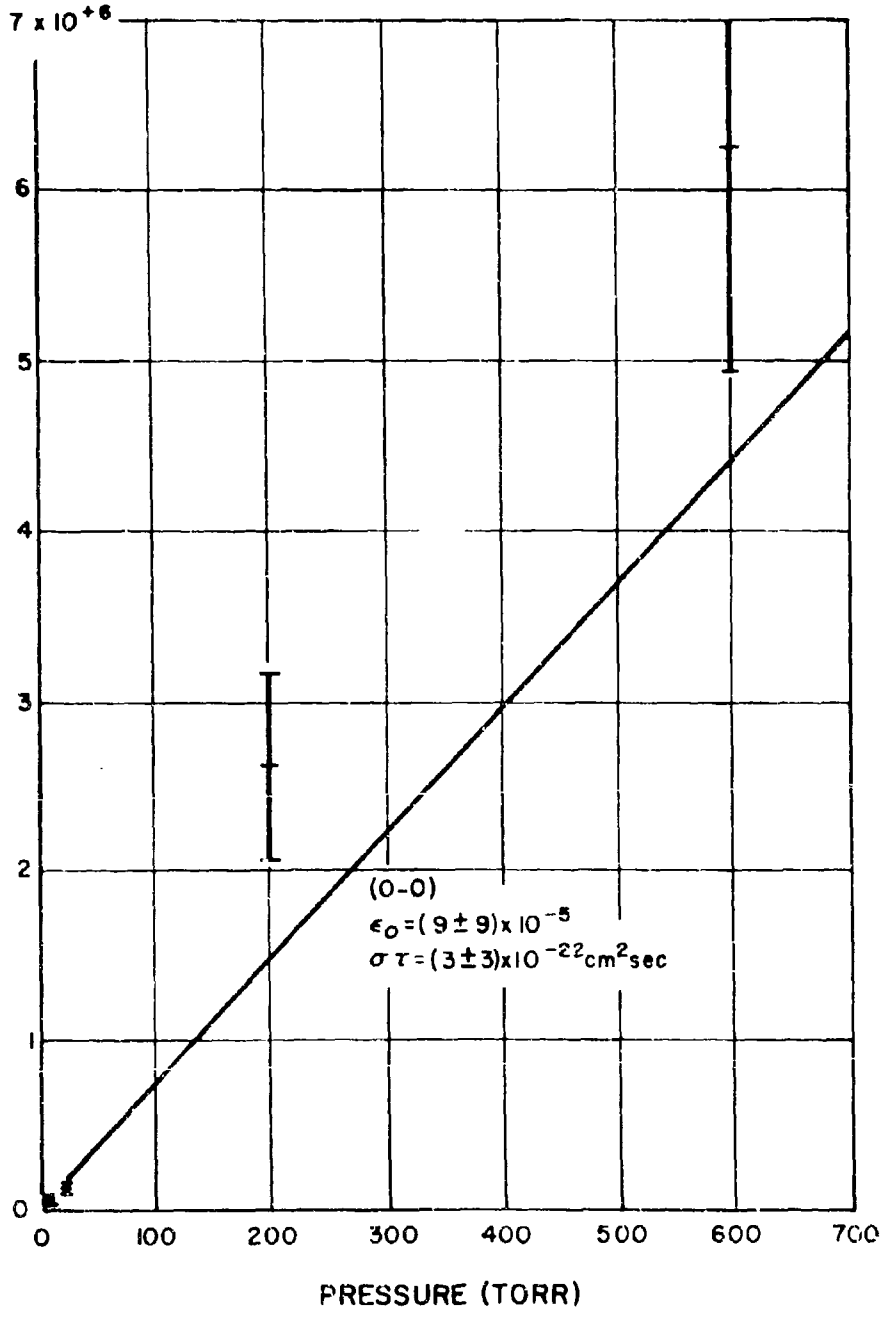

Figure 41

FLUORESCENT EFFICIENCY OF N_2 1P BANDS BY ELECTRON BOMBARDMENT OF AIR

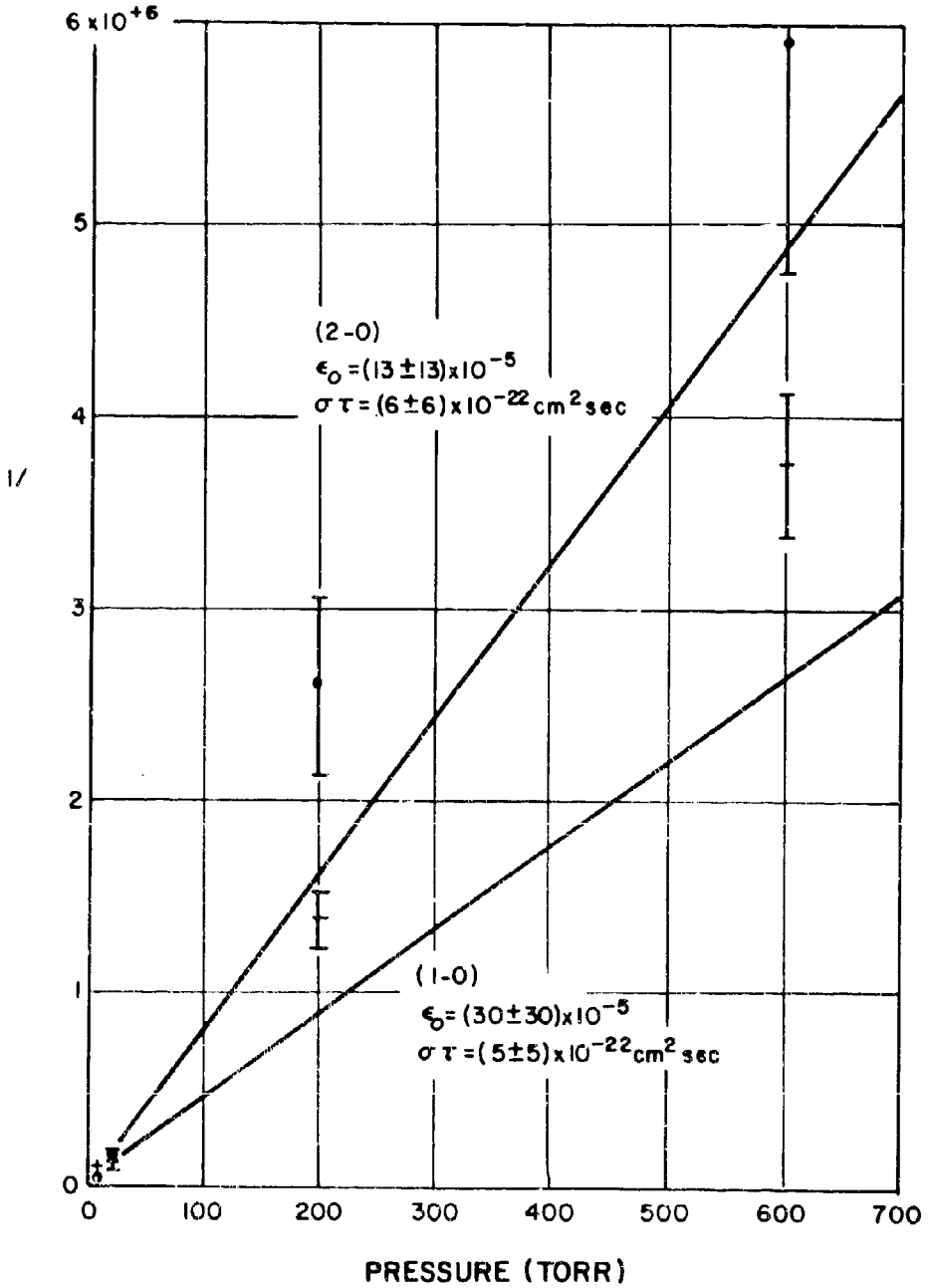

Figure 42

FLUORESCENT EFFICIENCY OF N_2 1P BANDS BY ELECTRON BOMBARDMENT OF AIR

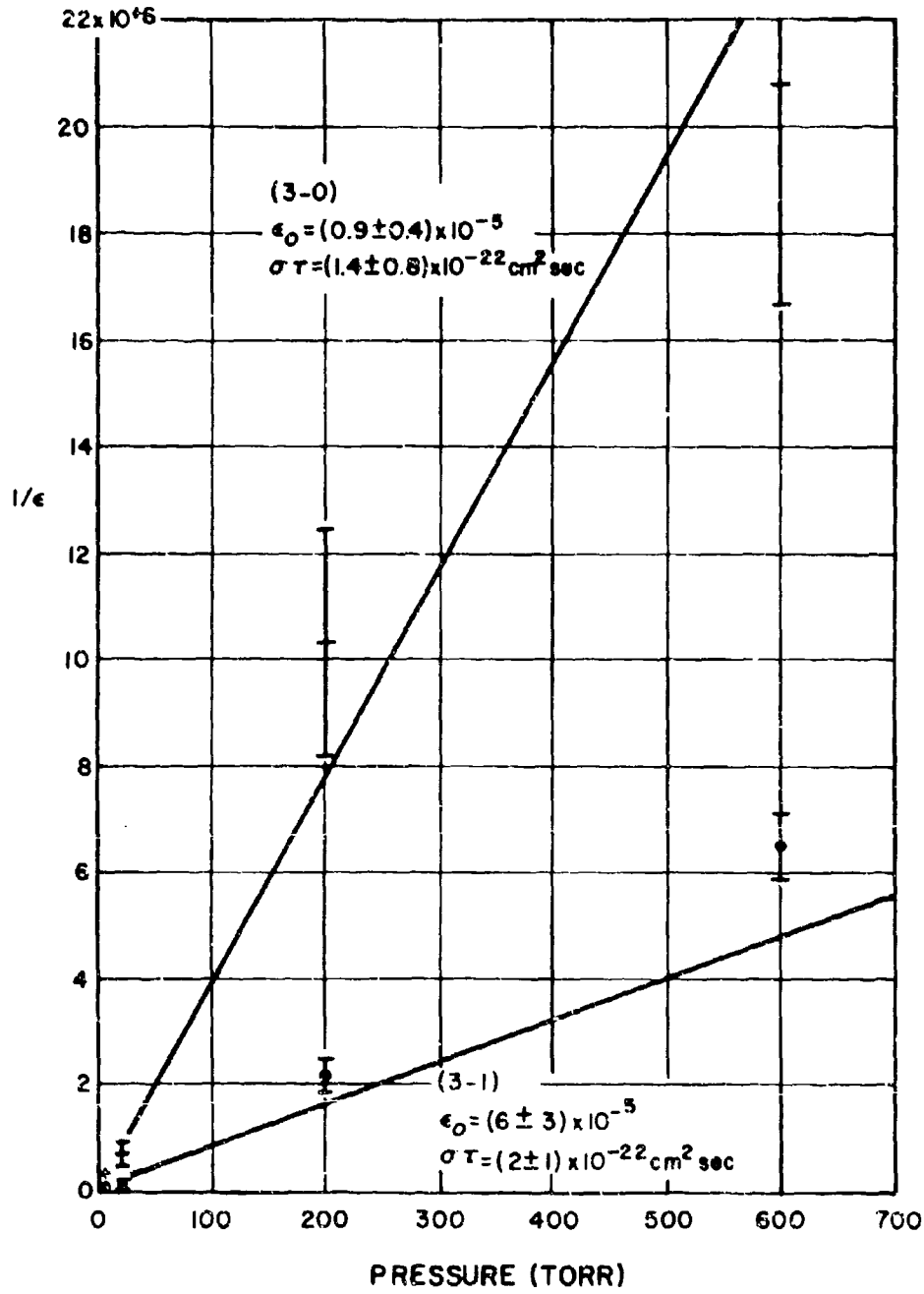

Figure 43

FLUORESCENT EFFICIENCY OF N_2 1P BANDS BY ELECTRON BOMBARDMENT OF AIR

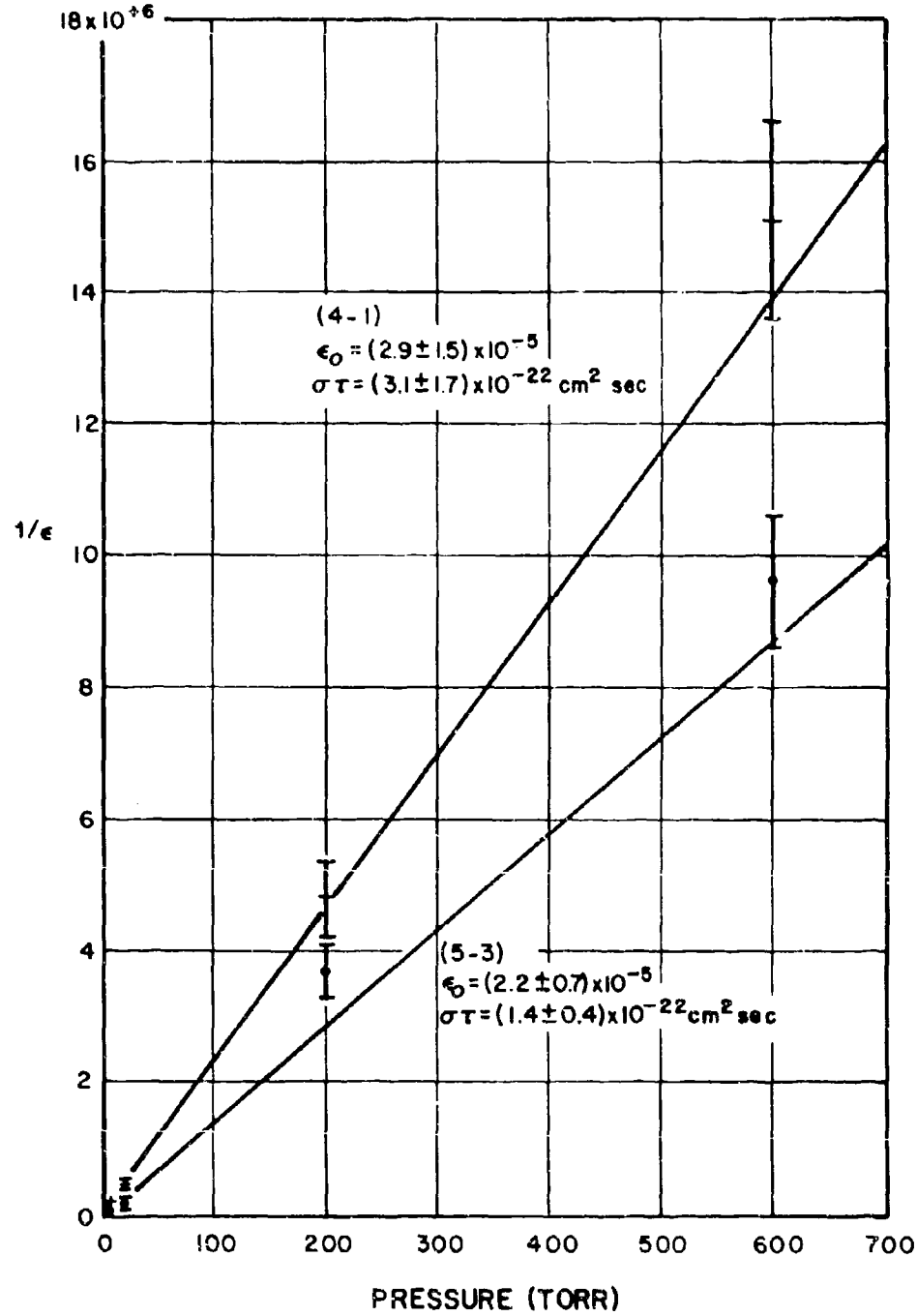

Figure 44

FLUORESCENT EFFICIENCY OF N_2 1P BANDS BY ELECTRON BOMBARDMENT OF AIR

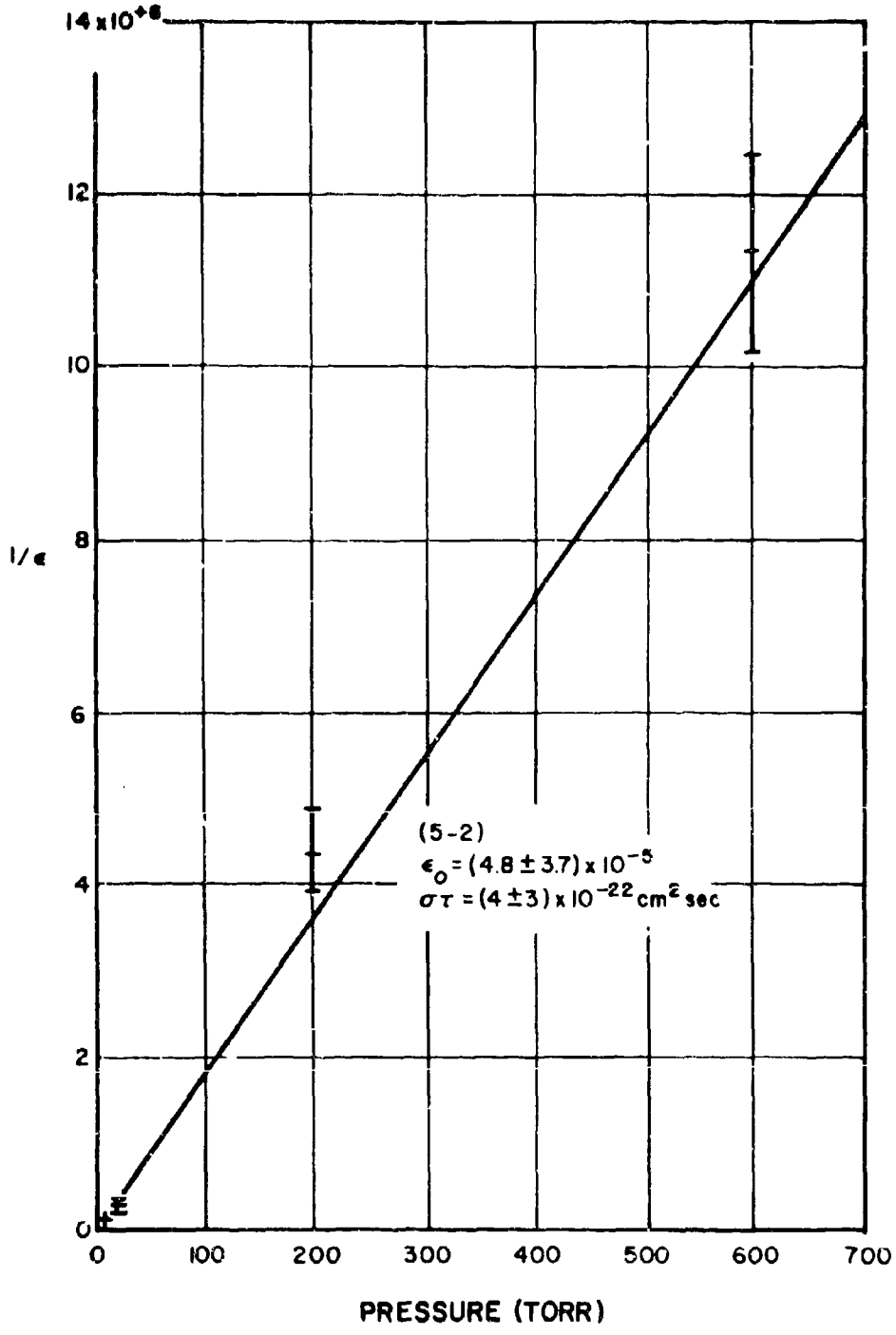

Figure 45

FLUORESCENT EFFICIENCY OF N_2 1P BANDS BY ELECTRON BOMBARDMENT OF AIR

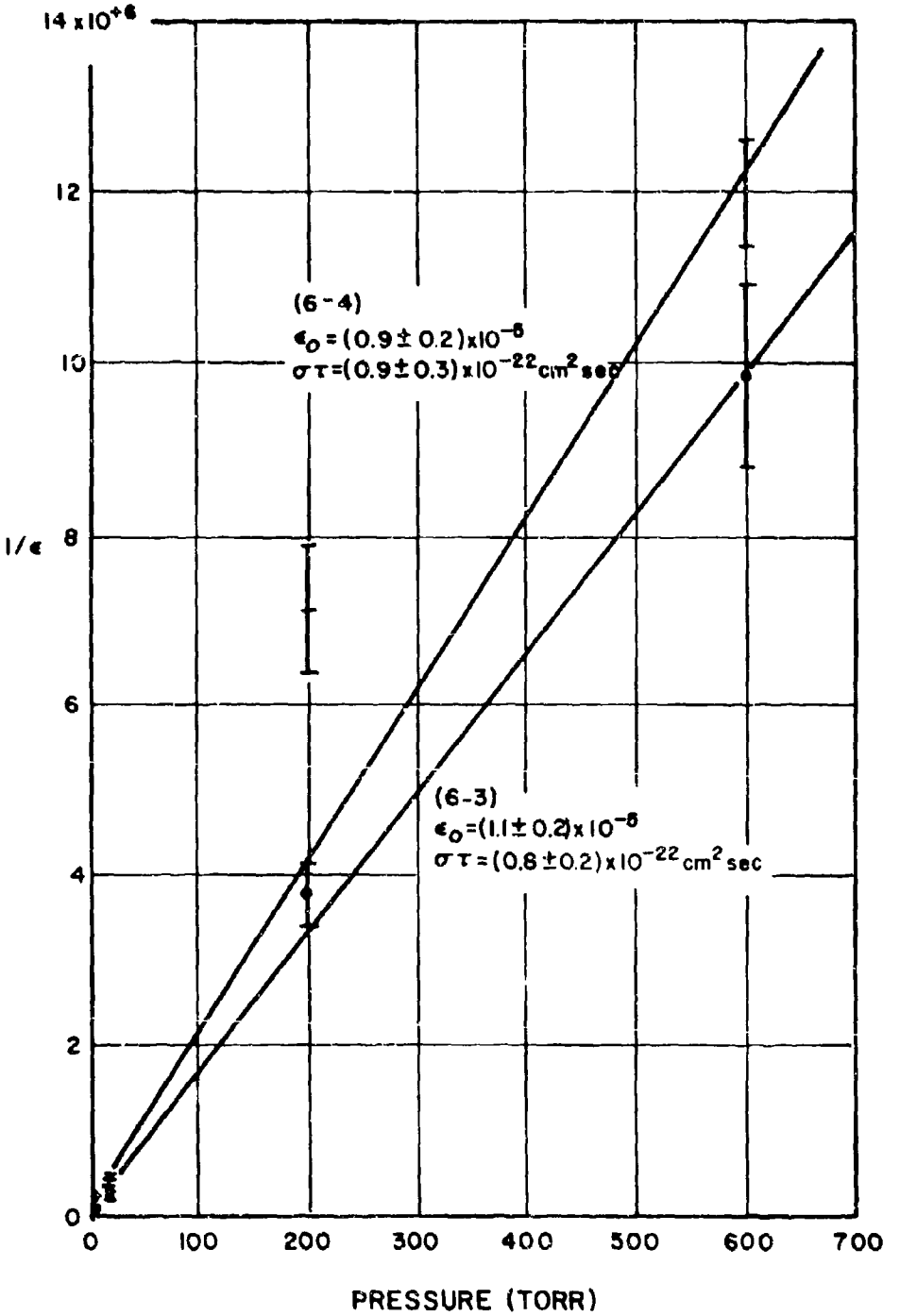

Figure 46

TABLE VIII

FLUORESCENT EFFICIENCIES OF THE N_2 FIRST POSITIVE BANDS EXCITED BY ENERGETIC ELECTRONS AND THE COLLISIONAL DEACTIVATION CROSS SECTIONS OF N_2 AND AIR

Transition	ϵ_c ($\times 10^{-5}$)		σ ($\times 10^{-17}$ cm^2)[a]	
	N_2	Air	N_2	Air
0-0		9 ± 9		5 ± 5
1-0	58 ± 16	30 ± 30	1.9 ± 0.5	7 ± 7
2-0	22 ± 6	13 ± 13	1.5 ± 0.4	6 ± 6
3-0		0.9 ± 0.4		2 ± 1
3-1		6 ± 3		3 ± 1.5
4-1		2.9 ± 1.5		4.8 ± 2.6
5-2		4.8 ± 3.7		6.5 ± 5
5-3	3.0 ± 0.6	2.2 ± 0.7	1.1 ± 0.3	2.2 ± 0.7
6-3		1.1 ± 0.2		1.4 ± 0.3
6-4		0.9 ± 0.2		1.4 ± 0.4

[a]The collisional deactivation cross sections are based on the radiative lifetimes of Jeunehomme.

4. THIN TARGET CONDITIONS

In the thin target studies the gas pressure was reduced such that the energetic primary electron lost a small fraction of its energy in crossing the observation region of the target chamber. The collimated energetic electron beam in the thin target case facilitates the distinction between primary and secondary electron excitation based on the spatial distribution of the emittance. The thin target measurements presented in this report are limited to the first negative and Meinel bands of N_2^+. As observed in this experiment these band systems were excited by primary energetic electrons.

4.1 Target Chamber

The target chamber design for the thin target measurements is shown in Figure 47. Wall effects, including emissions due to secondary electrons produced by the impact of the electron beam on the end of the target chamber, were isolated from the observation region by two copper baffles. Figure 48, photographs of the thin target fluorescence, illustrates the effectiveness of the baffles in isolating wall effects from the observation region where the thin target measurements were made.

A single 3 x 9 mm differentially pumped nozzle maintained a maximum pressure of 5×10^{-4} Torr in the electron gun section while the target pressure ranged from 10^{-4} to 5×10^{-2} Torr. The isolated target chamber functioned as a Faraday cup to measure the electron beam current.

Target chamber pressure was measured with a National Research Corporation "Alphatron" gauge. The "Alphatron" gauge was calibrated over the range of 0.02 to 1.0 Torr with a McLeod gauge which read approximately 10 percent lower than the "Alphatron" gauge. Recently, Schram et al[14] have discussed a pumping effect of mercury vapor in McLeod gauges previously reported by others. Mercury vapor diffusing from the reservoir causes a pressure gradient between the gauge and the cold trap conventionally used to isolate the vacuum system from the gauge. This effect results in a low McLeod gauge reading. Schram's pressure readings

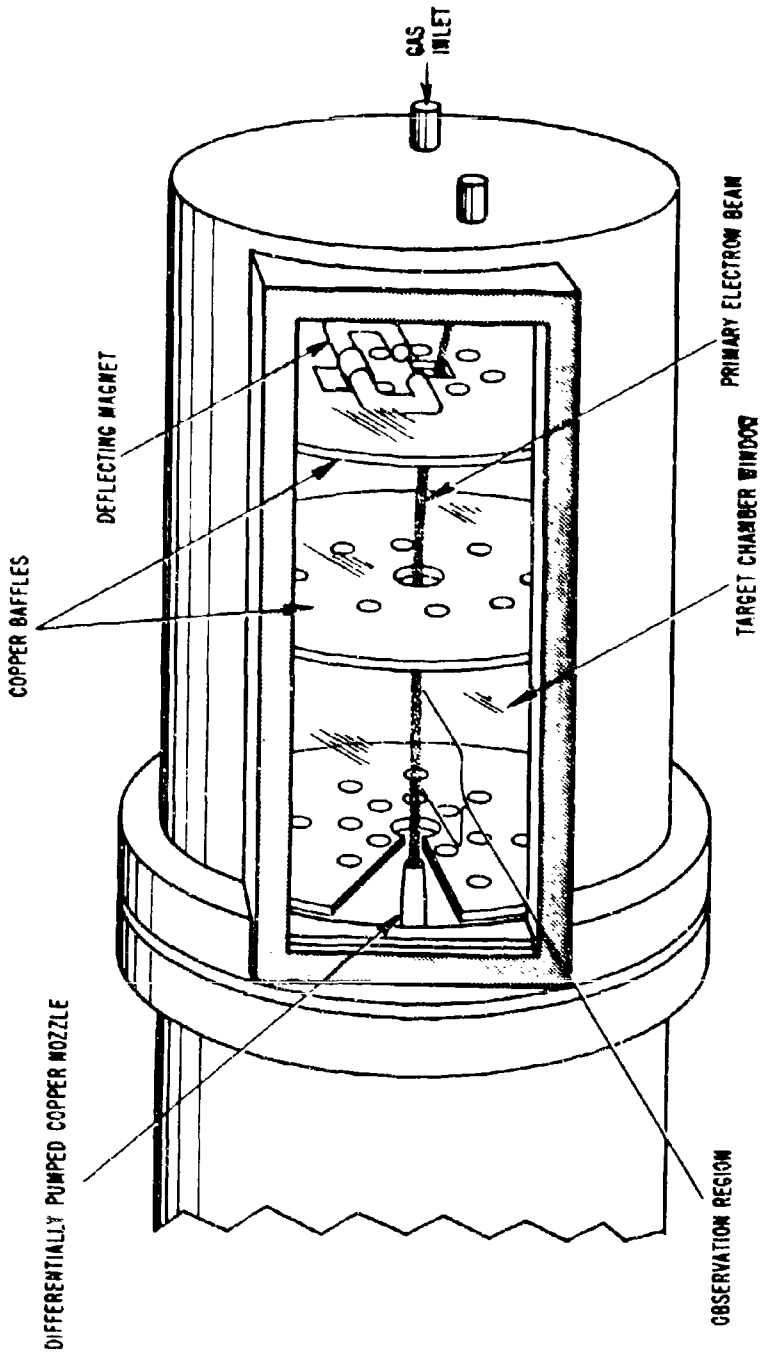

TARGET CHAMBER FOR THIN TARGET CASE

Figure 47

THIN TARGET FLUORESCENCE

N_2 AT 10^{-2} TORR, 50 keV ELECTRONS, 5 mg BEAM CURRENT, 10 PERCENT DUTY CYCLE

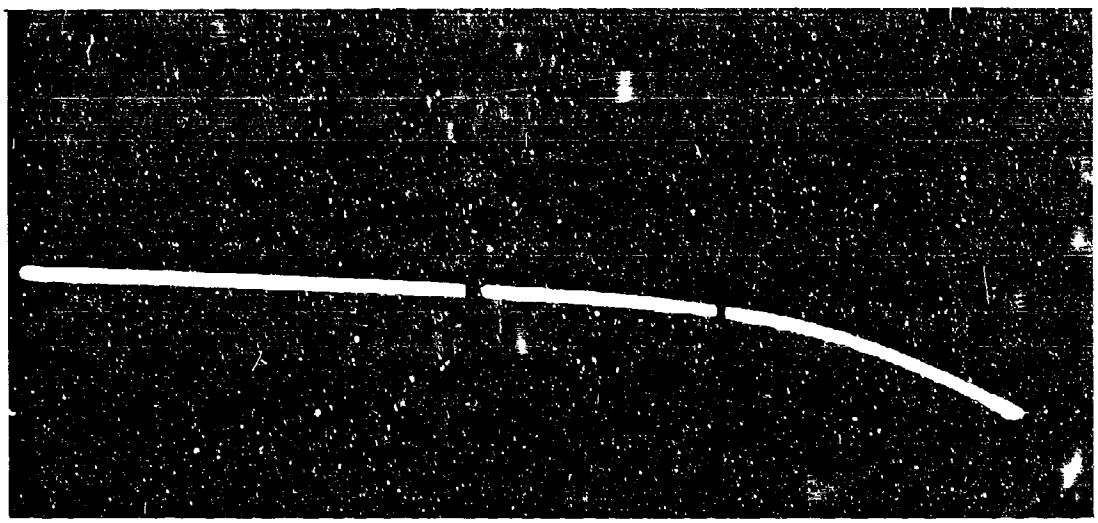

a. 1 MINUTE EXPOSURE

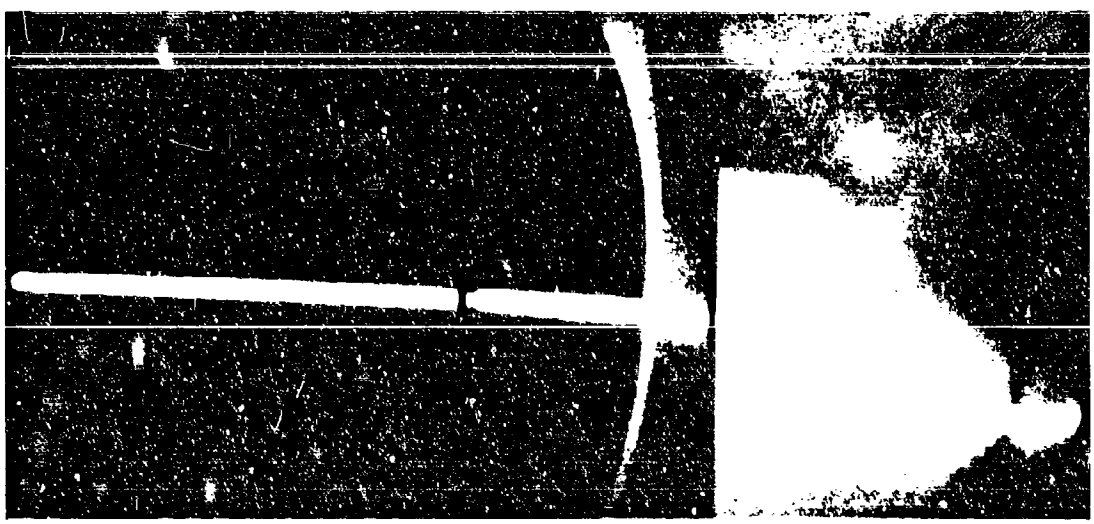

b. 10 MINUTE EXPOSURE

Figure 48

of nitrogen increased 8 percent by placing a cold trap immediately above the mercury reservoir. The magnitude of the mercury pumping effect is a function of the gas, mercury temperature and the dimensions of the gauge. Assuming this effect accounts in part for the lower McLeod gauge reading, the "Alphatron" gauge absolute accuracy is believed to be within five percent over the range 3×10^{-4} to 5×10^{-2} Torr.

4.2 Recording Spectra

Figure 49 is a spectrogram of the emission in N_2 at 5×10^{-2} Torr excited by 50 kev electrons. The spectra were recorded with a series of gratings and photomultipliers and corrected for the system spectral response as previously discussed in the thick target results. The monochromator was positioned such that the long dimension of the electron beam was parallel to the entrance slit. The electron beam was imaged on the 2 x 20 mm entrance slit by a condensing lens resulting in an optical gain that was inversely proportional to the width of the fluorescing beam. The optical gain was approximately one for the first positive bands and progressively increased for the second positive, Meinel and first negative system (optical gain of approximately ten). The long exposure of Figure 48 illustrates the emission was not confined to the path of the primary electron beam. The 3914 Å emission excited by the primary electron beam is an accurate measure of the beam width. Since little momentum is transferred in electron excitation, the velocities of the excited molecules are described by a room temperature Boltzman distribution. The average 3914 Å emitter travels only 3×10^{-2} mm over one radiative lifetime (6.58×10^{-8} sec). Sheridan, Oldenberg and Carleton[29] photographed the beam width of the 3914 Å band and the (2-0) Meinel band emission due to electron excitation and estimated the (2-0) Meinel band lifetime as 3×10^{-6} seconds based on the width of the fluorescent beam. This value yields an average single lifetime travel of 1.4 mm. The first and second positive bands of N_2 are excited principally by low energy secondary electrons and account for the emission outside the primary electron beam of Figure 48. Thompson and

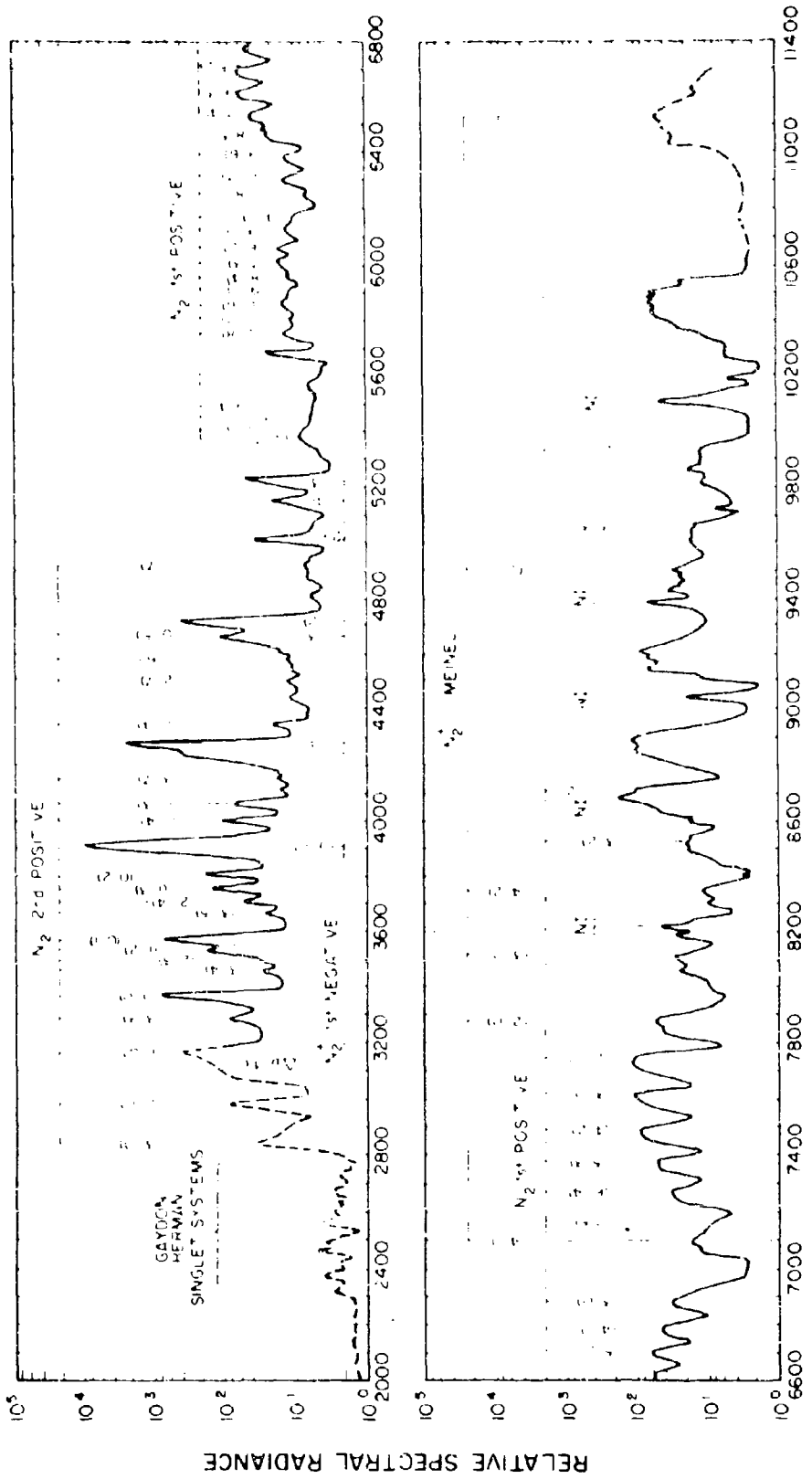

RELATIVE SPECTRAL RADIANCE OF NITROGEN AT 5×10^{-2} TORR EXCITED BY 50 kev ELECTRONS

Figure 49

Williams[30] as well as Stewart, Cribbon and Emeleus[31] have reported the same general effect for the first positive bands. Fan[32] presents the same general spatial distribution for electron beam excitation. However, Fan's spectrographic measurements indicate a wider electron beam fluorescence for the first negative bands than the Meinel bands.

The (2-0), (1-0) and (0-0) Meinel band measurements were made with three bandpass interference filters mounted on a liquid nitrogen cooled photomultiplier (RCA 7102) with S-1 response. A tubular collimator limited the angle of incidence to a maximum of 7.5 degrees off the normal. The collimator ensured that the bandpass of the filters did not substantially shift to lower wavelengths for off axis illumination. The filters were effective in isolating the Meinel bands from adjacent spectra for normal incidence illumination.

4.3 Meinel Band Lifetime Measurements

The Meinel bands of N_2^+, first identified in aurora, have been excited by an energetic electron beam by Sheridan, Oldenberg and Carleton.[29] In addition to a 3×10^{-6} second lifetime for the (2-0) band, a N_2 collisional quenching cross section of 2×10^{-14} cm^2 was presented.

In the present experiment the lifetimes of the (0-0), (1-0) and (2-0) Meinel bands were measured. A low signal to noise ratio prevented the fluorescence decay from being displayed on an oscilloscope and measured directly. Two experimental techniques were used to measure the radiative lifetimes. Figure 50 illustrates the experimental arrangement for the technique using a gated input to a phase sensitive amplifier. The gate width was controlled by a pulser which also provided a continuously variable delay from an external reference (electron beam pulse). This technique allowed the narrow band phase sensitive amplifier to scan the fluorescence decay of the photomultiplier output. Initial results indicated the Meinel band lifetimes to be pressure dependent and range from 2 to 5×10^{-6} seconds over the pressure range of 3 to 20×10^{-3} Torr. The gated sample width was 0.4×10^{-6} seconds and the electron beam

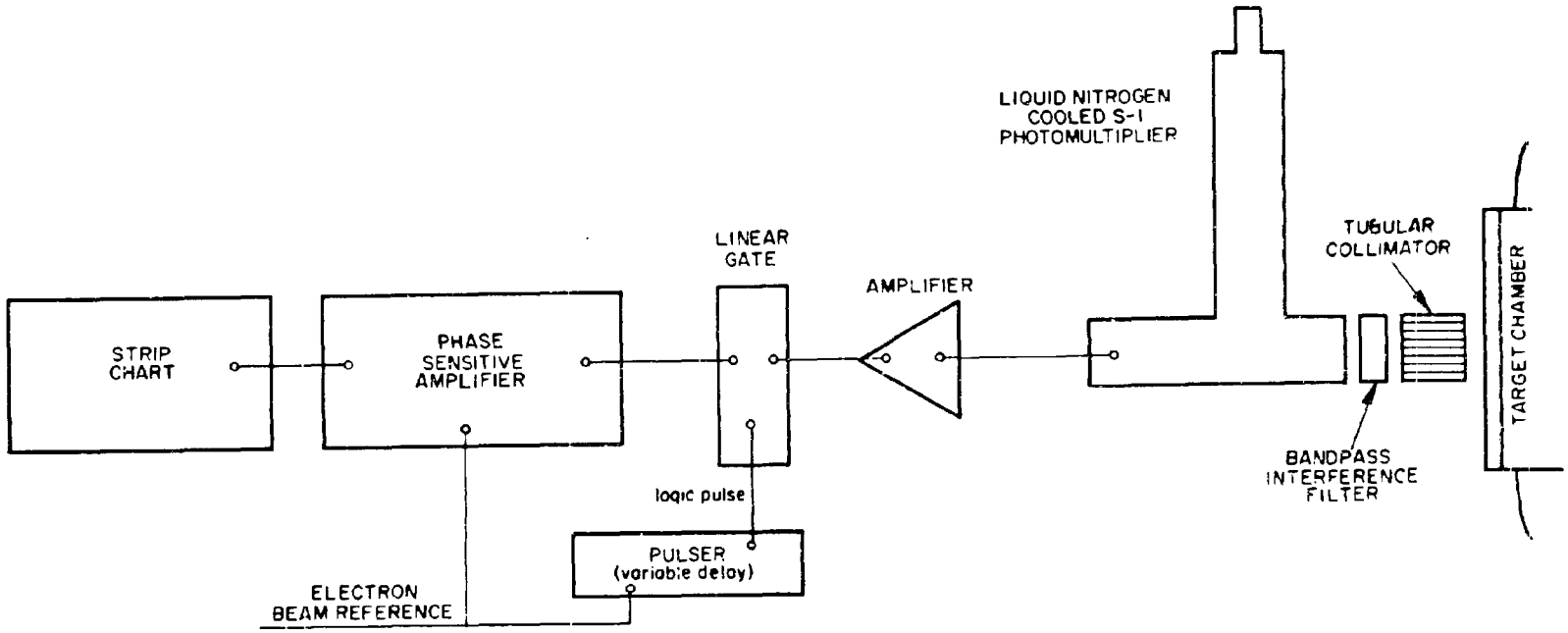

OSCILLOSCOPE DISPLAY

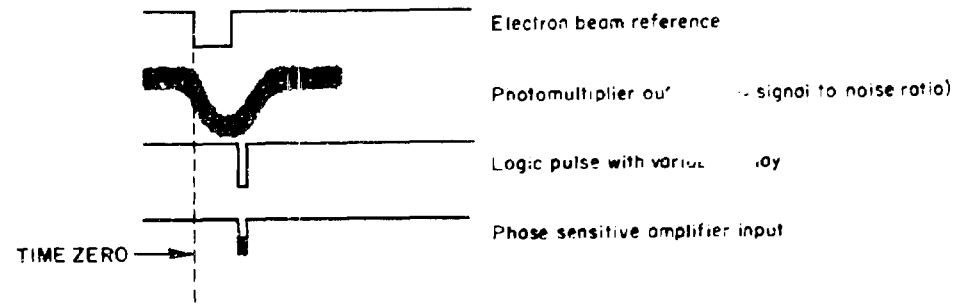

Figure 50

EXPERIMENTAL ARRANGEMENT TO MEASURE MEINEL BAND LIFETIMES

modulation frequency 2×10^4 Hz for most of the lifetime measurements with the linear gate technique. The phase sensitive amplifier was tuned for a logic pulse with no delay from the arbitrarily defined zero time. Introducing a delay to the logic pulse detuned the phase sensitive amplifier. The amplitude of the fluorescence decay was corrected for the effective decrease in the gain of the amplifier which was proportional to the cosine of the angular delay.

In the second experimental technique the amplifier output was applied to a Princeton Applied Research waveform eductor, an instrument designed to recover repititive waveforms from low signal to noise ratio inputs. In the waveform eductor, the repititive waveform is divided into one hundred segments which are switched sequentially and synchronously through a resistor to memory capacitors where the average signal is obtained and stored. The information in the memory was read out on a strip chart recorder. The minimum sample time per channel was one microsecond. The Meinel band lifetimes were corrected for a system rise time of about one microsecond caused by the limitation of the waveform eductor high frequency bandwidth.

The measured lifetimes are based on the exponential decay of the fluorescence over approximately an order of magnitude of intensity. It has been assumed that the fluorescence decay is described by a single exponential decay. Worsley[33] has treated the problem of extracting multiple exponential decays from experimental data. It is necessary that the experimental data be very accurate in order to be meaningfully described by a sum of exponentials. In addition, observation of the intensity decay over several orders of magnitude may be necessary. Even with these conditions satisfied, the determination of several coefficients and exponents by curve fitting can be ambiguous. With the accuracy of the data of this experiment and the limited range of intensity observed, a single exponential decay is the only meaningful interpretation.

The pressure dependence of the lifetimes of the (2-0), (1-0) and (0-0) Meinel bands are presented in Figures 51, 52 and 53. For most of the data the results the two experimental methods show no measurable difference. However, at the higher pressures the lifetimes measured for the (2-0) band with the waveform eductor are significantly larger than the values measured with the linear gate technique. This effect is believed to be due to overlapping by a first positive band which increases the lifetime measured with the waveform eductor at high pressures. As subsequently shown, the intensity of first positive bands increases faster than pressure while the Meinel band intensity increases less than the pressure in this range. Thus, fluorescence within the bandpass of the interference filter of the overlapping first positive emission should increase at higher pressures. Figure 10 indicates the relatively weak (7-6) first positive band coincides with the (2-0) Meinel band. Jeunehomme[28] has shown the fluorescence decay of the first positive bands in an rf discharge are described by tne sum of three exponential decays. The natural radiative lifetime (presumably the fastest exponential decay) for the seventh upper vibrational level is 5.3×10^{-6} seconds. This minimum value of the several first positive decay rates is larger than the (2-0) Meinel band lifetime at the higher N_2 target gas pressures. In the case of the linear gate technique the modulation frequency was 2×10^{4} Hz compared to 5×10^{3} Hz for the waveform eductor. Operating at a 10 percent duty cycles, the electron beam pulse width was 5×10^{-6} seconds for the linear gate and 20×10^{-6} seconds for the waveform eductor measurements. The narrow beam pulse used in the linear gate case has reduced the relative intensity of the longer lived overlapping first positive bands. This interpretation is supported by Figure 54 which shows lifetime measurements of the (2-0) Meinel band as a function of pulse width at two N_2 gas pressures $(5.3 \text{ and } 23) \times 10^{-3}$ Torr. The 5.3×10^{-3} Torr lifetime is independent of pulse width, while the 23×10^{-3} Torr data shows a significant decrease in lifetime at narrow pulse widths.

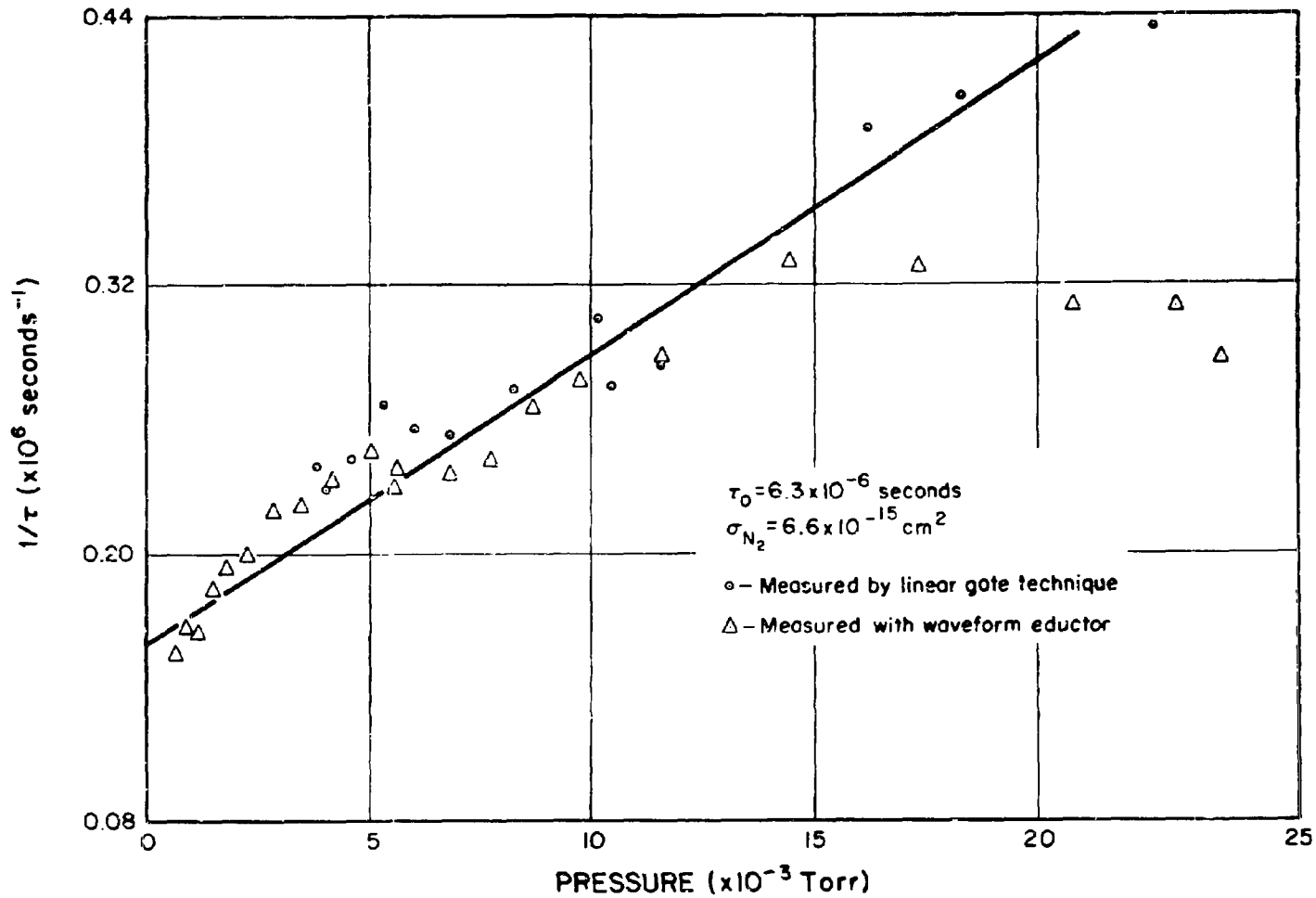

Figure 51

PRESSURE DEPENDENCE OF THE (2-0) MEINEL BAND LIFETIME

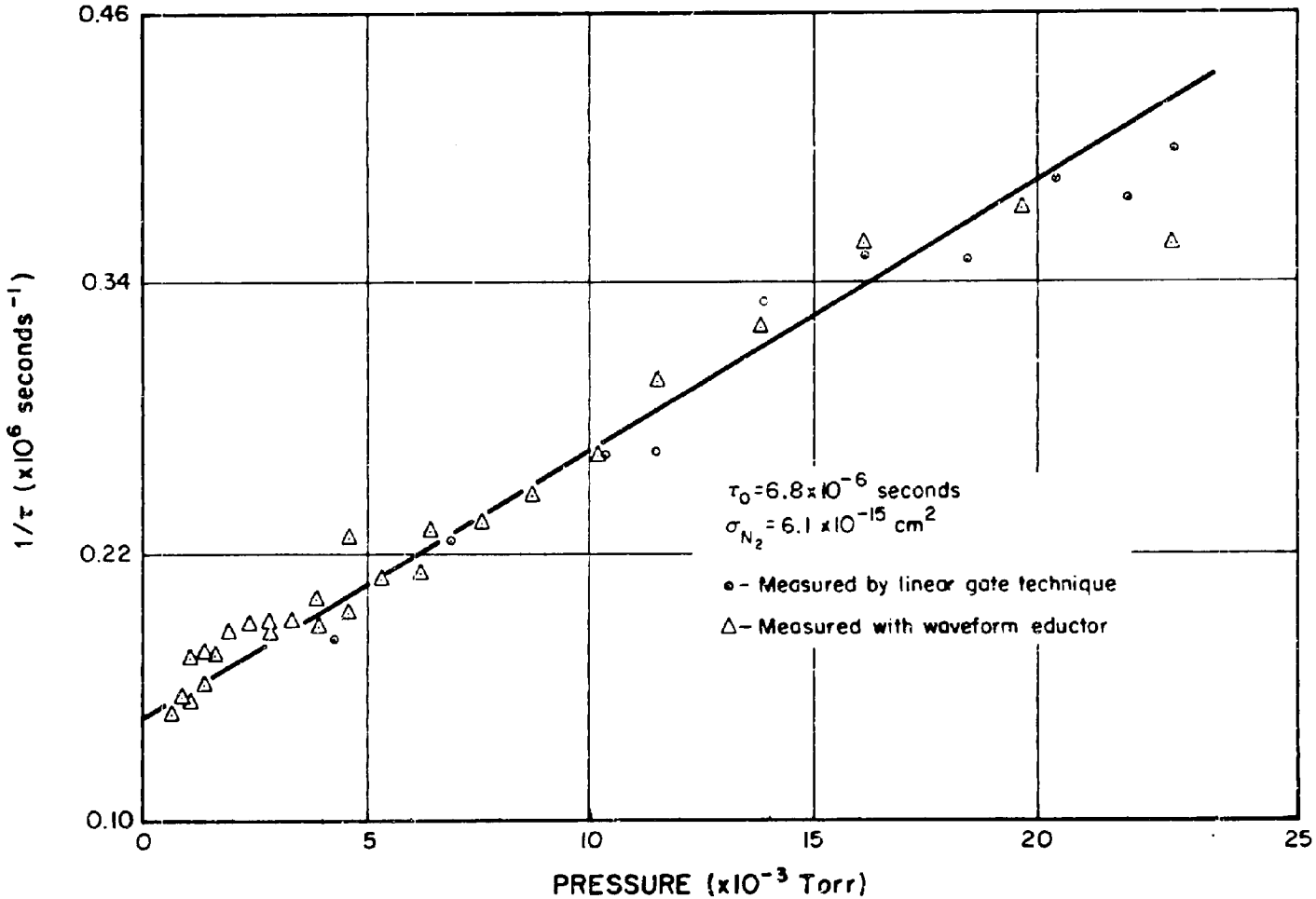

Figure 52

PRESSURE DEPENDENCE OF THE (1-0) MEINEL BAND LIFETIME

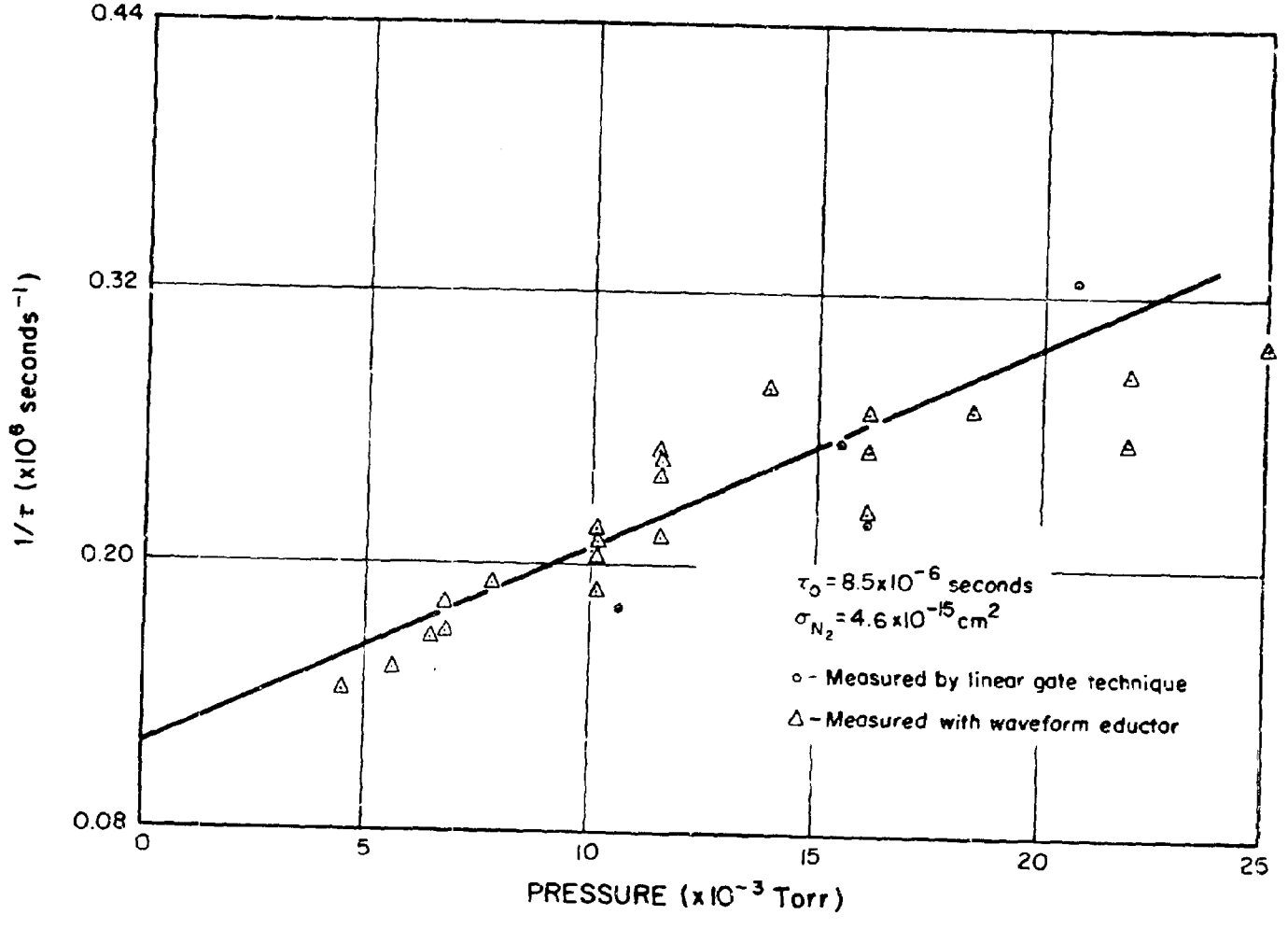

Figure 53

PRESSURE DEPENDENCE OF THE (0-0) MEINEL BAND LIFETIME

MEASURED LIFETIME FOR (2-0) MEINEL BAND VS ELECTRON BEAM PULSE WIDTH

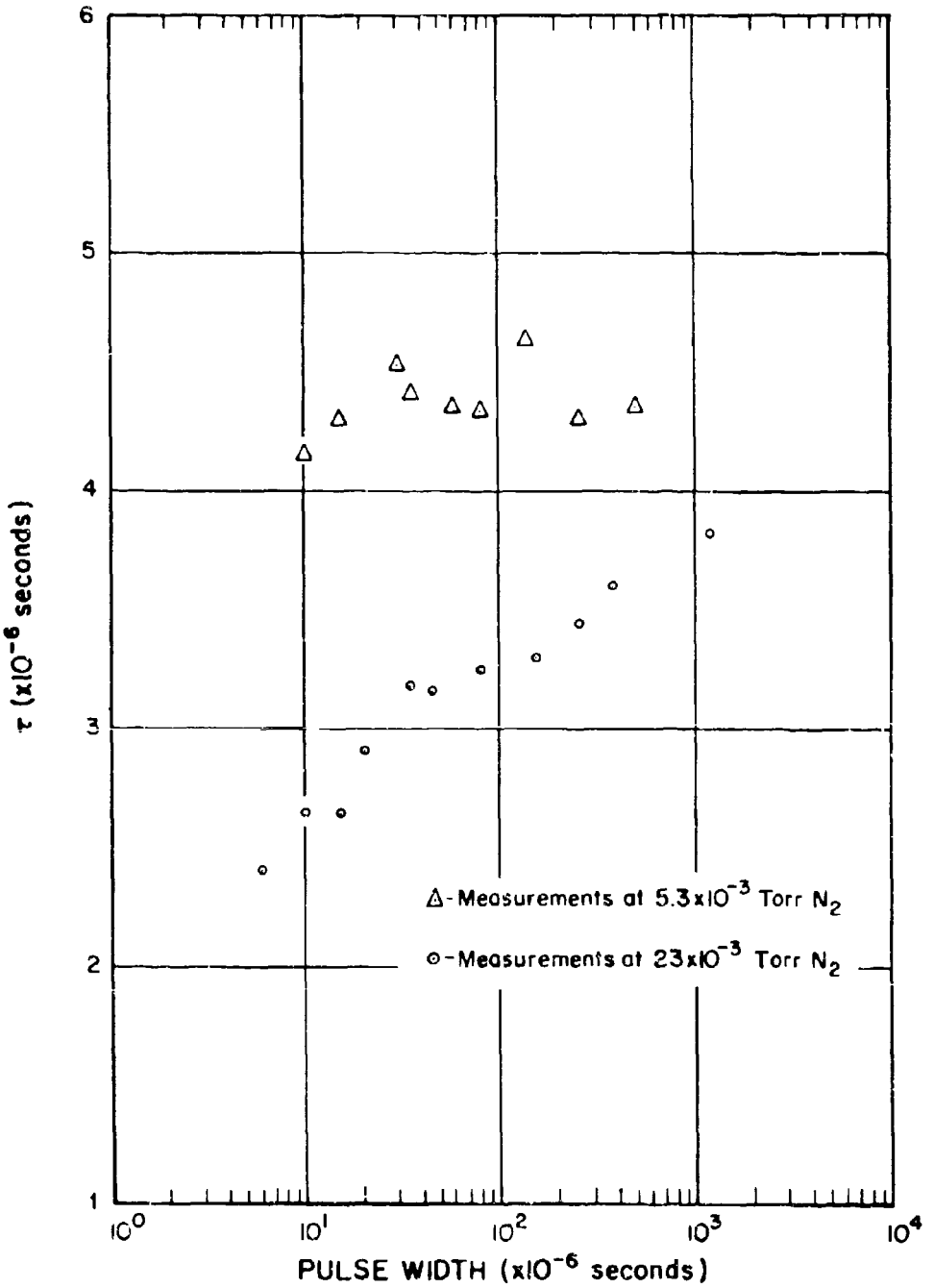

Figure 54

Figures 51, 52 and 53 have been analyzed by a Stern-Volmer quenching expression of the form

$$1/\tau = 2.2.10^{21} \sigma P + 1/\tau_o$$

where τ is the observed fluorescence decay time, σ the collisional quenching cross section of N_2, P the pressure in Torr and τ_o the natural radiative lifetime. The collisional quenching cross section of N_2 has been estimated as 6.6×10^{-15} cm^2 for the (2-0) band, 6.1×10^{-15} cm^2 for the (1-0) band and 4.6×10^{-15} cm^2 for the (0-0) band. The respective values of τ_o are 6.3×10^{-6}, 6.8×10^{-6}, and 8.5×10^{-6} seconds. Sheridan, Oldenberg and Carleton measured a value of 6×10^{-20} cm^2 seconds for the product of the (2-0) band lifetime and the N_2 quenching cross section. This experiment indicates a value of 4.2×10^{-20} cm^2 seconds for this quantity.

4.4 Meinel Band Collisional Deactivation Cross Sections

In the previous section the N_2 collisional quenching cross section was measured by observing the pressure dependence of the exponential decay of the Meinel band fluorescence. Measuring the less than linear increase of the Meinel band intensity with pressure in the range of 0.3 to 20×10^{-3} Torr is an alternative method of measuring the collisional deactivation cross section. In this method two photomultipliers were used to observe the electron beam fluorescence as a function of target gas pressure. A cooled photomultiplier with S-1 response was fitted with either one of the three Meinel band interference filters and the tubular collimator. A narrow band interference filter that isolated the first negative (0-0) band at 3914 Å was mounted on a second photomultiplier with an S-11 photocathode response. The intensities of both the 3914 Å band and either the (2-0), (1-0) or (0-0) Meinel band were measured by the phase sensitive amplifier as a function of the target gas pressure measured by the "Alphatron" gauge. The pressure dependence of the 3914 Å band for a typical case is presented in Figure 55. The slight scatter about the linear relationship is due to errors in the pressure measurement. The best linear fit of the data has been used to define a corrected pressure for each

THIN TARGET 3914Å BAND RADIANCE EXCITED BY 50 keV ELECTRONS

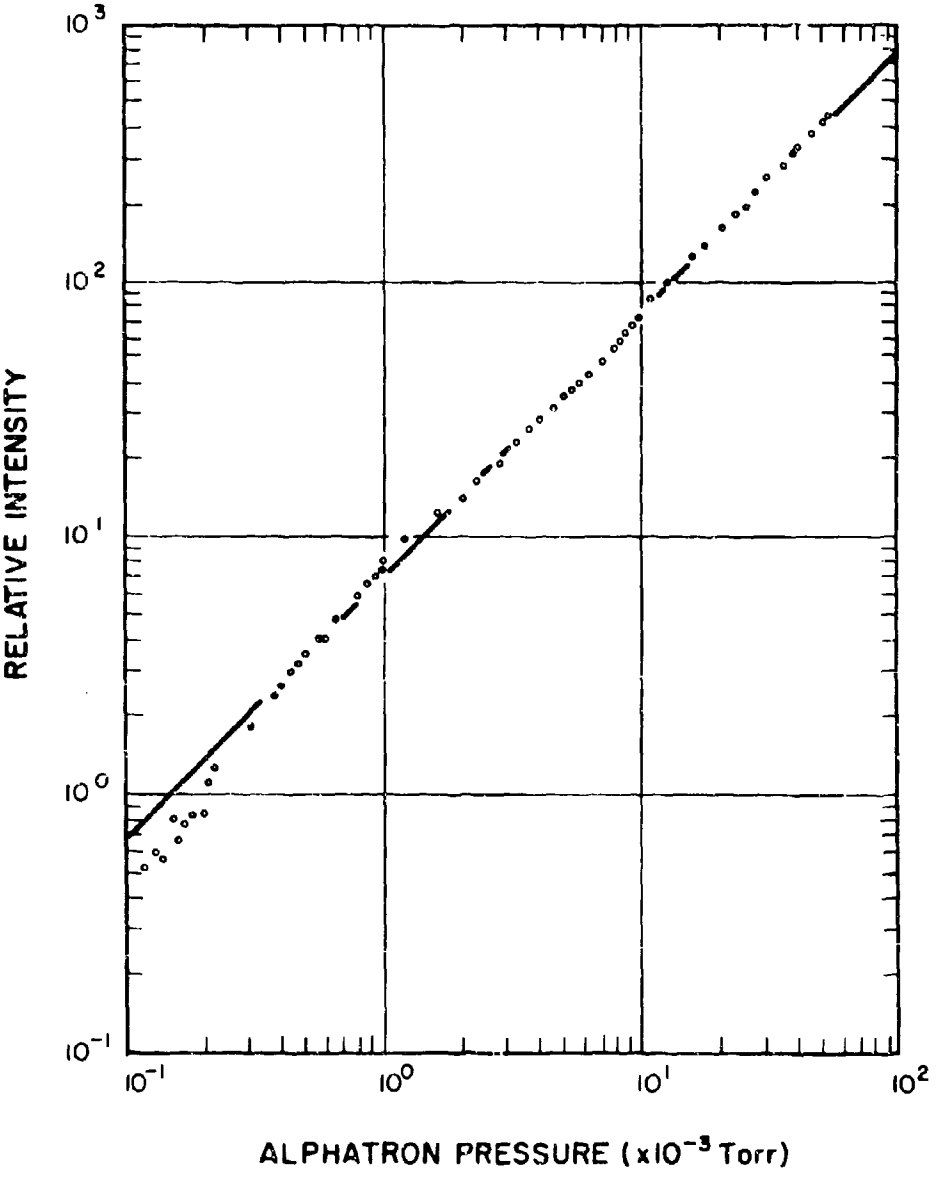

Figure 55

1602

data point. The corresponding Meinel intensity at each pressure is plotted against the corrected pressure value in the form of a Stern-Volmer plot in Figures 56 through 61. The figures indicate that the Stern-Volmer quenching expression is valid over limited pressure ranges and, the Meinel band intensity as recorded, is frequency dependent.

The fundamental harmonic of the fluorescence in a given transition excited by a modulated electron beam is shifted in phase because of a finite radiative lifetime. The magnitude of the phase shift is expressed by

$$\angle\ \theta = \arctan 2\ \pi\ f\ \tau$$

where f is the electron beam modulation frequency and τ is the radiative lifetime. In addition to the phase shift, the amplitude of the fundamental harmonic is attenuated as described by an expression of the form

$$A = [\ 1 + (2\ \pi\ f\ \tau)^2\ ]^{-1/2}$$

where A represents the amplitude attenuation. The phase sensitive amplifier was tuned in each instance for maximum signal output for the 3914 Å band. For the modulation frequencies used (2×10^4 Hz maximum) the 3914 Å band ($0.58 \cdot 10^{-8}$ second lifetime) was essentially a measure of the electron beam phase. The Meinel band intensity as measured in the fundamental harmonic by the phase sensitive amplifier is proportional to the product of the amplitude and the cosine of the angular delay. Thus the frequency dependence of the Meinel band intensity is described by

$$I = [\ 1 + (2\ \pi\ f\ \tau)^2\ ]^{-1}$$

as measured by the phase sensitive amplifier tuned for 3914 Å band. The previous section indicates the Meinel band lifetimes are on the order of 6×10^{-7} seconds. Thus at 6×10^3 Hz, it is anticipated the Meinel intensities will be reduced on the order of five percent from the magnitude measured at lower frequencies. However collisional quenching competes with fluorescence decay at higher pressures and causes an increase in the depopulation rate of the excited state. Thus in order to measure Meinel intensity as a function of the single variable pressure, modulation frequencies less than 6×10^3 Hz were used to avoid intensity attenuation at the longer decay times (low pressures).

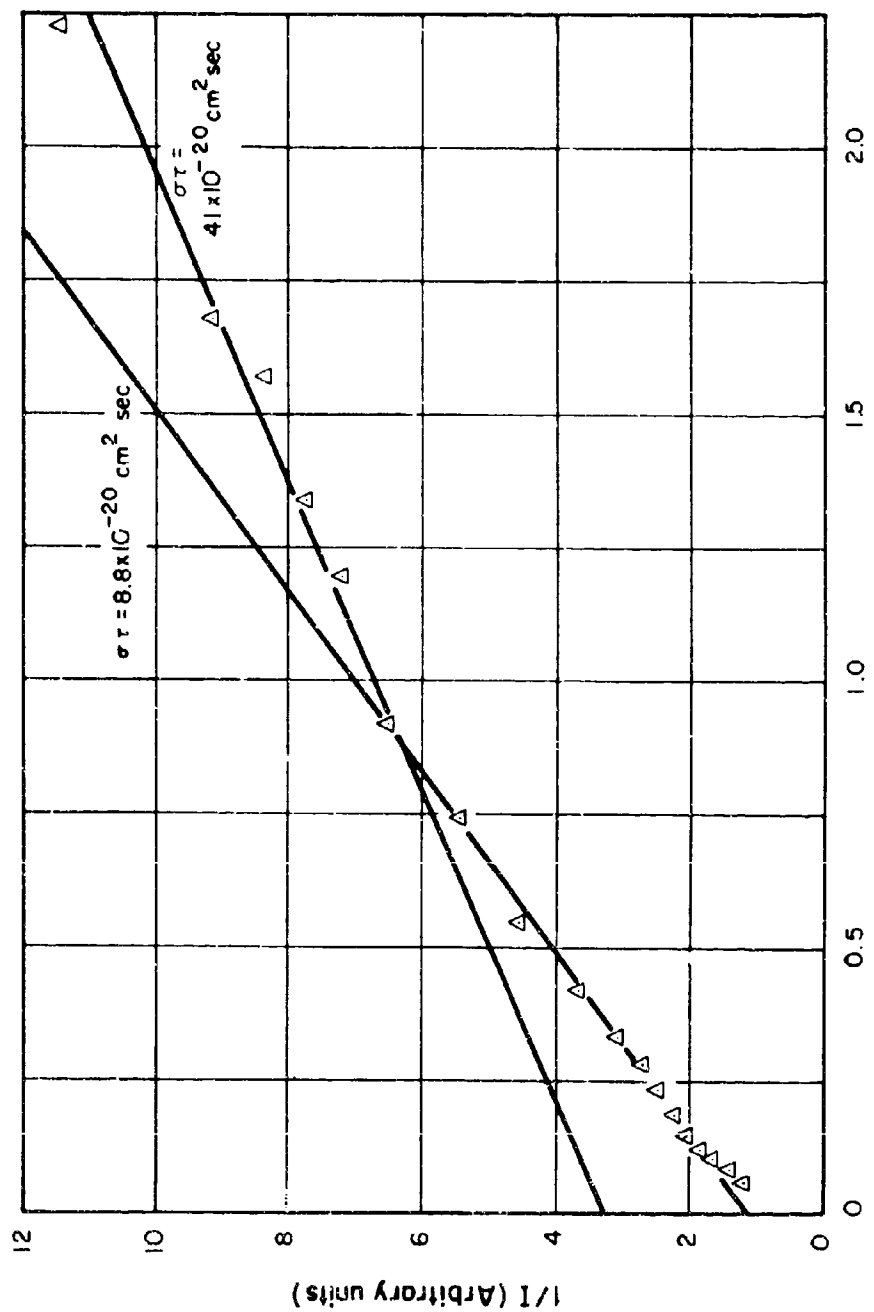

STERN-VOLMER PLOT (2-0) MEINEL BAND
150 HERZ MODULATION FREQUENCY

Figure 56

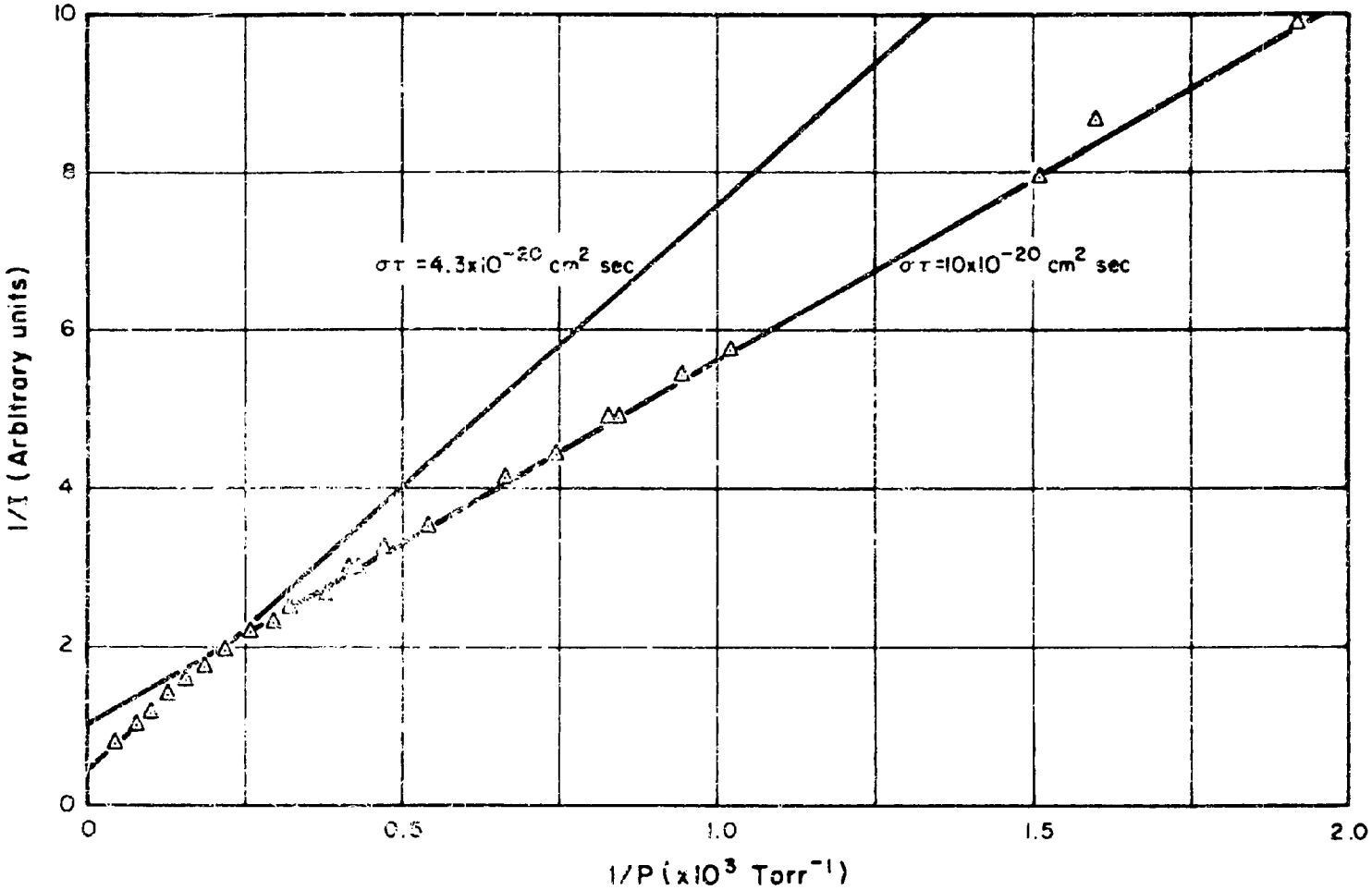

STERN-VOLMER PLOT (2-0) MEINEL BAND

5x10³ HERZ MODULATION FREQUENCY

Figure 57

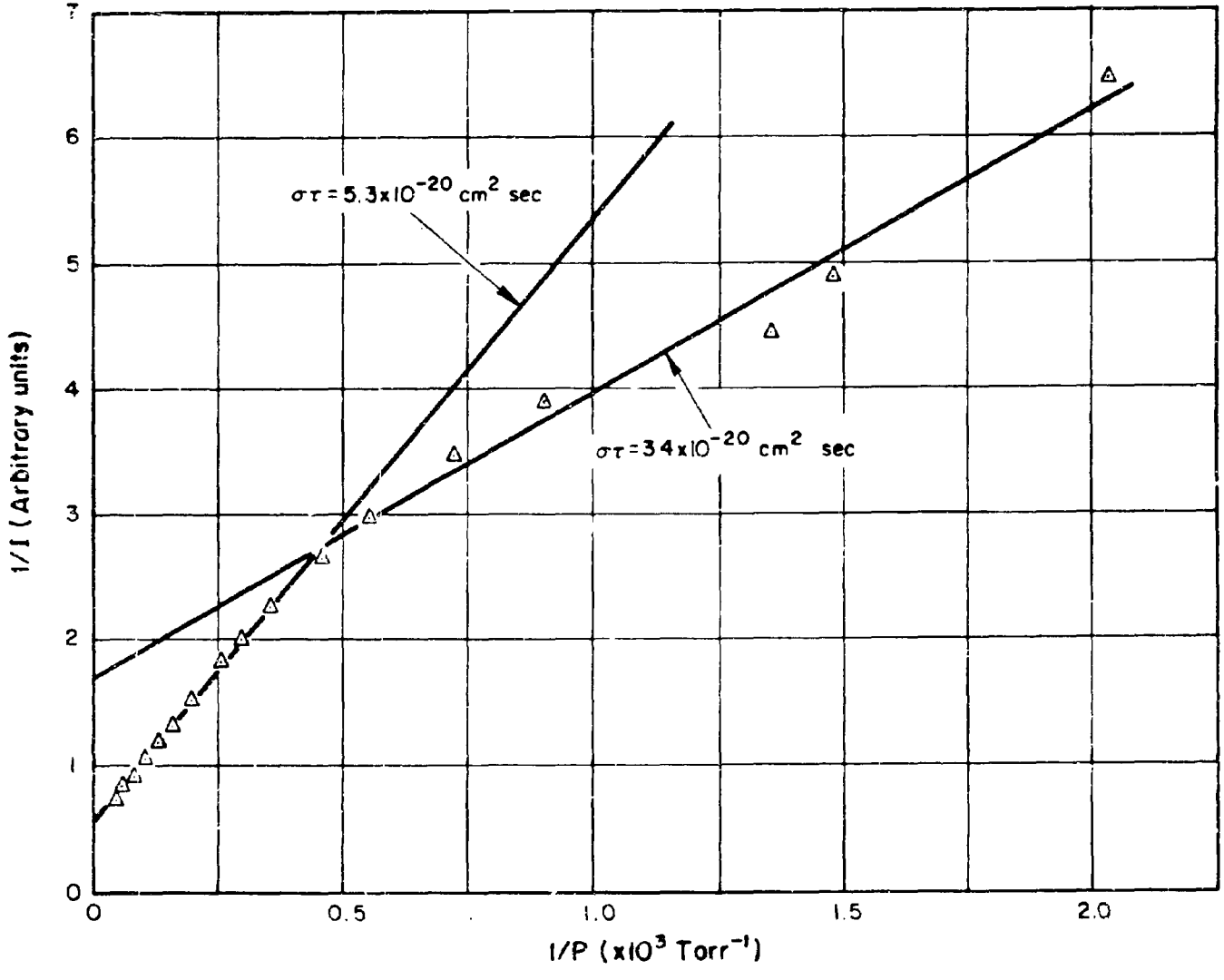

Figure 56

STERN-VOLMER PLOT (1-0) MEINEL BAND
150 HERZ MODULATION FREQUENCY

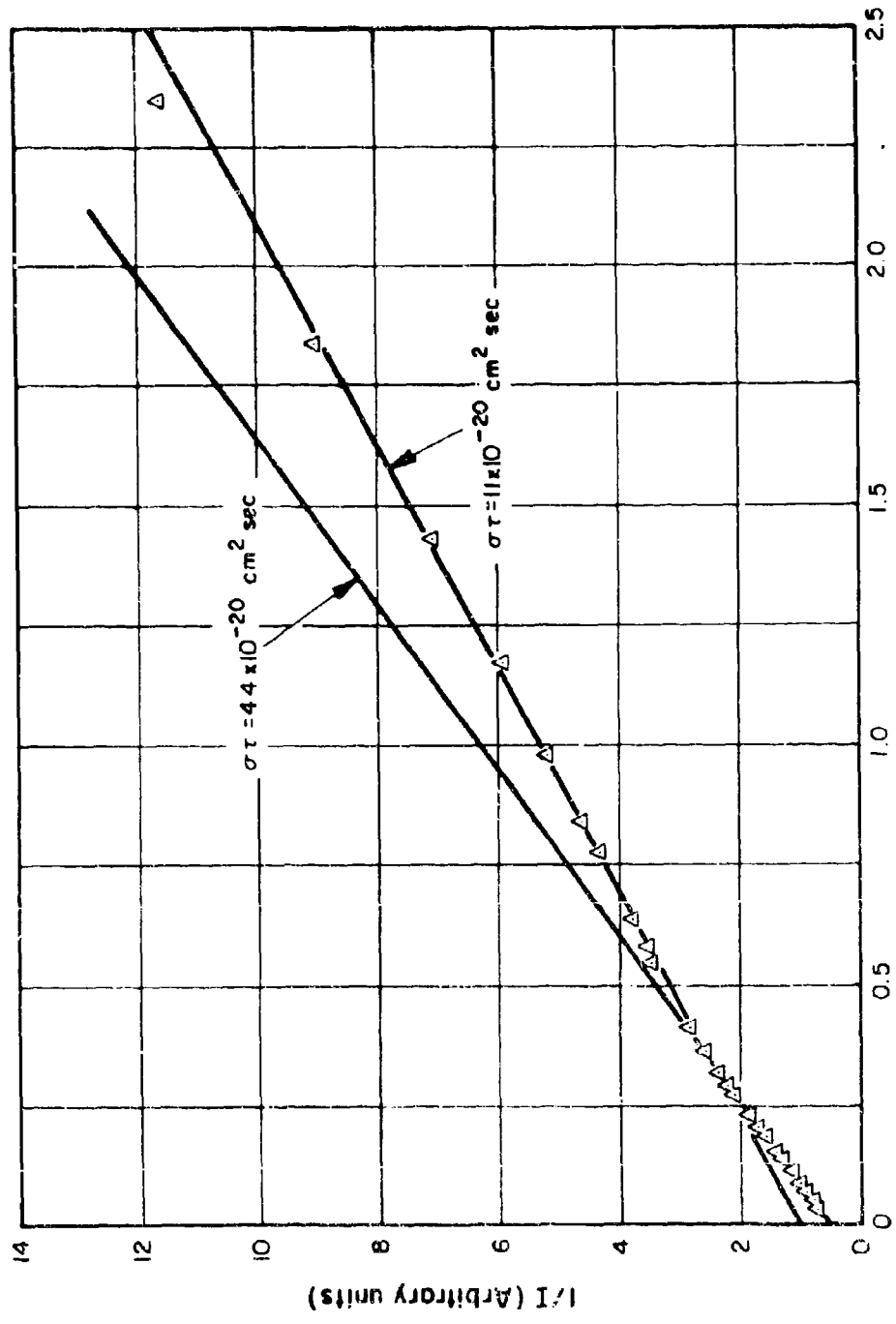

STERN-VOLMER PLOT (1-0) MEINEL BAND

5×10^3 HERZ MODULATION FREQUENCY

Figure 50

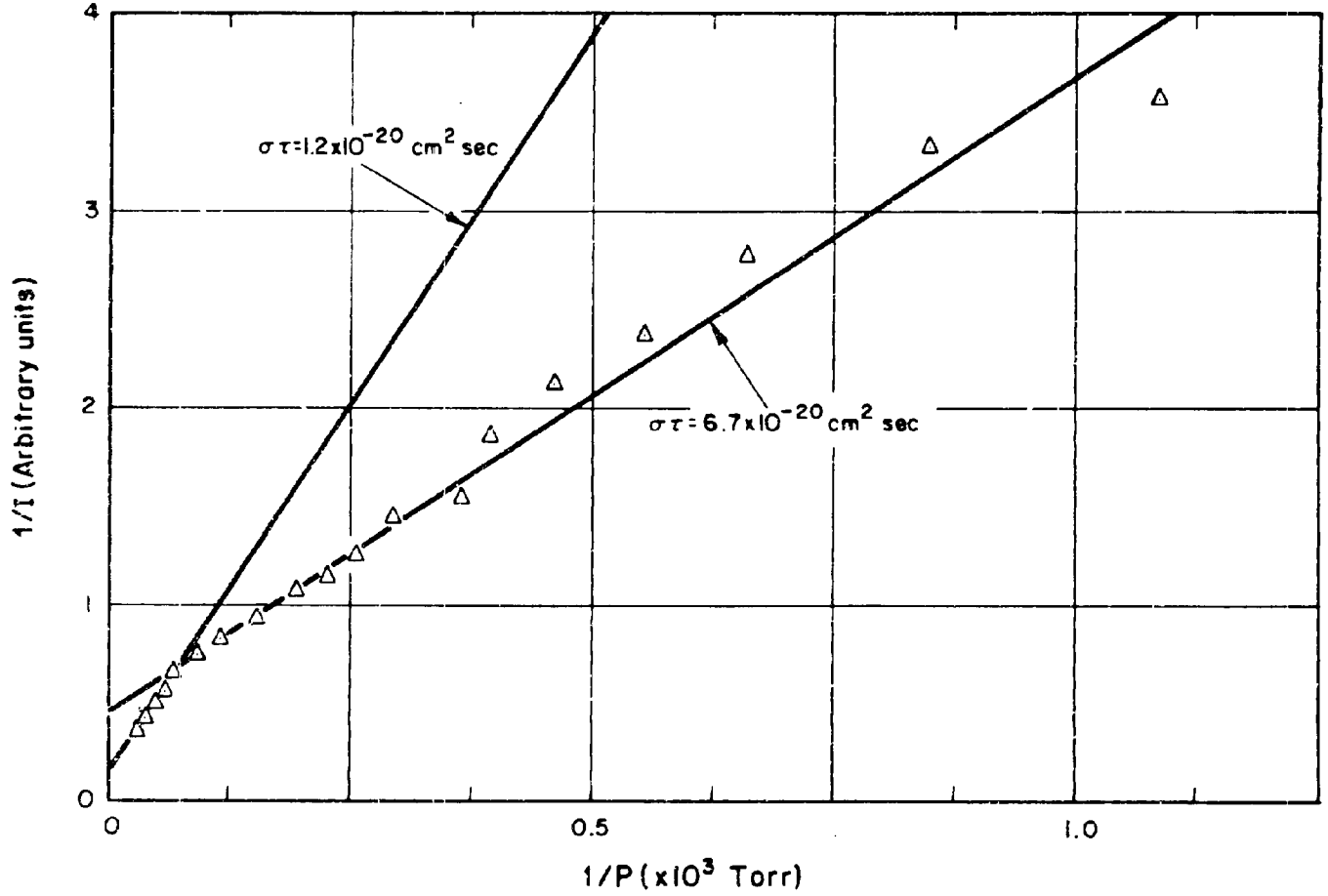

Figure 60

STERN-VOLMER PLOT (0-0) MEINEL BAND
150 HERZ MODULATION FREQUENCY

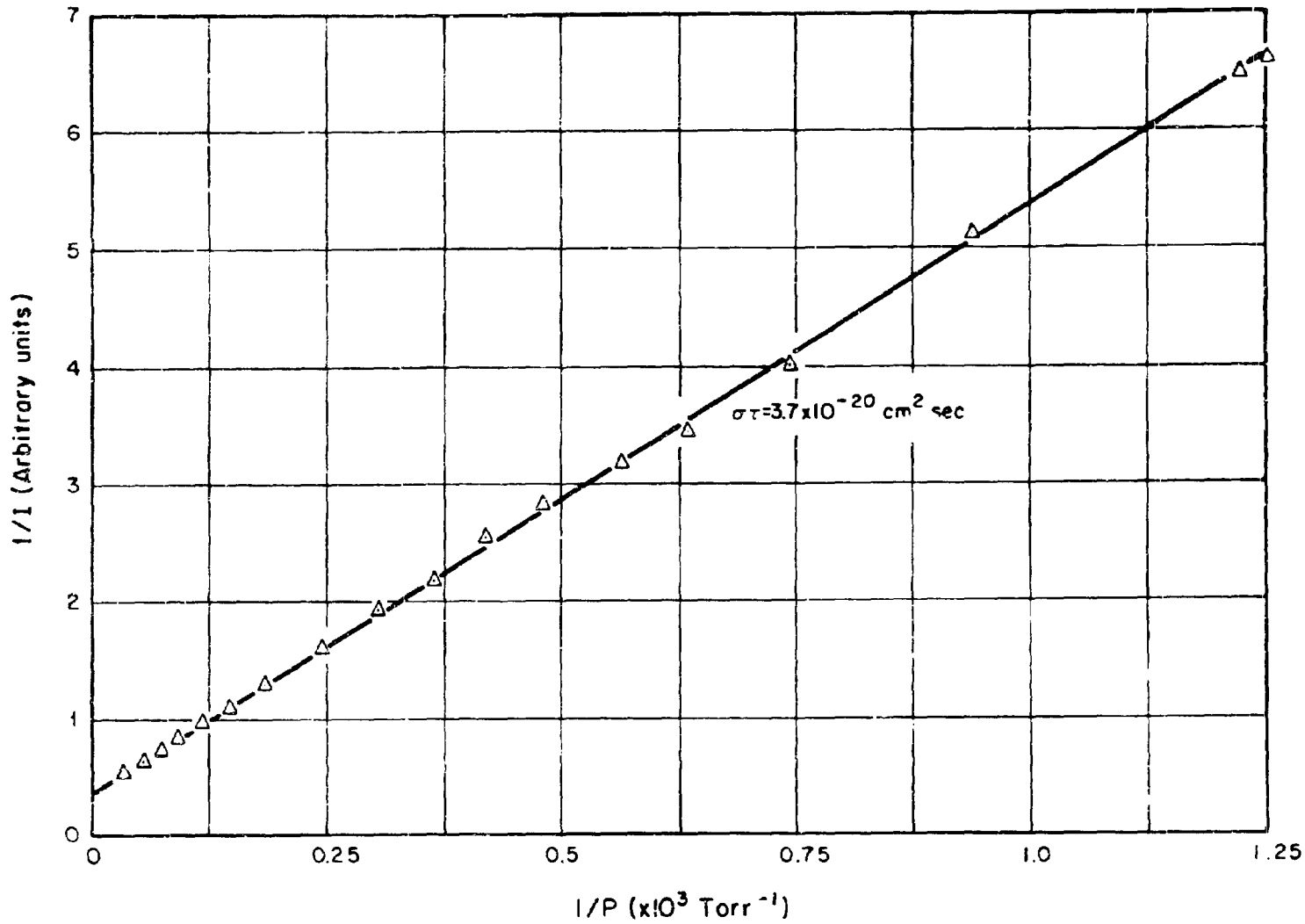

STERN-VOLMER PLOT (0-0) MEINEL BAND
5x10³ HERZ MODULATION FREQUENCY

Figure 61

In Figures 56 through 61 Stern-Volmer quenching was analyzed by an expression of the form

$$I^{-1} = \frac{2.16 \times 10^{21} \sigma\tau}{K} + \frac{1}{KP}$$

where I is the Meinel band intensity, K is a constant, τ the natural radiative lifetime, σ the collisional quenching cross section of N_2, and P the pressure in Torr. For the several linear sections of the figures the ratio of the intercept to the slope was calculated and expressed in the form of the $\sigma\tau$ product. The lifetime measurements of the previous section indicate that this quantity is 4.2×10^{-20} cm^2 seconds for the (2-0) bands, 4.1×10^{-20} cm^2 seconds for the (1-0) band, and 3.9×10^{-20} cm^2 seconds for the (0-0) band. Figures 56, 58 and 60 indicate that under similar conditions of modulation frequency (5×10^3 Hz) and pressure (2 to 20×10^{-3} Torr) this experiment confirms these values within experimental error. However, at lower modulation frequencies and lower pressures the magnitude of this parameter increases. The frequency dependence may be interpreted as emission within the bandpass of the interference filter with an apparent lifetime substantially greater than 6×10^{-6} seconds. The longer lived emission may be either overlapping spectra or Meinel band radiation due to an indirect excitation process.

The only known potentially overlapping emitter are the relatively weak first positive bands of N_2 that are coincident in wavelength with the Meinel bands. Figure 62 indicates the pressure dependence of several first positive bands near 6600 Å. The greater than linear intensity increase with pressure occurs until the range of the secondary electrons is confined within the field of view. Considering the less than linear intensity increase of the Meinel bands with pressure, first positive band overlap is anticipated at higher pressures. As discussed in the previous section, the first positive overlap recorded by the phase sensitive system is expected to decrease at higher modulation frequencies due to amplitude attenuation and phase shift of the fundamental frequency caused by first positive longer radiative lifetimes. Thus if first positive band overlap is proposed as the reason for

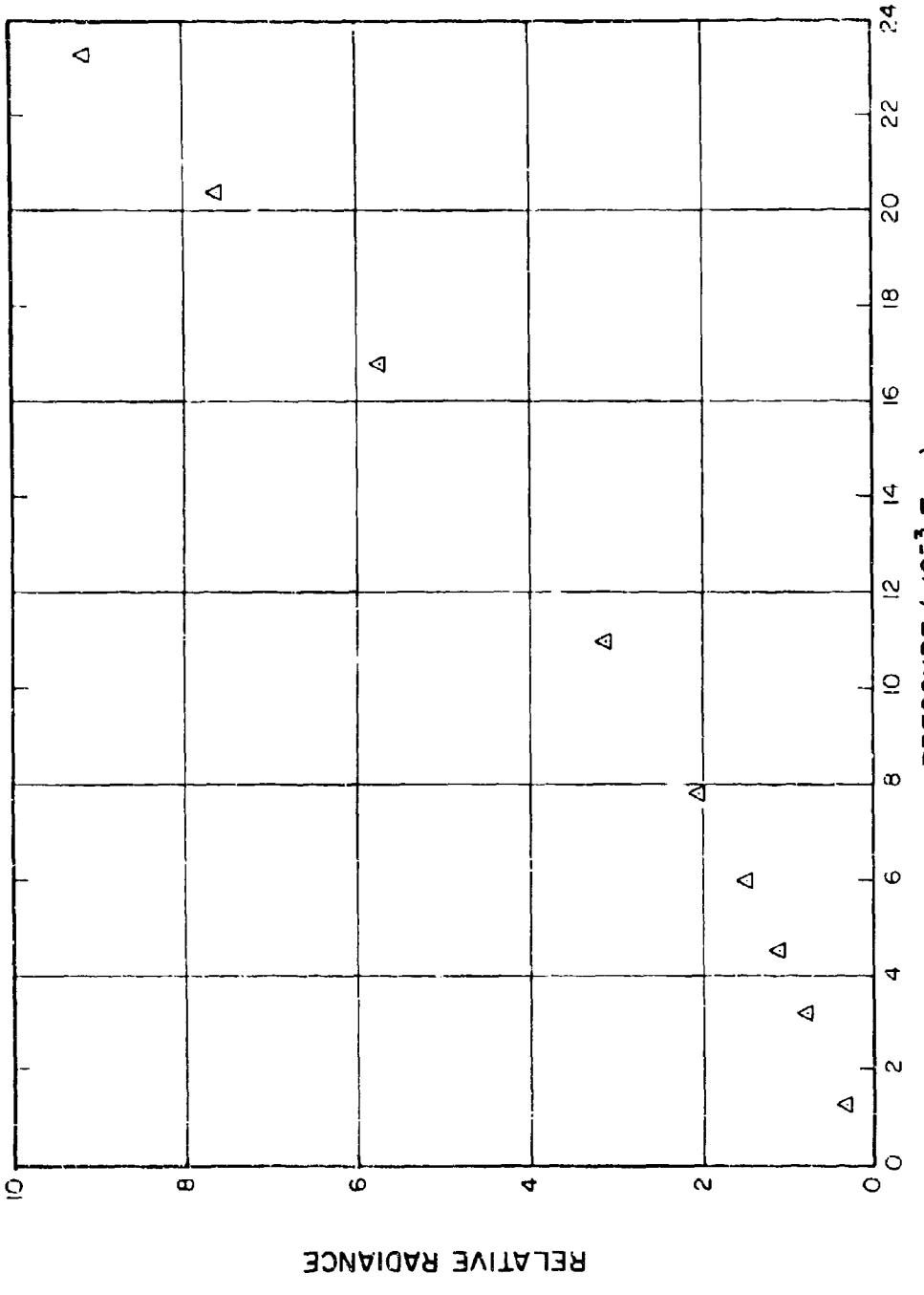
INTENSITY OF FIRST POSITIVE BANDS AT 6600Å
RELATIVE RADIANCE
PRESSURE (x10⁻³ Torr)
0
2
4
6
8
10
12
14
16
18
20
22
24

Figure 62

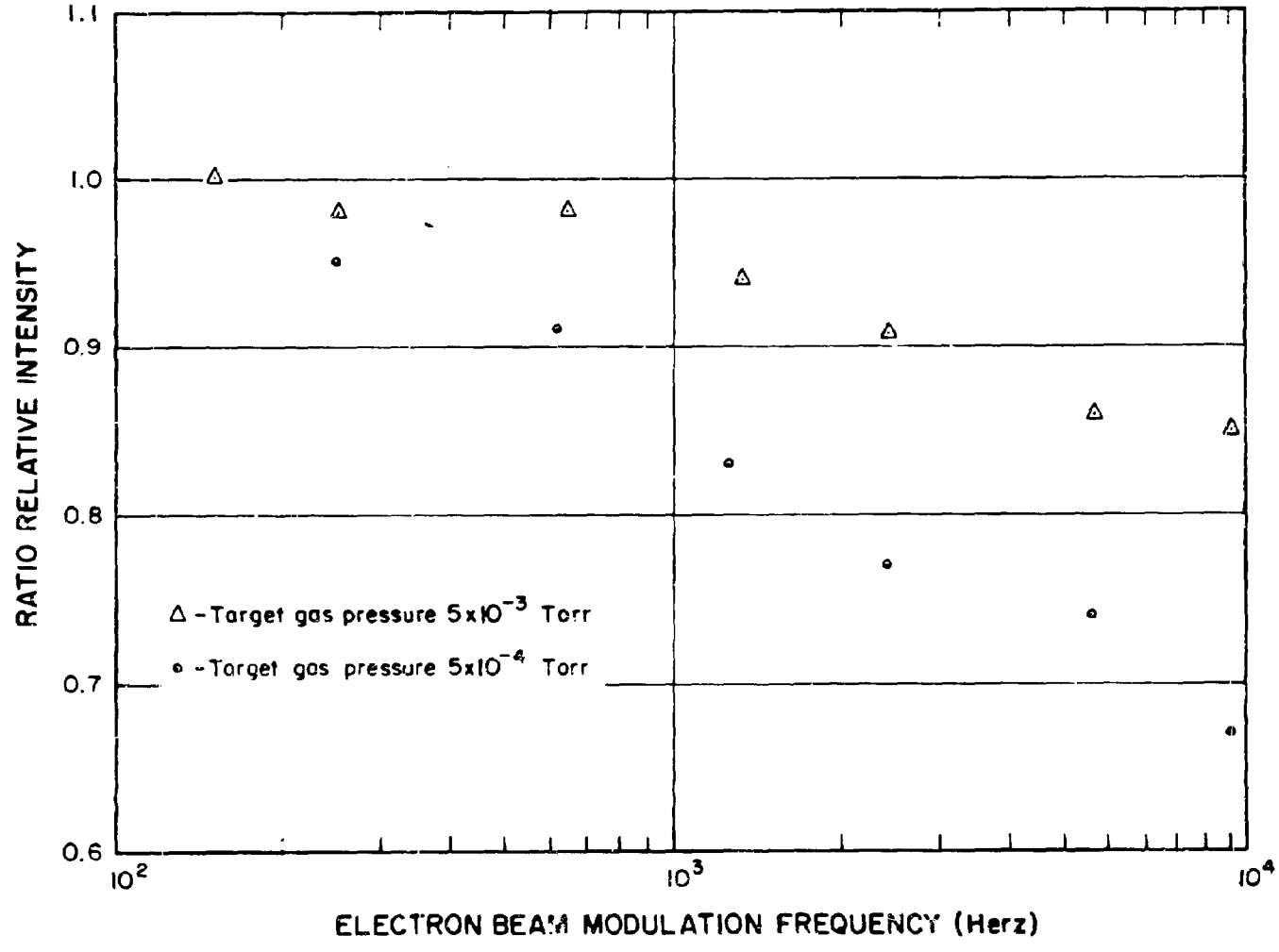

Figure 63

RATIO MEINEL (1-0) BAND INTENSITY TO 1st NEGATIVE (0-0) BAND INTENSITY AS MEASURED BY PHASE SENSITIVE AMPLIFIER

the departure of Figures 56 through 61 from the description of the Stern-Volmer expression, an increase in absolute intensity would be expected at high pressures and low modulation frequencies. This is not the case. The intensity of the (1-0) Meinel band relative to the 3914 Å band is presented in Figure 63 as a function of the electron beam modulation frequency. The Meinel band shows a significant increase in intensity at the lower modulation frequencies for the lower pressure case. In addition, the Meinel band intensity is linear with electron beam current for the low pressure-low frequency conditions. Thus the emission is the result of a single electron collision resulting in one or more excitation mechanisms.

The variation of the intensity of the Meinel bands at lower pressures with modulation frequency suggests a multiple excitation process. The data is consistent with a direct and an indirect populating mechanism which is characterized by a substantially longer fluorescence decay, the phase sensitive amplifier is detuned to the indirect excitation at the higher modulation frequencies. The prominence of the indirectly excited emission at low pressures suggests a collisional process competes with the relatively slow process which indirectly populates the Meinel system.

In view of the complexity of the proposed model, the values presented for the collisional deactivation cross sections are tentative values until further experiments define the excitation and de-excitation mechanisms.

4.5 Absolute Cross Sections for Production of N_2^+ First Negative and Meinel Bands by Electron Impact

4.5.1 Introduction

The importance of a knowledge of absolute and relative cross sections in understanding excitation phenomena in gases has been pointed out many times in the past. This knowledge is particularly applicable to the phenomena of auroral and ionospheric processes.

Laboratory studies of electron interactions with atmospheric gases were carried out at least as early as 1931 by Lindh.[34] It was observed

that at low pressures the more prominent emissions in the visible region of the spectrum were from the N_2^+ first negative band system. Later, it was observed in aurora by Meinel[35] and in the laboratory by Fan[32] that under certain conditions the intensity of the Meinel system of N_2^+ may appear with an intensity of the same order of magnitude as the N_2^+ first negative system.

Absolute cross sections for production of N_2^+ first negative emissions by electron impact have been measured in various energy regions from threshold to 20 Kev by by Stewart[36]; Sheridan, Oldenberg and Carleton[37]; Hayakawa and Nishimura[38]; McConkey and Latimer[39]; McConkey, Woolsey and Burns[40]; Holland[41]; Srivastava and Mirza.[42] The results differ by approximately a factor of two in the overlap regions between the first three and the last three references. In an effort to isolate the source of this discrepancy, a series of joint measurements were made in Los Alamos with Dr. R. Holland[41] of the Los Alamos Scientific Laboratory and in Cambridge with Dr. N. P. Carleton of Harvard University. The nature of the joint measurements are included in a recent report by Holland.[41] Based on the results of the cross checks with Dr.'s Holland and Carleton the originally reported[43] cross section for electron production of the 3914 Å band has been revised, increased by a factor of two to agree with the results of Holland[41] and other recently reported values.[39,40,42]

Zapesochnyi and Skubenich[27] have measured the absolute cross section for low energy electron production of the $A^2\Pi_g$ state of N_2^+. Relative electron excitation cross sections for several Meinel bands have been given by Stewart.[26] Absolute cross sections for production by protons have been given by Carleton and Lawrence[44] and by Sheridan, Oldenberg and Carleton.[37] Fan[32] compares the relative intensity of 3914 Å band and the Meinel bands excited by protons and electrons.

The data presented in this section are in the form of absolute effective cross sections for production of the radiation observed independent of excitation path. It is generally assumed that the bands of the N_2^+ first negative system are excited directly from the ground state of N_2, rather

than as a result of a cascade process. Recent results of Lassettre et al [45] on electron energy loss in collisions with nitrogen fail to show the characteristic loss at 18.7 ev that is expected for direct excitation. Fink and Welge[8], and Jeunehomme [10] in the measurement of first negative band radiative lifetimes have interpreted anomalous effects as indications of a dual excitation process.

It is of interest to compare the results of the excitation cross section measurements with the measured cross sections for ionization of N_2 as given by Schram, et al.[14] Experimental results indicate for electron production the ratio of the total ionization cross section to the 3914 Å cross section is constant. This ratio, when combined with the observed 35 ev average energy loss by electrons stopping in N_2 or air for each ion pair, is used to estimate the efficiency for producing 3914 Å emission by energetic electrons.

Results are presented for the absolute cross sections for production of the (0-0) band of the N_2^+ first negative system and the (0-0), (1-0) and (2-0) bands of the N_2^+ Meinel system by electrons of energies between 3 kev and 60 kev.

4.5.2 Experimental Method

The absolute cross section for electron excitation of the 3914 Å band was measured by observing a 2.5 cm path length of the electron beam in the observation region of the target chamber (Figure 46) at a distance of several meters. The emission was assumed to approximate an isotropic point source. The target chamber and baffles had been painted with a flat black paint to minimize reflections. It was verified that the black paint did not alter or add to the relative emission of the observed band systems. A standard tungsten ribbon lamp was used to calibrate the photomultiplier filter detector. The photomultiplier response was assumed to be constant over the 75 Å bandwidth of the interference filter. Knowing the transmission of the filter to both a continuous source and the 3914 Å band, absolute pressure, beam current, window transmission, and path length observed,

the absolute cross section was determined for a given energy. The relative cross section energy dependence was measured by using the two phase sensitive amplifiers and dual channel strip chart to record the 3914 Å signal and beam current as a function of energy. The Meinel band cross sections were measured by mounting the three bandpass interference filters successively on the cooled S-1 photomultiplier which was positioned several centimeters from the target chamber window. The absolute cross sections were determined by measuring the intensity relative to the 3914 Å band with the nitrogen target chamber pressure 5×10^{-4} Torr. The signal was recorded by a phase sensitive amplifier and strip chart recorder. The maximum angle of incidence through the filters was approximately 7 degrees as determined by a cathode surface mask and the filter mount geometry. An RCA 6199 photomultiplier with an S-11 response with a field of view similar to the S-1 tube was used as a measure of the relative 3914 cross section. Both tubes were calibrated with the tungsten ribbon lamp. The cooled S-1 tube with each of the three Meinel band filters was also calibrated with a 1150°C blackbody. Knowing the transmission of each filter to the molecular band as well as a continuous source and the response of the photomultiplier filter detectors to the standard sources, the relative cross sections were determined assuming the same path length and solid angle of the source was observed.

The correction in the originally published cross section is based principally on a revised measurement of absolute pressure. To avoid spurious currents generated by the electron beam, the "Alphatron" gauge was mounted approximately 30 cm from the observation region of the target chamber in a pipe leading to the large mechanical pump. It was previously observed for a given 3914 Å radiance, the "Alphatron" pressure increased when the gas flow through the target chamber was substantially reduced. This was erroneously treated as a pressure gradient with the value measured at minimum gas flow accepted as an accurate measure of the pressure in the region of the 3914 Å emission. Additional recent tests indicate the pressure increase with decreasing gas flow is due to outgassing contaminants generated by

electron beam impact with the target chamber. Increasing gas flow more than an order of magnitude while maintaining the same target chamber pressure reduces the partial pressure of the outgassing constituents to negligible proportions.

4.5.3 Results

The revised cross section measured for electron excitation of the 3914 Å band is compared with some of the previously published values in Figure 64. The recent results (not shown in Figure 64) of McConkey, Woolsey and Burns[40], of Holland[41] and of Srivastava and Mirza[42] support the cross section of McConkey and Latimer[39] and extend the electron energy to 2 kev.

As discussed in Section 4.4, the absolute intensity of the Meinel bands at low pressure as measured in this experiment was dependent on the modulation frequency. This is interpreted as a dual excitation process, presumably a direct and an indirect populating mechanism. At a modulation frequency of 5×10^{3} Hz and target gas pressure of 5×10^{-4} Torr, the ratios of the (2-0), (1-0) and (0-3) Meinel band cross sections to the 3914 Å band are 0.60 ± 0.06, 1.40 ± 0.14 and 1.20 ± 0.18 respectively. The revised cross sections for this case are presented in Figure 65. As indicated by the Stern-Volmer plots of Figures 56 through 61, for these conditions the direct excitation process dominates. At the lower modulation frequency of 150 Hz, the magnitude of the Meinel cross sections also measured at a gas pressure of 5×10^{-4} Torr increased by a factor of 1.5. The increase is presumably due to an indirect populating mechanism. As shown in Figure 66, no measurable difference was observed in the energy dependence of the Meinel bands compared to the 3914 Å band. The target chamber pressure was 5×10^{-4} Torr and the emission of each Meinel band and the 3914 Å band were recorded simultaneously through the dual channel recording system. The increase in experimental error at the lower energies was caused by the decrease in target chamber beam current and at the longer wavelengths by the lower quantum efficiency of the photomultiplier.

ELECTRON EXCITATION CROSS SECTION FOR THE N_2^+ FIRST NEGATIVE (0-0) BAND AT 3914A

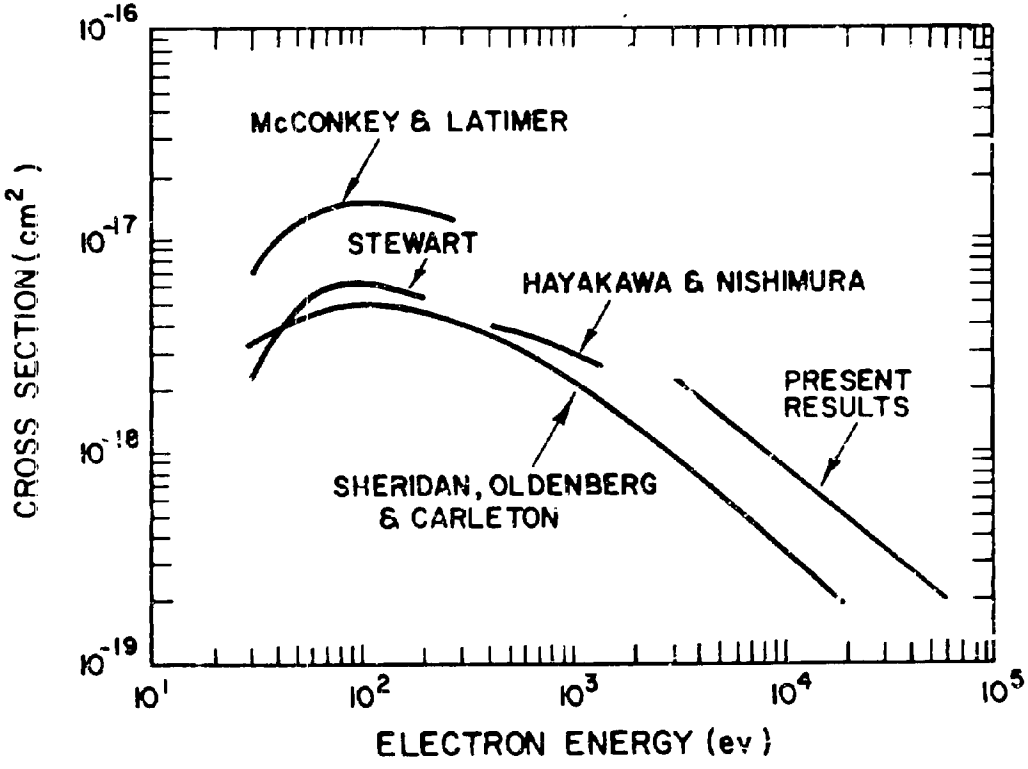

Figure 64

ELLCTRON EXCITATION CROSS SECTIONS FOR N_2^+ BANDS

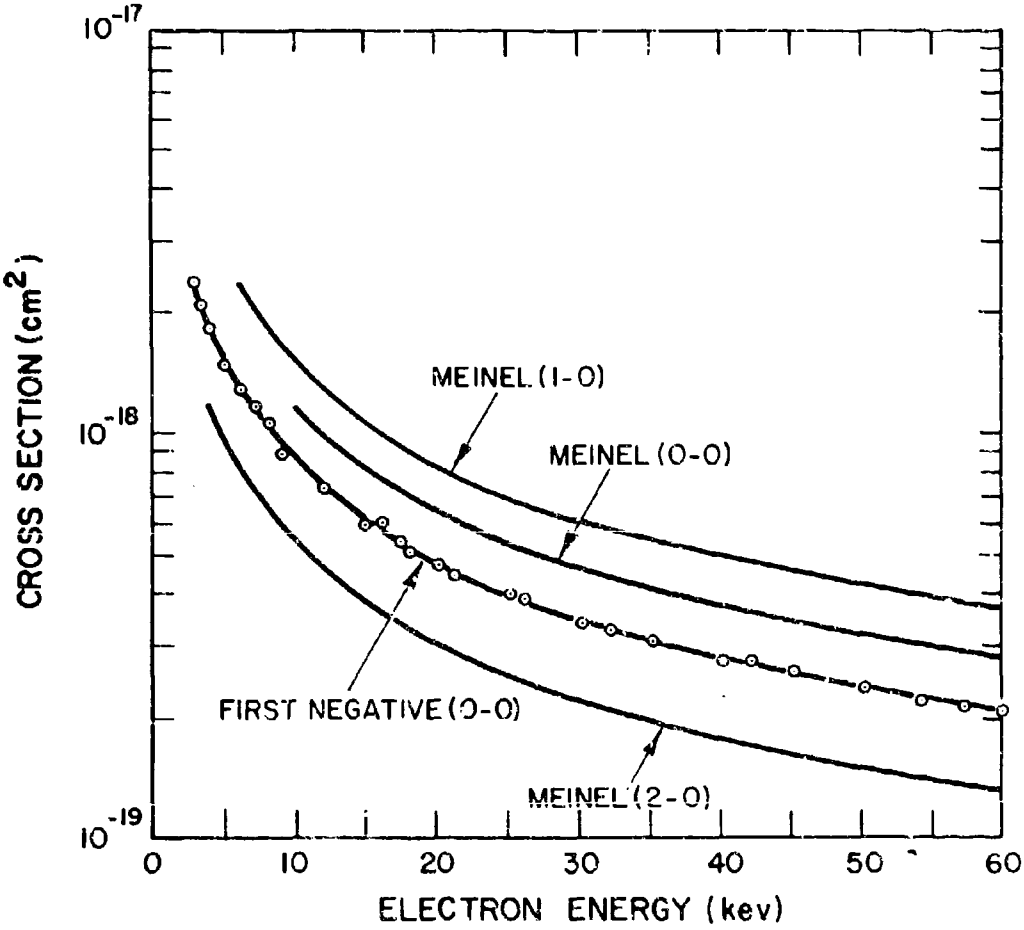

Figure 65

NORMALIZED RATIO MEINEL TO 3914Å CROSS SECTIONS

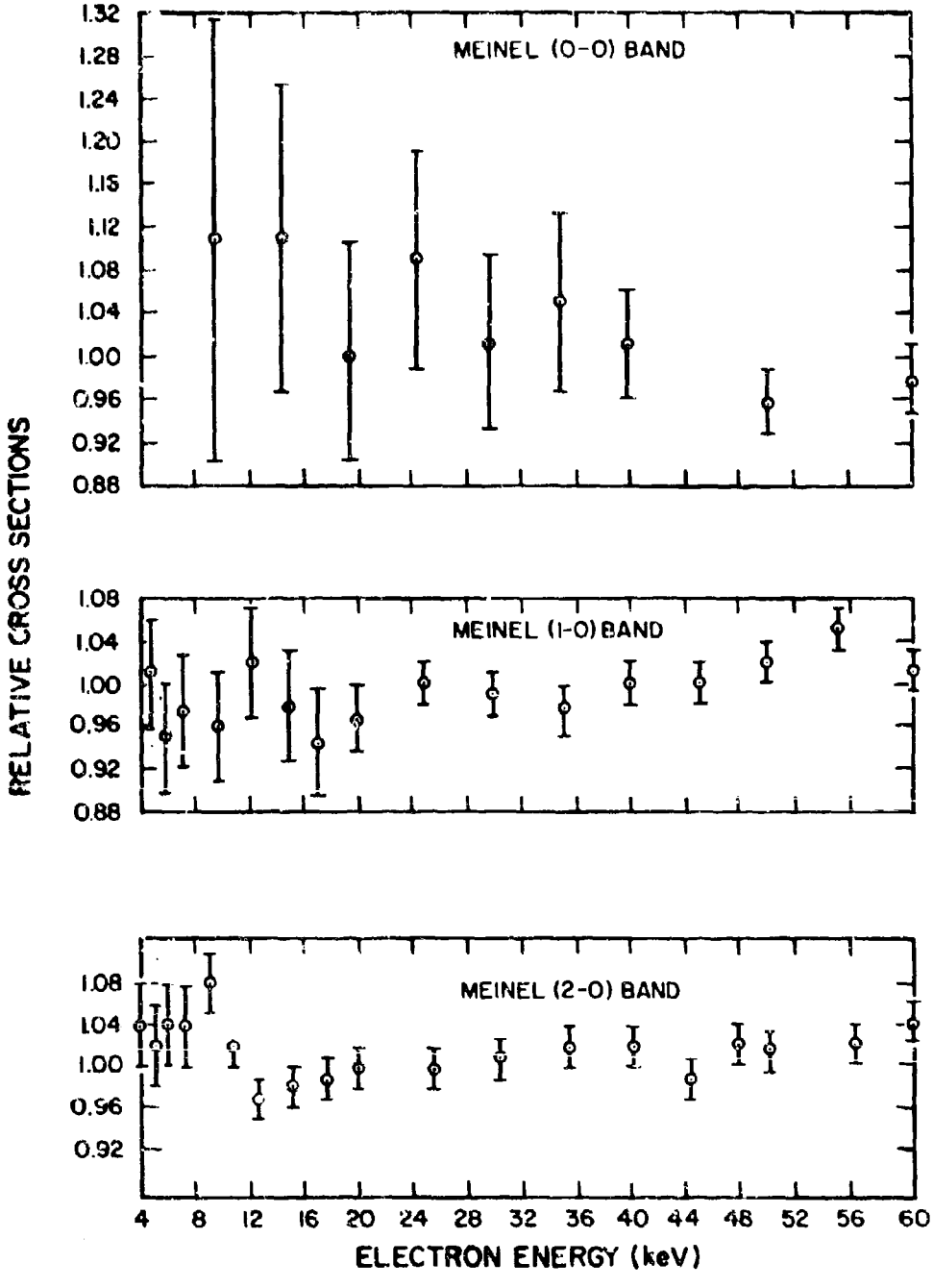

Figure 66

4.5.4 Discussion

Schram, et al[14] have analyzed a measured cross section for the ionization of nitrogen by electrons of from 0.6 to 20 kev energy in terms of the Born approximation. The resulting expression has the form

$$\sigma_{N_2^+} = \frac{A}{E'} \log_e CE'$$

where $\sigma_{N_2^+}$ is the cross section in cm^2 per molecule, $E' = 1/2\, m_o v^2$ (m_o = rest mass of the electron) and A and C constants. Schram found the Born approximation to be an accurate description of the non-relativistic energy dependence. The constants A and C are $(1.84 \pm 0.01) \times 10^{-14}$ ev cm^2 and 0.078 ± 0.001 ev^{-1}, respectively.

For analysis of the excitation cross section for the 3914 Å band by electrons of from 3 to 60 kev energy, where relativistic effects become significant, the expression

$$\sigma_{3914\,Å} = \frac{A}{E'} \left[\log_e CE' - \log_e (1-\beta^2) - \beta^2 \right]$$

is used where β is the ratio of the electron velocity to the velocity of light. In Figure 67 ($\sigma_{3914\,Å}$ E') is plotted as a function of the quantity $\log_e E' - \log_e (1-\beta^2) - \beta^2$. The linear relationship indicates the Born approximation accurately describes the energy dependence of the 3914 Å band cross section. A least squares analysis of the data presented in Figure 67 yields values of A and C of $(12.6 \pm 0.4) \times 10^{-16}$ ev cm^2 and $(0.08\,^{+\,0.04}_{-\,0.02})$ ev^{-1}, respectively. An additional estimated error of $\pm$ 15% exists in the value of A due to the error in the absolute cross section measurement. Schram's value of A is 15 times the value presented for the 3914 Å band while the values of C agree within experimental error.

A comparison of the published[36-43] 3914 Å band electron excitation cross sections and the total ionization cross sections of Tate and Smith[13], Cook and Peterson[46], and Schram et al[14] indicates a similar energy dependence for all the measurements. For electrons with energy in excess of 100 ev, an essentially constant ratio exists between given 3914 Å band

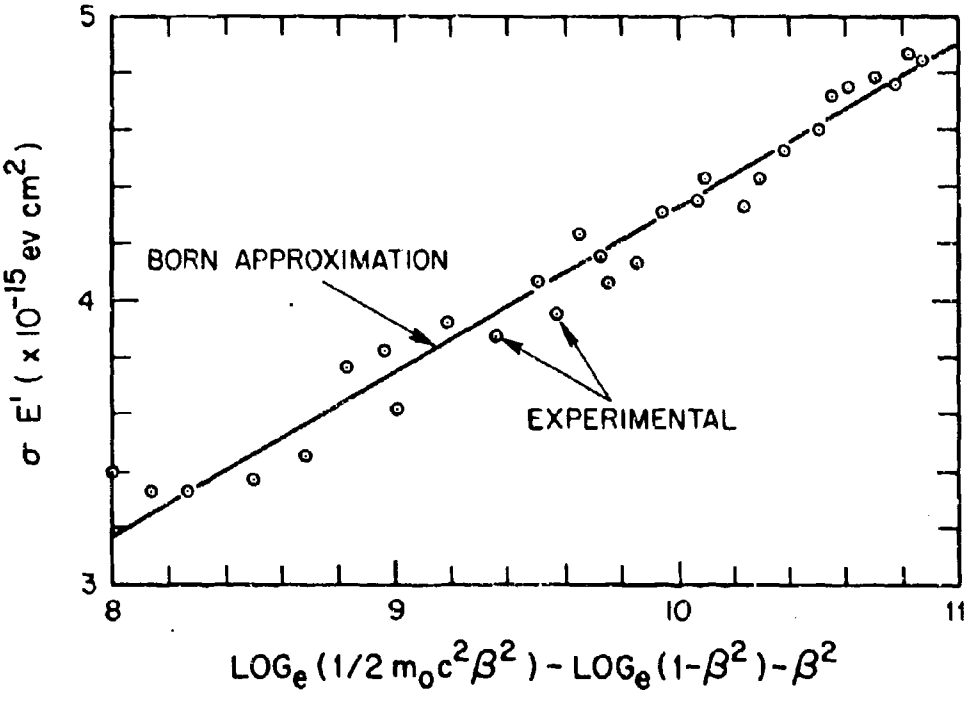

Figure 67 Comparison of Measured Energy Dependence of 3914A Electron Excitation Cross Section with Born Approximation

excitation and N_2 total ionization cross section measurements. However, the magnitude of this ratio varies from approximately 13 to 50 among the various results due to discrepancies in the magnitude of the cross sections. The bulk of this discrepancy is in the excitation cross sections. The total ionization cross sections of Tate and Smith[13] and Schram et al[14] agree within 20 percent.

Valentine and Curran[23] present a review of experimental evidence that indicates energetic electrons incident on nitrogen lose an average 35 ev per ion pair produced. The average energy lost is independent of electron energy for electrons with energy in excess of approximately 100 ev.

Based on the ratio of 15 ion pairs per 3914 Å photon and 35 ev lost per ion pair produced, a fluorescent efficiency of 6.0×10^{-3} is indicated for production of the 3914 Å band in N_2 by electrons. Values of 13 to 15 ion pairs per 3914 Å photon are indicated by recently reported[39-42] excitation cross sections based on the total ionization cross section of Schram et al.[14] Similar analysis using the originally reported[36,37,38,43] excitation cross sections yield approximately 35 ion pairs per photon and a fluorescent efficiency of 2.6×10^{-3} for electrons incident on N_2. The cross section measured by Schram et al for electron ionization is 16 percent larger for O_2 than N_2. Assuming negligible competing inelastic electron collisions with other atmospheric constituents, the 6.0×10^{-3} 3914 Å electron induced fluorescent efficiency in N_2 reduces to 4.6×10^{-3} in air. The fluorescent efficiency calculated in this manner is independent of electron energy for electrons with energies in excess of approximately 100 ev. Hartman[47] in an experiment designed to measure fluorescent efficiency directly in air at pressures low enough to exclude collisional deactivation presents a value of 3.4×10^{-3} for production of the 3914 Å band by electrons. This value confirms a tentative result given in an earlier report.[48] Green and Barth[49] present a theoretical estimate of the fraction of a 30 kev electron's kinetic energy lost by inelastic collisions resulting in the population of the electronic states of N_2 and N_2^+. A fluorescent efficiency of 1.4×10^{-3} is

indicated for excitation of the 3914 Å band by [illegible] nitrogen. Frankenthal, Manley and Treve[5] calculate a fluorescent efficiency of 3 to 5 x 10^{-3} for production in nitrogen by electrons with energy in the range of 1 to 10^3 kev. However both of these calculated fluorescent efficiencies are based on initially reported values of the electron excitation cross section for the 3914 Å band. Use of the larger more recently reported values would increase the fluorescent efficiencies by a factor of slightly greater than two.

Nicholls[51] has calculated Frank-Condon factors for the first negative and the Meinel systems of N_2^+. In addition to calculations of the relative Frank-Condon factors for transitions of a given progression, values are presented for the transitions to various upper vibrational levels excited from the ground state. Based on these Frank-Condon factors and assuming the electronic transition moment is a constant, the relative Meinel band cross sections have been calculated. The calculation also assumes the vibrational levels are populated by electron excitation in proportion to their Frank-Condon factors. The calculated and experimental values are compared in Table IX. The Frank-Condon factors indicate the (2-0), (1-0) and (0-0) bands represent 10, 24 and 18 percent of all the Meinel band transitions. Similar analysis indicates the 3914 Å band represents 65 percent of all the first negative transitions. On the basis of these percentages and the cross sections for direct excitation (the Meinel band cross sections measured at 5 x 10^3 Hz), the ratio of the population by direct electron excitation of the $N_2^+ A^2 \Pi_u$ to the $B^2 \Sigma_u^+$ state is 4 to 1. Since it is also known the 3914 Å excitation cross section represents one out of 15 ionizing collisions, a maximum value for the relative population of the $X^2 \Sigma_g^+$ state of N_2^+ may be calculated. Assuming the first three electronic states represent the total ionization cross section, the X, A and B states are populated in the ratio of 5:4:1. Zapesochnyi and Skubenich[27] have measured the cross section for the electron excitation of the $A^2 \Pi$ and $B^2 \Sigma_u^+$ electronic states of N_2^+ by summing the cross sections for the more intense Meinel and first negative

TABLE IX

RELATIVE MEINEL BAND EXCITATION CROSS SECTIONS

Transition	This Experiment	Theoretical[a]
2-0	1.0 ± 0.1	1.0
1-0	2.3 ± 0.23	2.4
0-0	2.0 ± 0.3	1.8

[a]The theoretical values are based on the Frank-Condon factors of Nicholls

transitions. At the maximum electron energy of 140 ev the ratio of the A to B state excitation cross section is approximately 2.5:1. While a maximum error of 40% is given for the absolute values of the cross sections, the error in the relative cross sections and the target gas pressure for the Meinel band measurements are not specified.

The (2-0), (1-0) and (0-0) Meinel bands have excitation cross sections (including the indirect populating process) that are 0.9, 2.1 and 1.8 times the 3914 Å band. At pressures below 5×10^{-4} Torr where collisional quenching is an ineffective depopulating process the cross sections represent fluorescent efficiencies of 2.7×10^{-3}, 5.4×10^{-3} and 3.9×10^{-3}. At this pressure, it is estimated that approximately 55 percent of the emission is due to direct electron excitation and the remainder the result of an indirect populating mechanism.

5. CONCLUSIONS

The absolute intensity of the optical emissions resulting from electron bombardment of nitrogen and air have been measured. The intensities have been expressed in the form of fluorescent efficiencies, the fraction of the electron's kinetic energy converted into optical radiation in a given transition. Data are presented for the first negative and Meinel systems of N_2^+ and the first and second positive systems of N_2. The measurements have been made in the pressure range where collisional deactivation and radiative transitions are competing depopulating processes. With the exception of the Meinel bands of N_2^+, Stern-Volmer quenching describes the pressure dependence of the fluorescent efficiencies. The Meinel bands are excited by a dual excitation mechanism. One of the excitation mechanisms is pressure dependent and is not described by the Stern-Volmer quenching process.

Figures 68 and 69 present fluorescent efficiencies as a function of pressure in N_2 and air for representative transitions of the band systems considered. The fluorescent efficiency for the (1-0) Meinel band is for direct excitation exclusive of the cascade mechanism. The magnitude of the efficiency is based in part on the cross section measured at 5×10^3 Hz at a N_2 pressure of 5×10^{-4} Torr. Figure 59 indicates at 5×10^{-4} Torr the excitation cross section for direct excitation represents 80 percent of the total cross section. The fluorescent efficiency for the (1-0) Meinel band given in Figure 68 is based on the cross section measured at 5×10^3 Hz reduced by 20 percent. Thus the fluorescent efficiency is a minimum value and at lower pressures an increasing additional contribution to the fluorescence is made by an indirect populating mechanism.

The data of Figures 68 and 69 aid in the interpretation of atmospheric radiative phenomena produced by electron excitation. The magnitude of the fluorescent efficiencies are estimated to be independent of electron energy for electrons with energy in excess of approximately 100 ev in agreement

EFFICIENCY FOR PRODUCTION OF OPTICAL RADIATION BY ELECTRONS INCIDENT ON NITROGEN

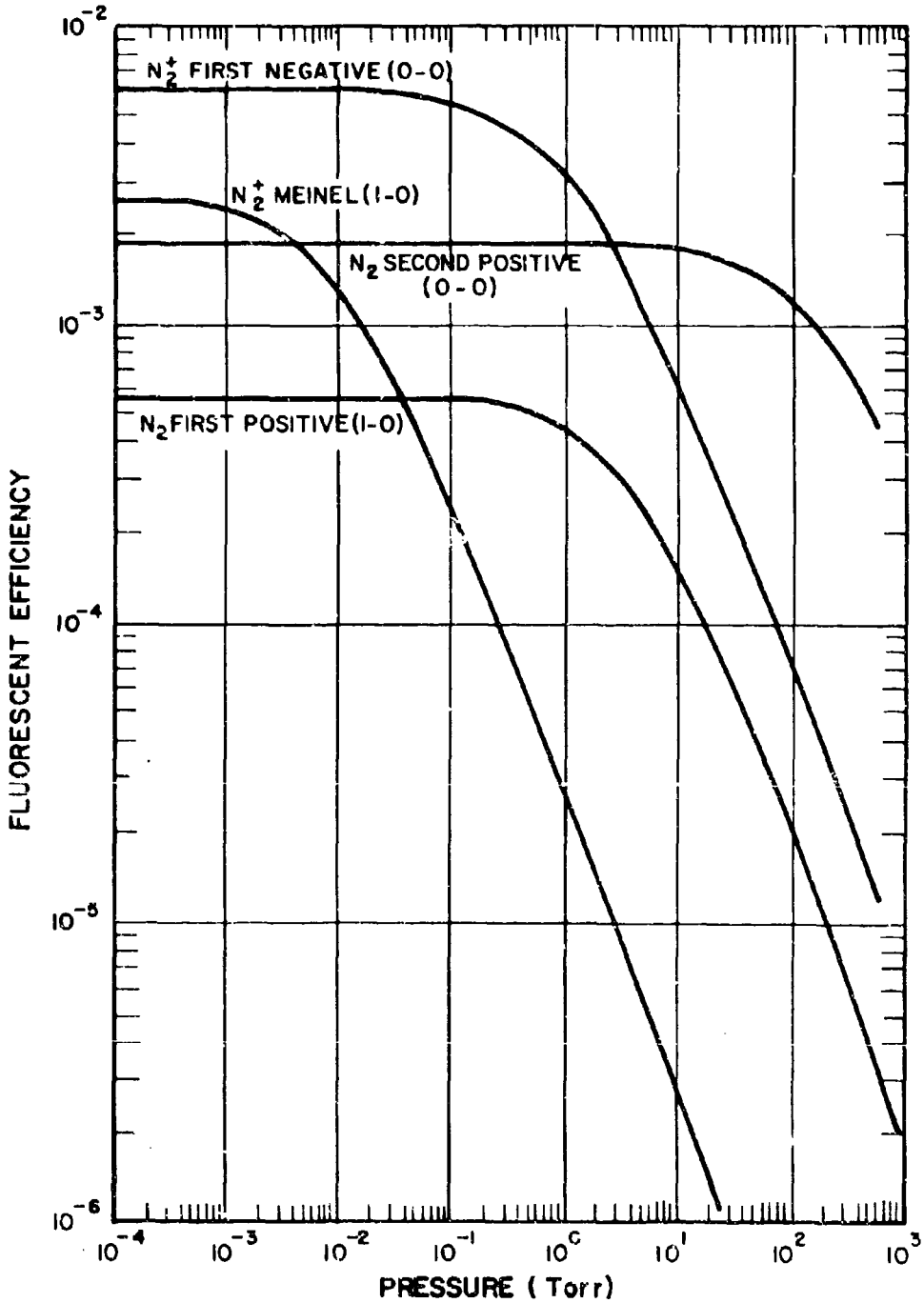

Figure 68

EFFICIENCY FOR PRODUCTION OF OPTICAL RADIATION BY ELECTRONS INCIDENT ON AIR

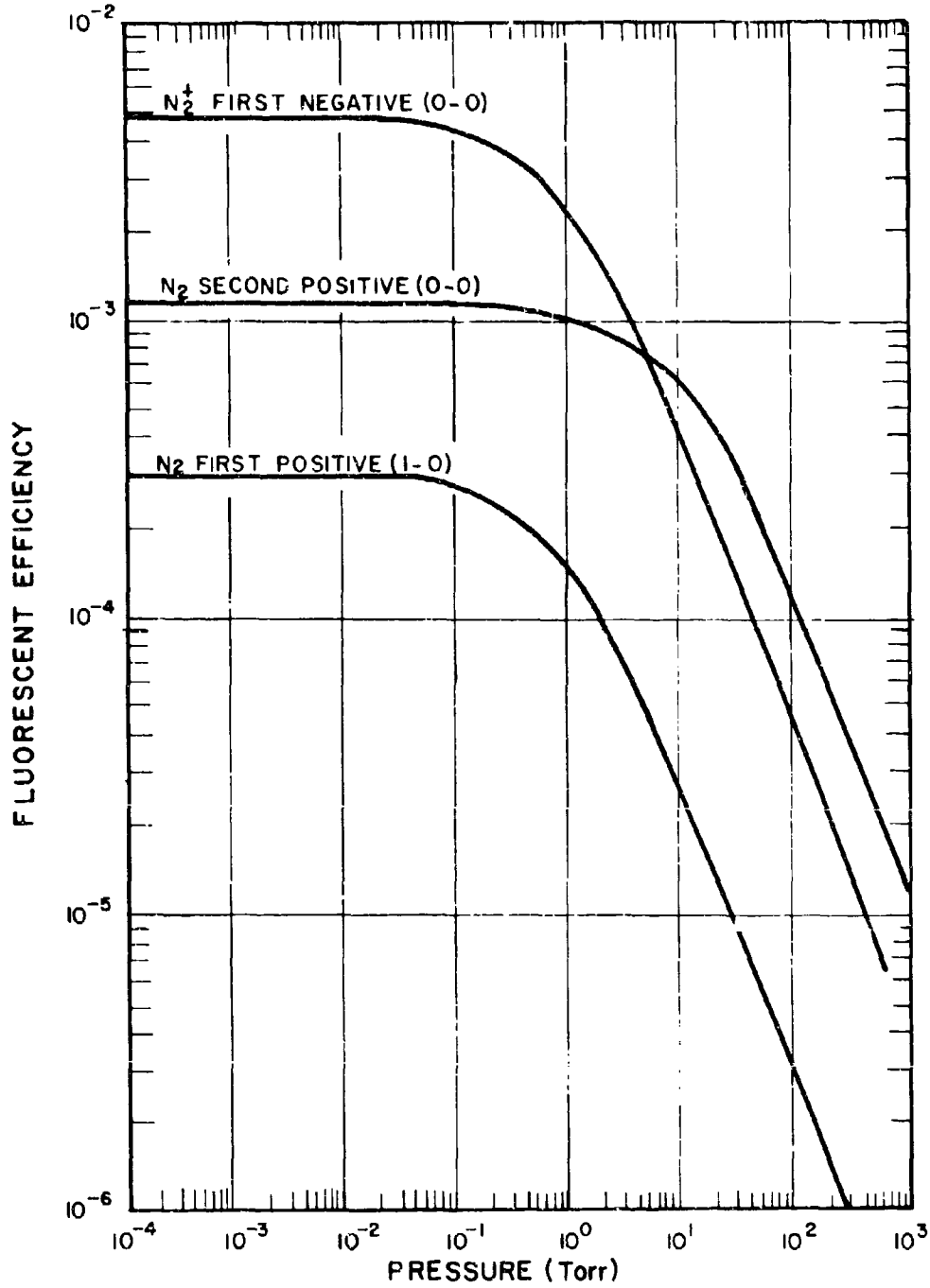

Figure 69

with the calculations of Stolarski and Green[52]. Below 80 km, photochemical reactions are minimal, the atmosphere is almost completely N_2 and O_2 in the ratio of 4 to 1 and the fluorescent efficiencies of Figures 68 and 69 apply directly. Above 80 km, the increasing concentration of atomic species offer alternative energy dissipating mechanisms to the molecular process presented in this report.

REFERENCES

1. G. Davidson and R. O'Neil, U. S. Air Force Cambridge Research Laboratories Report, AFCRL-64-466 (1964).
2. G. Davidson and R. O'Neil, J. Chem. Phys., 41, 3946 (1964).
3. A. E. Grün, Z. Naturforsch, 9a, 55 (1954).
4. B. W. Schumacher, Ontario Research Foundation, Report #5806 (1958).
5. S. Dondes, P. Harteck and C. Kunz, Radiation Res., 27, 174 (1966).
6. R. A. Young and R. L. Sharpless, Discussions Faraday Soc., 33, 228 (1962).
7. R. G. Bennett and F. W. Dalby, J. Chem. Phys., 31, 434 (1959).
8. E. Fink and K. H. Welge, Z. Naturforsch, 19A, 1193 (1964).
9. D. I. Sebacher, J. Chem. Phys., 42, 1368 (1965).
10. M. Jeunehomme, J. Chem. Phys., 44, 2672 (1966).
11. R. G. Fowler and T. M. Holzberlein, J. Chem. Phys., 45, 1123 (1966).
12. J. E. Hesser and K. Dressler, J. Chem. Phys., 45, 3149 (1966).
13. J. T. Tate and P. T. Smith, Phys. Rev., 39, 270 (1932).
14. B. L. Schram, F. J. DeVeer, M. J. Van Der Wiel and J. Kistemaker, Physica, 31, 94 (1965).
15. B. Brocklehurst and F. A. Downing, J. Chem. Phys., 46, 2976 (1967).
16. M. H. Hirsh, G. M. Halpern, J. A. Slevin and N. Wolf, U. S. Army Electronic Command Technical Report, ECOM-01354-F.
17. B. Brocklehurst, Trans. Faraday Soc., 60, 2151 (1964).
18. M. Jeunehomme, Private communication.
19. G. Culp and A. T. Stair, J. Chimie Physique, 64, 57 (1967).
20. G. Herzberg, Spectra of Diatomic Molecules, D. Van Nostrand Co., Inc., Princeton, New Jersey, 1950.
21. D. T. Stewart and E. Gabathuler, Proc. Phys. Soc., (London) 72, 287 (1958).
22. J. D. Jobe, F. A. Sharpton and R. M. St. John, J.O.S.A., 57, 106 (1967).
23. J. M. Valentine and S. C. Curran, Rep. Progr. Phys., 21, 1 (1958).
24. A. E. Grün, Can. J. Phys., 36, 858 (1958).
25. G. O. Langstroth, Proc. Roy. Soc. A, 146, 167 (1934)

26. D. T. Stewart, Proc. Phys. Soc. (London) A68, 404 (1955).

27. I. P. Zapesochnyi and V. V. Skubenich, Optics and Spectr., 21, 83 (1966).

28. M. Jeunehomme, J. Chem. Phys., 45, 1805 (1966).

29. W. F. Sheridan, O. Oldenberg and N. P. Carleton, Atomic Collision Processes, ed. by M. R. C. McDowell, Wiley and Sons, New York (1964).

30. N. Thompson and S. E. Williams, Proc. Roy. Soc. A, 147, 583 (1934).

31. D. T. Stewart, P. W. F. Gribbon and E. G. Emeleus, Proc. Phys. Soc. A, 67, 188 (1954).

32. C. Y. Fan, Phy. Rev., 103, 1740 (1956).

33. B. H. Worsley, Comm. of the Acm, 7, 39 (1964).

34. A. E. Lindh, Z. Physik, 67, 67 (1931).

35. A. B. Meinel, Astrophys. J., 112, 562 (1950).

36. D. T. Stewart, Proc. Phys. Soc. (London) A69, 437 (1956).

37. W. F. Sheridan, O. Oldenberg and N. P. Carleton, Abstr. 2nd Intern. Conf. Phys. Electronic and Atomic Collisions, Boulder, Colo., 1961, W. A. Benjamin, New York.

38. S. Hayakawa and H. Nishimura, J. Geomagnetism and Geoelectricity (Japan), 16, 72 (1964).

39. J. W. McConkey and I. D. Latimer, Proc. Phys. Soc., 86, 463 (1965).

40. J. W. McConkey, J. M. Woolsey and D. J. Burns, Planet. Space Sci., 15, 1332 (1967).

41. R. F. Holland, Los Alamos Scientific Laboratory Report LA-3783.

42. B. N. Srivastava and I. M. Mirza, Phys. Rev., 168, 86 (1968).

43. G. Davidson and R. O'Neil, Astr. IVth Intern. Conf. Phys. Electronic and Atomic Collisions, Quebec, 1965, Science Bookcrafters, Inc., New York.

44. N. P. Carleton and T. R. Lawrence, Phys. Rev., 109, 1159 (1958).

45. E. N. Lassettre, F. M. Glaser, V. D. Meyer, and A. Skerbele, J. Chem. Phys., 42, 3429 (1965).

46. C. J. Cook and J. R. Peterson, Peterson, Phys. Rev. Letters, 9, 164 (1962).

47. P. L. Hartman, Los Alamos Scientific Laboratory Report, LA-3793.

48. P. L. Hartman, Los Alamos Scientific Laboratory Report, LA-3147-MS.

49. A. E. S. Green and C. A. Barth, J. Geophys. Res., 70, 1083 (1965).

50. S. Frankenthal, O. P. Manley and Y. M. Treve J. Chem. Phys., 44, 257 (1966).

51. R. W. Nicholls, U. S. Air Force Cambridge Research Laboratories Report, AFCRL-605 (1961).

52. R. S. Stolarski and A. E. S. Green, J. Geophys. Res., 72, 3967 (1967).

UNCLASSIFIED
Security Classification

DOCUMENT CONTROL DATA - R&D

(Security classification of title, body of abstract and indexing annotation must be entered when the overall report is classified)

1 ORIGINATING ACTIVITY *(Corporate author)*
American Science and Engineering, Inc.
11 Carleton Street
Cambridge, Massachusetts 02142

2a. REPORT SECURITY CLASSIFICATION
Unclassified

2b. GROUP

3 REPORT TITLE

THE FLUORESCENCE OF AIR AND NITROGEN EXCITED BY ENERGETIC ELECTRONS

4 DESCRIPTIVE NOTES *(Type of report and inclusive dates)*
Scientific. Final. 12 March 1964 - 11 February 1968 - Approved, 13 June 1968

5 AUTHOR(S) *(First name, middle initial, last name)*

Robert R. O'Neil and Gilbert Davidson

6. REPORT DATE	7a. TOTAL NO. OF PAGES	7b. NO. OF REFS
1 January 1968	146	52

8a. CONTRACT OR GRANT NO.	9a. ORIGINATOR'S REPORT NUMBER(S)
AF 19 (628)-4080	ASE-1602
b. PROJECT, TASK, WORK UNIT NOS. 5710, 571000, 57100001	
c. DOD ELEMENT 62600601D	9b. OTHER REPORT NO(S) *(Any other numbers that may be assigned this report)* AFCRL-67-0277
d. DOD SUBELEMENT 68920G0535	

10. DISTRIBUTION STATEMENT
1- Distribution of this document is unlimited. It may be released to the Clearinghouse, Department of Commerce, for sale to the general public.

11. SUPPLEMENTARY NOTES	12. SPONSORING MILITARY ACTIVITY
TECH, OTHER	Air Force Cambridge Research Labs. (CRO) L. G. Hanscom Field Bedford, Massachusetts 01730

13. ABSTRACT

The optical radiation from air and nitrogen bombarded by energetic (kev) electrons has been measured over a wide range of gas pressures. Absolute fluorescent efficiencies of spectra from 3,200 to 11,000 Å are presented for air and nitrogen at both 22 Torr excited by 10 kev electrons and 600 Torr excited by 50 kev electrons. At lower pressures, absolute intensity measurements have been made in the form of electron excitation cross sections for the first negative and Meinel bands of N_2^+. The radiative lifetimes of the Meinel bands are also given.

The pressure dependence of the first and second positive systems of N_2 and the first negative and Meinel systems of N_2^+ has been analyzed. With the exception of the Meinel bands, the Stern-Volmer collisional quenching mechanism accurately describes the pressure dependence of these systems in nitrogen and air.

Based on the Stern-Volmer analysis, the absolute intensity of the electron induced fluorescence is determined for various transitions of these four band systems for any pressure of air or nitrogen.

DD FORM 1 NOV 65 1473

UNCLASSIFIED
Security Classification

14. KEY WORDS	LINK A		LINK B		LINK C	
	ROLE	WT	ROLE	WT	ROLE	WT
Optical Radiation	8	2				
Air and Nitrogen	8	2				
Gas Pressure	6	3				
Absolute Fluorescent Efficiency	7	3				
Excitation Cross Sections	8	2				
Radiative Lifetimes	8	2				
N_2 First Positive System			8	2		
N_2 Second Positive System			8	3		
N_2^+ First Negative System			8	3		
N_2^+ Meinel Band System			8	3		
Collisions			6	2		
Quenching			7	2		